FEDERAL UNIVERSITY OF SÃO CARLOS
CENTER OF EXACT SCIENCES AND TECHNOLOGY
DEPARTMENT OF CHEMISTRY
POSTGRADUATE PROGRAM IN CHEMISTRY

EVALUATION OF THE CHEMICAL COMPOSITION AND SURFACE ACIDITY OF MESOPOROUS ACIDIC CATALYSTS IN THE PRODUCTION OF 5-HYDROXYMETHYLFURFURAL AND FURFURAL FROM MONOSACCHARIDES

José Lucas Vieira*

Thesis presented as part of the requirements for obtaining the title of DOCTOR OF SCIENCE, concentration area: INORGANIC CHEMISTRY

Advisor: Dr. Caue Ribeiro de Oliveira
Co-advisor: Dr. Jean Marcel R. Gallo

***São Paulo Research Foundation (FAPESP): grants 2017/17042-9, 2018/10536-9, 2019/02132-8, and 2020/04109-0**

São Carlos - SP
2024

UNIVERSIDADE FEDERAL DE SÃO CARLOS

Centro de Ciências Exatas e de Tecnologia
Programa de Pós-Graduação em Química

Folha de Aprovação

Defesa de Tese de Doutorado do candidato José Lucas Vieira, realizada em 22/07/2024.

Comissão Julgadora:

Prof. Dr. Cauê Ribeiro de Oliveira (EMBRAPA)

Prof. Dr. Marco André Fraga (INT)

Prof. Dr. Wagner Alves Carvalho (UFABC)

Prof. Dr. Luiz Carlos Alves de Oliveira (UFMG)

Prof. Dr. Thiago Faheina Chaves (BRASKEM)

O Relatório de Defesa assinado pelos membros da Comissão Julgadora encontra-se arquivado junto ao Programa de Pós-Graduação em Química.

“All the mountains are high!”

- Zé da Timba & Zé Latinha

ACKNOWLEDGMENT

I would like to thank God for life and health! Thank you for giving me the energy to finish this thesis and this journey!

I would like to thank my parents, my dad José Adriano Vieira, and my mom Elaine Cristina Martins! More than the financial support, your psychological support was invaluable! At the beginning of this academic journey, you really did not know where I was heading (I still think you do not fully understand what I have been working on, haha), but without judgment, you supported me! I love you both!

I would like to thank my darling wife, Mikaely Cristina Vaz! She is my physical and psychological support as well. After a very bad/sad day of work, she was there for me! After a very good/happy day, she was there for me! I want to be there for you every day of our lives! If I finished this thesis, you and our future family are one of the reasons. All I have done, I did thinking of us!

I would like to thank my sister Aleska Caroline Vieira! She is so kind and so silly, haha. Love you, my little sis!

I would like to thank Prof. Dr. Jean Marcel R. Gallo. I was your first and will be the last student of your GreenCat group. You were my mentor; you gave the tips. You are my inspiration.

I would like to thank Dr. Caue Ribeiro and his group CatFert at Embrapa. Thank you all for hosting and accepting me into your group!

I would like to thank Profa. Dra. Clelia Mara de Paula Marques, and Prof. Dr. José Maria Corrêa Bueno. This couple is amazing! Profa. Clelia was my

first professor in inorganic chemistry, and during her lessons, I met Dr. Jean Marcel R. Gallo (her tutor at that time). She was also so kind to me and my wife, as was José Maria. I wish both of you the best!

I would like to thank my old group GreenCat. This group was amazing! The work, the discussions, the laughter, the good environment, the partnership… In particular, my close friends M.Sc. Gustavo Duran Iga and M.Sc. Marcelo de Assis Lima. I love you, my friends, you made this journey easier!

I would like to thank my pagode band "Pagode Catalítico", again M.Sc. Gustavo Iga and M.Sc. João Lucas Barros. You guys have no idea how important you were in my life when I was alone in the lab in 2023…

I would like to thank all my relatives: my grandmother Dona Cida, my uncles (Fernando, Marcelo, and Marcos), aunts (Janaína and Luciana), cousins (especially my brother Murilo), mother-in-law (Nalvinha), father-in-law (Nivaldo), sisters-in-law (Nayara and Taynara), and brothers-in-law (Mateus and Murilo).

I would like to thank my friends from Itaí, São Carlos (especially Débora and Gustavo), Campinas (especially Érick), and abroad! The days were chill with you!

I would like to thank Prof. Dr. Edson Rodrigues Filho for the gatherings and football games that we watched together during this journey!

I would like to thank FAPESP for financing me during this whole journey (grants 2019/02132-8 and 2020/04109-0).

TABLE LIST

FIGURE LIST

RESUMO

AVALIAÇÃO DA COMPOSIÇÃO QUÍMICA E ACIDEZ SUPERFICIAL DE CATALISADORES ÁCIDOS MESOPOROSOS NA PRODUÇÃO DE 5-HIDROXIMETILFURFURAL E FURFURAL A PARTIR DE MONOSSACARÍDEOS. Esta tese investigou a síntese, composição e acidez superficial de vários catalisadores ácidos mesoporosos e seus impactos na desidratação catalítica de monossacarídeos nas moléculas plataforma 5-hidroximetilfurfural (HMF) e furfural. Fosfatos de nióbio com diferentes razões molares *P/Nb* foram preparados, afetando suas razões de sítios ácidos de Lewis/Brønsted (razão *L/B*) e suas atividades catalíticas. Catalisadores com altas razões *P/Nb* exibiram baixas razões *L/B*, enquanto que catalisadores com baixas razões *P/Nb* apresentaram altas razões *L/B*. Além disso, foi demonstrada uma correlação linear entre a razão *L/B* e as velocidades de reação para a produção de HMF e furfural a partir de glicose e xilose, respectivamente. Com base nisso, sintetizamos um catalisador de carbono bifuncional mesoporoso controlado para produzir de forma mais fácil um catalisador com razões *L/B* para a produção de moléculas plataforma. Primeiro, preparamos carbonos sulfonados com apenas acidez de Brønsted para a desidratação de frutose e xilose em HMF e furfural, respectivamente. Eles apresentaram diferentes concentrações de sítios ácidos mais fortes (grupos sulfônicos) e mais fracos (grupos ácido carboxílico, álcool, fenol). A proporção entre sítios ácidos mais fortes e mais fracos (N_S/N_W) foi encontrada como significativamente influente no desempenho catalítico, com rendimentos e números de turnover ótimos observados nas razões N_S/N_W de 2 – 4, sugerindo um papel sinérgico de ambos os tipos de sítios ácidos no mecanismo catalítico. Finalmente, dois carbonos sulfonados promissores do estudo anterior foram selecionados e passaram por troca iônica parcial com cátions metálicos com acidez de Lewis (Al^{3+}, Sc^{3+}, Fe^{3+}, Cu^{2+}, Sn^{4+}, Yb^{3+}) para produzir carbonos bifuncionais ionicamente trocados com diferentes razões *L/B* para a desidratação

de glicose e xilose em HMF e furfural, respectivamente. Embora ainda não tenha sido realizada uma caracterização quanto à acidez superficial desses materiais, a força dos sítios ácidos de Lewis provavelmente desempenha um papel crucial na conversão dos monossacarídeos, com sítios mais fortes (Al^{3+}, Cu^{2+} e Yb^{3+}) levando a isômeros; sítios de força intermediária (Sc^{3+}) levando a isômeros e moléculas plataforma; e sítios mais fracos (Sn^{4+}) levando a moléculas plataforma. O catalisador com 20 % de sítios ácidos de Brønsted trocados por Sn^{4+} (20%-Sn(IV)-Amb-45) mostrou resultados promissores, alcançando seletividade de 41 % para HMF com 57 % de conversão de glicose e seletividade de 47 % para furfural com 65 % de conversão de xilose, enquanto 100%-Al(III)-Amb-45, 100%-Cu(II)-Amb-45 e 100%-Yb(III)-Amb-45 foram promissores para reações de isomerização.

ABSTRACT

EVALUATION OF THE CHEMICAL COMPOSITION AND SURFACE ACIDITY OF MESOPOROUS ACIDIC CATALYSTS IN THE PRODUCTION OF 5-HYDROXYMETHYLFURFURAL AND FURFURAL FROM MONOSACCHARIDES. This thesis investigates the synthesis, composition, and surface acidity of various mesoporous acidic catalysts and their impacts on the catalytic dehydration of monosaccharides into the platform molecules 5-hydroxymethylfurfural (HMF) and furfural. Niobium phosphates with different *P/Nb* molar ratios were prepared, affecting their Lewis/Brønsted acid site (*L/B*) ratio and catalytic activity. Catalysts with high *P/Nb* ratios exhibited low *L/B* ratios, whereas catalysts with low *P/Nb* ratios, high *L/B* ratios. Additionally, a linear correlation between the *L/B* ratio and reaction rates for HMF and furfural production from glucose and xylose, respectively, was demonstrated. Based on that, we synthesize a controlled mesoporous bifunctional carbon catalyst to more easily produce a catalyst with *L/B* ratios for platform molecules production. First, we prepared sulfonated carbons with only Brønsted acidity for the dehydration of fructose and xylose into HMF and furfural, respectively. They had different concentrations of stronger (sulfonic acid groups) and weaker acid sites (carboxylic acid, alcohol, phenol groups). The ratio between stronger and weaker acid sites (N_S/N_W) was found to significantly influence catalytic performance, with optimal yields and turnover numbers observed at N_S/N_W ratios of 2 – 4, suggesting a synergistic role of both types of acid sites in the catalytic mechanism. Finally, two promising sulfonated carbons from the previous study were selected and underwent partial ion-exchange with metallic cations with Lewis acidity (Al^{3+}, Sc^{3+}, Fe^{3+}, Cu^{2+}, Sn^{4+}, Yb^{3+}) to produce ion-exchanged bifunctional carbons with different *L/B* ratios for dehydrating glucose and xylose into HMF and furfural, respectively. Even though no characterization regarding surface acidity has been performed yet, the strength of the Lewis acid sites likely plays a crucial role in the

monosaccharide conversion, with stronger sites (Al^{3+}, Cu^{2+}, and Yb^{3+}) leading to isomers; intermediate strength sites (Sc^{3+}) leading to both isomers and platform molecules, and weaker sites (Sn^{4+}) leading to platform molecules. The catalyst with 20 % of Brønsted acid sites exchanged with Sn^{4+} (20%-Sn(IV)-Amb-45) showed promising results, achieving 41 % HMF selectivity at 57 % glucose conversion and 47 % furfural selectivity at 65 % xylose conversion, whereas 100%-Al(III)-Amb-45, 100%-Cu(II)-Amb-45, and 100%-Yb(III)-Amb-45 were promising for isomerization reactions.

TABLE OF CONTENTS

1 - GENERAL INTRODUCTION

1.1 - Strategies for Carbon Neutrality

The world population will reach 9.9 billion by 2050, leading to an 80 % increase in energy demand and a 70 % rise in food production [1,2]. This demand has based on non-renewable fossil fuels (petroleum, natural gas and coal), exacerbating environmental issues such as energy scarcity, greenhouse gas emissions, and climate change. Without intervention, for example, greenhouse gas emissions are projected to increase by 50 % by 2050, mainly due to energy-related CO_2 emissions [1,3]. In response, the Paris Agreement was signed by all nations in 2015, aiming to limit global warming to below 2.5 °C, and striving for less than 1.5 °C by achieving carbon neutrality, the state of net-zero carbon emission, by 2050 [4]. To fulfill these targets, strategies based on carbon absorption technologies, CO_2 capture, storage, and usage methods, and transitioning to renewable energy sources are being pursued [1,3].

Carbon sinks, such as forests and oceans, are natural systems that absorb more CO_2 from the atmosphere than they release, with forests alone accounting for around 45 % of greenhouse gas absorption [1,3]. Strategies to enhance carbon sinks and hence decrease CO_2 concentration in the atmosphere include reforestation, afforestation, and innovative soil management practices [1,3]. Additionally, CO_2 capture technologies, such as post-combustion, pre-combustion, and oxygen-fuel combustion, offer methods of reducing CO_2 emissions [1,3,5]. The captured CO_2 can then be either stored in geological structures, such as onshore saline aquifers or saline aquifers on the seabed, or used for producing high-value chemicals (syngas, methane, formic acid, and alcohols). However, long-term safety and reliability remain significant challenges for the first option, whereas thermodynamic challenges are observed for the second one due to CO_2 stability and inertness [1,3,6,7].

Transitioning from non-renewable to renewable energy sources that

produce minimal or zero net CO_2 emissions is considered the most promising strategy for achieving carbon neutrality, with solar, wind, ocean, nuclear, and hydrogen energies being one of the key players [1,3,6,7]. Wind and solar energies have been used in recent years; however, their intermittency is a big challenge that must be overcome. While energy storage appears to be a solution to this issue, its scalability and cost-effectiveness are still limitations [1]. Nuclear energy plays a significant role in clean energy, accounting for 40 % of global low-carbon electricity generation, nevertheless it faces uncertainties due to waste disposal and safety concerns. Hydrogen energy, in turn, is very promising since its energy system is similar to an electricity grid, but its widespread adoption is hindered by storage challenges [1]. For all these reasons, biomass remain as the key renewable energy source to achieve the targets pointed out in the Paris Agreement [1,2,5,7].

1.2 - Biomass as a Renewable Energy Source

Biomass is a naturally occurring, non-fossil organic material, including agricultural and forest residues, biogenic materials in municipal waste, animal waste, human sewage, and industrial wastes. It is estimated that biomass could provide 3000 terawatt hours of electricity by 2050 and save 1.3 billion tons of CO_2 equivalent emissions per year [2]. Biomass, as a renewable energy source, can be utilized for bioenergy, biochar, and bio-based products. Bioenergy stands as the oldest and largest source of renewable energy. In 2017, modern bioenergy, excluding energy for cooking and space heating in developing countries, accounted for 50 % (460 megatons of oil equivalent – Mtoe) of global renewable energy consumption. Within this, bioheat represented 70 % (323 Mtoe), biofuels 19 % (86 Mtoe), and bioelectricity 11 % (51 Mtoe) [5].

Additionally, biomass can be thermo-chemical decomposed by pyrolysis or gasification in inert atmosphere to produce a material with high carbon content called biochar. This material can be used as soil supplement in

agriculture, which has been seen as a promising approach to reduce CO_2 concentration, since it retards the return of soil fixed carbon to the atmosphere [1,2]. It can also hinder the emission of other greenhouse gases, such as N_2O and CH_4 from soil. Besides, it also has positive effects on physical aspects of soil such as density, porosity, and texture; as well as chemical features, including cation exchange capacity, pH, soil carbon, water retention, and soil carbon. Apart from agricultural benefits, biochar has also been used as a substrate in hydrogen formation, as a filter in pyrolysis and gasification technologies, and as a fuel when pelletized [1,2].

Furthermore, biomass has been utilized for the production of bio-based products, with approximately 50 million tons of bio-based and bio-polymer materials manufactured globally [2,8], indicating a reduced dependency on fossil sources, thus resulting in lower greenhouse gas emissions. Among the biorefineries responsible for producing these products, 134 (42 %) have been dedicated to generating building blocks (FIGURE 1.1), also referred to as platform molecules [9]. These compounds are versatile molecules that serve as crucial starting materials for synthesizing a wide range of products. Notably, 5-hydroxymethylfurfural (HMF) and furfural are considered among the most significant platform molecules by North American and European agencies [10], and have received a lot of attention by the academic community since 2007 (FIGURE 1.2). The higher interest in furfural compared to HMF in the literature is attributed to the larger global market size of furfural. In 2023, the furfural market was valued at approximately US$ 770 million, with a projected growth rate of 5.7 % during 2024 – 2032 [11]. In contrast, the HMF market was valued at around US$ 62.2 million at the same year, with a projected growth rate of 1.8 % during the same period [12]. The central focus of this thesis is the production of both platform molecules from biomass.

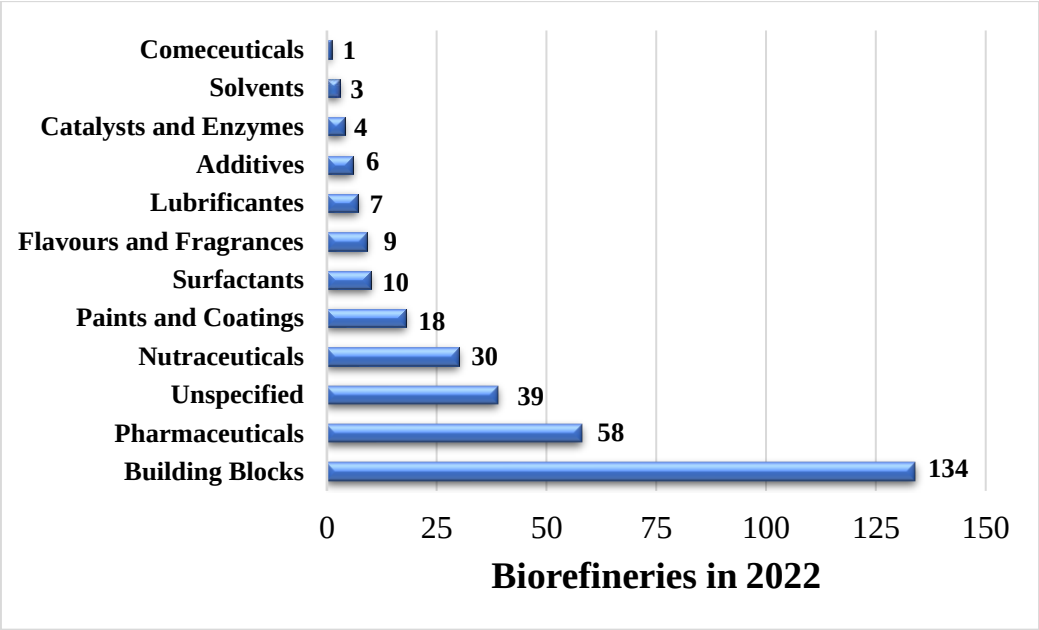

FIGURE 1.1 – Amount of worldwide biorefineries producing bio-based products in 2022.

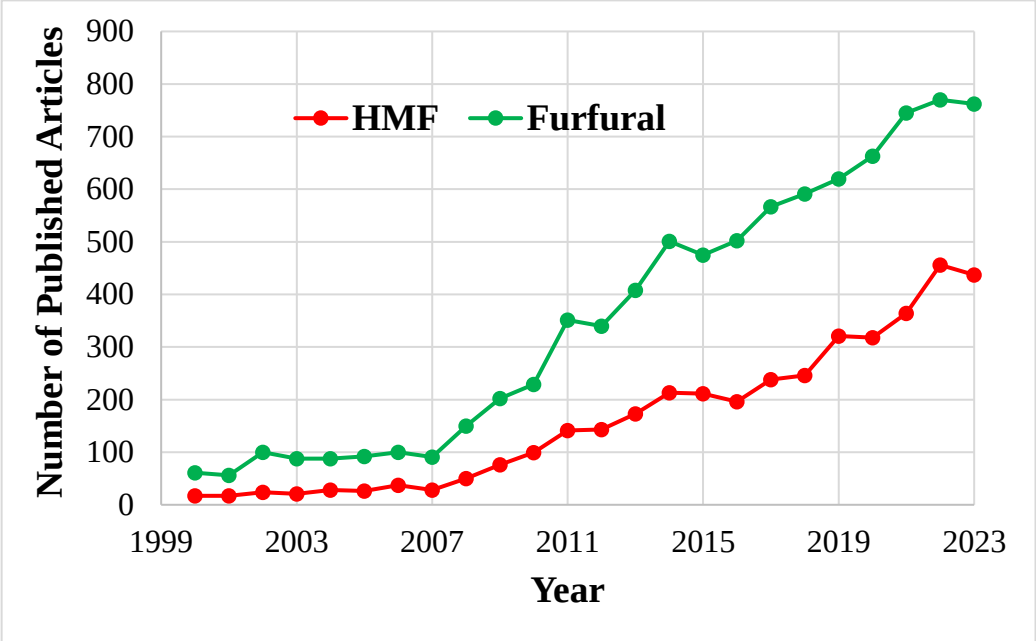

FIGURE 1.2 – Number of published articles on HMF and furfural annually from January 2000 to December 2023. Source: Scopus (keyword: "5-hydroxymethylfurfural", and "furfural").

1.3 - HMF and Furfural as Platform Molecules

HMF is a molecule with a furan ring, containing both aldehyde and alcohol functional groups (FIGURE 1.3). It is a white solid (although commercial

samples are often yellow) with a melting point between 30 and 34 °C, boiling point between 114 and 116 °C, and density of 1.29 g mL^{-1}. It is highly soluble in both water and organic solvents. Furfural, in turn, presents the furan ring with only the aldehyde group attached to it (FIGURE 1.3). It is a colorless liquid (although commercial samples are often brown) with a melting point of – 37 °C, boiling point of 162 °C, and a density of 1.16 g mL^{-1}. Furfural is also very soluble in water and organic solvents.

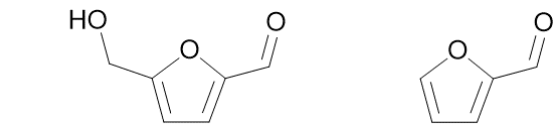

5-Hydroxymethylfurfural (HMF) **Furfural**

FIGURE 1.3 – Molecular structures of HMF and furfural.

Both molecules are highly reactive and can be readily transformed into various products depending on the catalytic process applied, which explains why they are considered excellent platform molecules. For example, in FIGURE 1.4, HMF can be oxidized with Au/TiO_2 to produce 2,5-furandicarboxylic acid (FDCA), a bio-based monomer used in plastic packaging [13]. HMF can also be transformed into chemicals typically derived from petroleum, such as terephthalic acid. In this process, HMF must first be converted into the fuel additive 2,5-dimethylfuran (DMF) using CuRu/C catalyst [14]. Subsequently, DMF undergoes a Diels-Alder reaction with ethylene to form ρ-xylene using the WO_x/ZrO_2 catalyst, which exhibits both Lewis and Brønsted acidity [13]. Finally, ρ-xylene is oxidized to terephthalic acid, which, when combined with ethylene glycol, produces polyethylene terephthalate (PET) for plastic packaging [15]. Another example involves the hydrogenation of HMF with a Ru/CeO_x catalyst to yield 2,5-dihydroxymethyl tetrahydrofuran, a precursor for solvents and monomers [16].

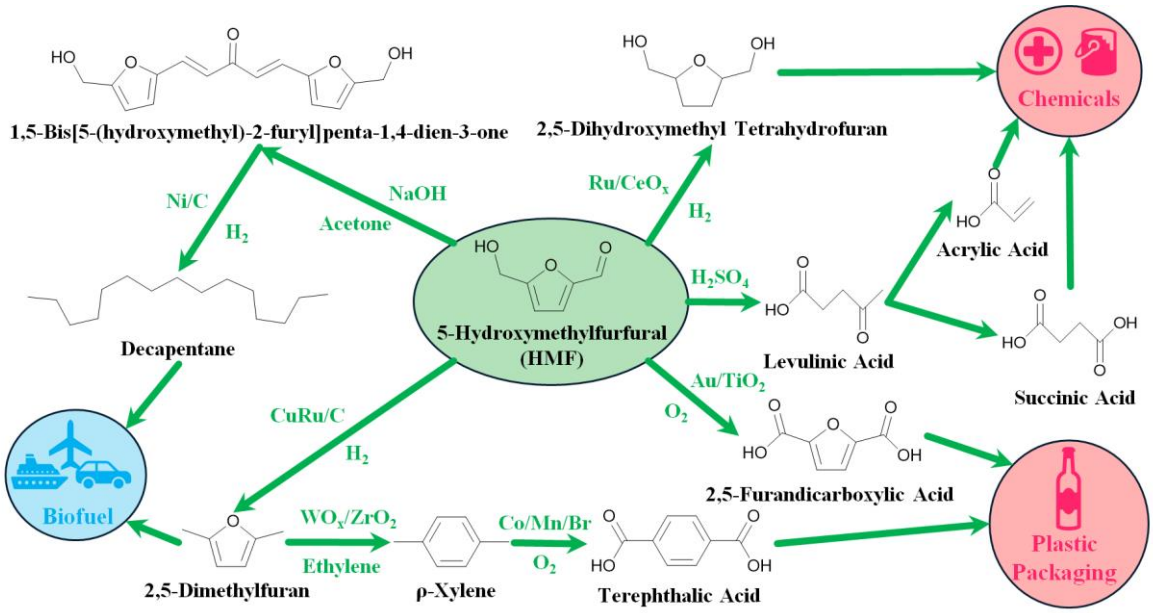

FIGURE 1.4 – Some of the products obtained from HMF and their potential application.

In a similar way, furfural can also be converted into biofuels and biochemicals (FIGURE 1.5). The primary derivative that drives the value of the global furfural market is furfuryl alcohol. It is used as a binder in resin-bonded sand-casting processes for ferrous foundries and as a precursor for resins and plastics [17]. The hydrogenation of furfural to furfuryl alcohol can be achieved using Cu/SiO_2 catalysts [15]. Additionally, furfural can be transformed into tetrahydrofuran and maleic acid, two products derived from petroleum, through its decarbonylation with Pd/SiO_2 [18] and its oxidation with titanium silicate and hydrogen peroxide as the oxidizing agent [19], respectively. These products serve as an industrial solvent and a precursor for resins, respectively. Moreover, furfural can undergo basic aldol condensation with acetone to generate larger molecules, which can be fully hydrogenated to produce hydrocarbons for biofuels [20]. Another possible route is the aerobic oxidation of furfural with PtPb/C catalyst to furoic acid, a precursor for chemical and pharmaceutical industry [21].

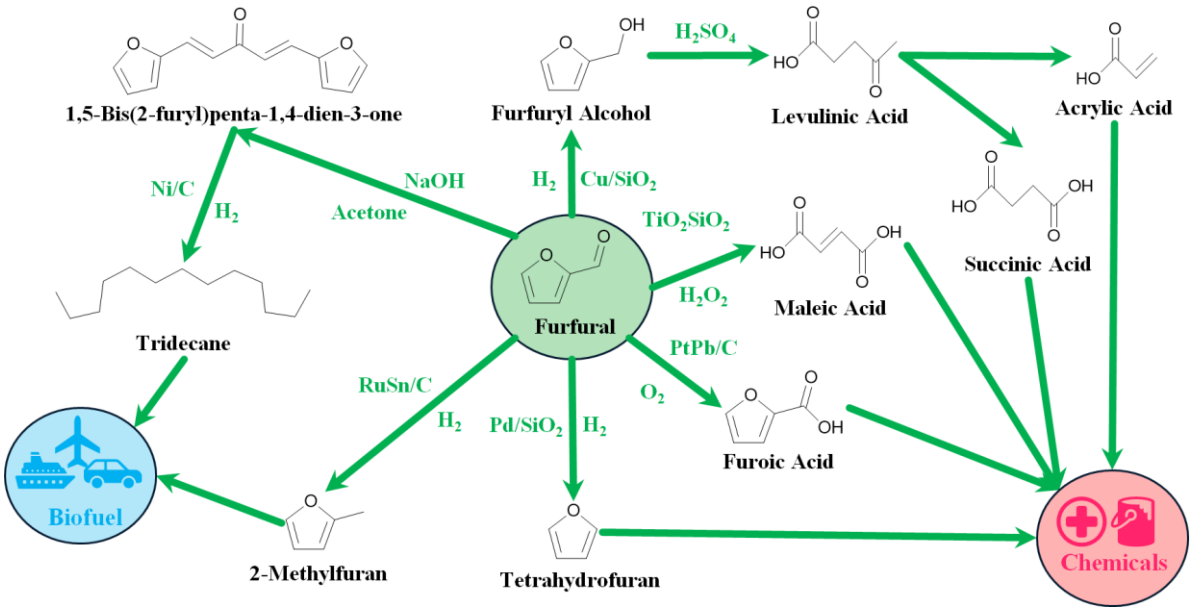

FIGURE 1.5 – Some of the products obtained from furfural and their potential application.

1.4 - HMF and Furfural Obtainment from Biomass: A Mechanistic Point of View

HMF and furfural are obtained from different fractions of lignocellulosic biomass, which is derived from plants. Regardless of their appearance, plants are composed of three fractions: cellulose, hemicellulose, and lignin. Cellulose, the first fraction, constitutes 40 – 50 % of the plant composition and is a crystalline polymer of the aldohexose D-glucose. The second fraction, comprising 25 – 35 % of the total composition, is a polymer of various monosaccharides, predominantly the aldopentose D-xylose. Lignin, constituting 15 – 20 % of the plant, is a polymer of phenolic units, including coniferyl, coumaryl, and syringyl alcohols [15]. HMF is commonly derived from the cellulose fraction and furfural, from hemicellulose.

For obtaining these compounds, both cellulose and hemicellulose must first be depolymerized into their monomers: D-glucose and D-xylose, respectively. In both cases, Brønsted homogeneous acid and basic catalysts are often used, with sulfuric acid and hydrochloric acid being the most common

catalysts [22]. Considering these acidic catalysts, in both reactions, the oxygen atom which links the monomers is protonated (FIGURE 1.6), resulting in the scission of the unit linkage, followed by a nucleophilic attack of a water molecule to produce the respective monomer [23].

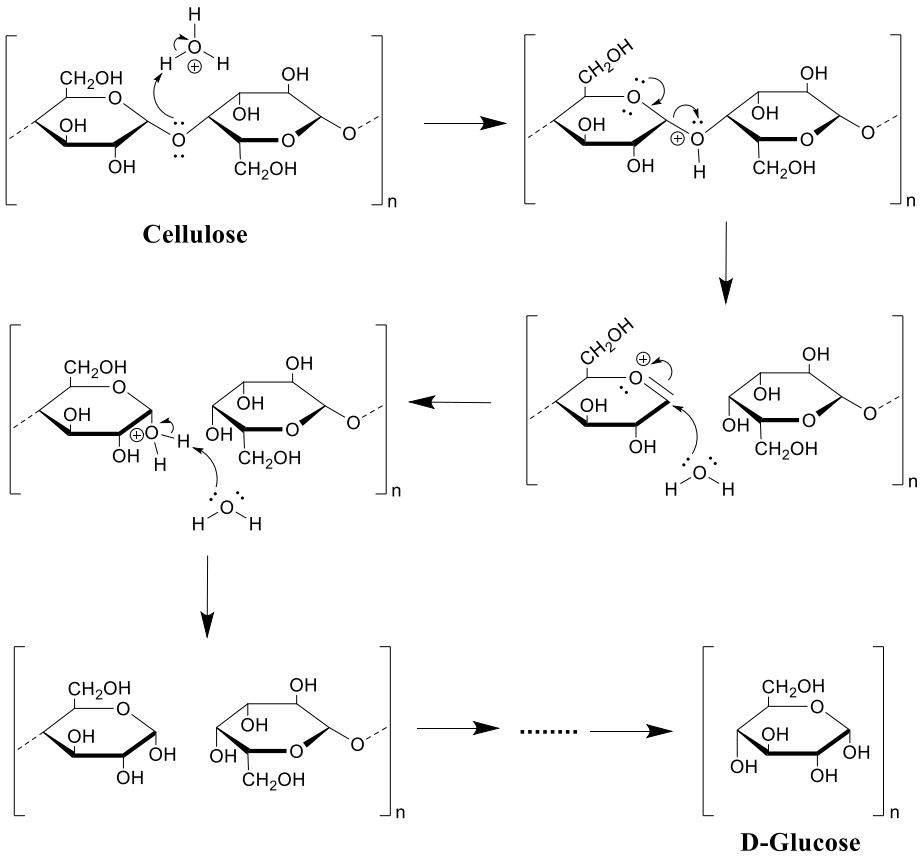

FIGURE 1.6 – Cellulose hydrolysis mechanism to glucose in acidic media.

Glucose and xylose, as well as any monosaccharide, exhibit either a cyclic or acyclic form in solution (FIGURE 1.7). Those monosaccharides are aldoses, thus they present a pyranose ring in their cyclic form; whereas ketoses, such as their respective isomers D-fructose and D-xylulose, exhibit a furanosic ring (FIGURE 1.7) [24]. To produce their platform molecules, glucose and xylose must undergo dehydration in acidic catalysis, releasing three molecules of water. Two different mechanisms have been accepted in the literature: one starting with protonation at O_1H for the cyclic mechanism [25], which is the most favorable

according to DFT studies [24,26]; and another starting with protonation at oxygen in the ring for the acyclic mechanism [24] (FIGURE 1.8). Even though protonation at O_1H is the most favorable, under the reaction conditions (temperature between 130 °C to 160 °C), both protonations can occur [26].

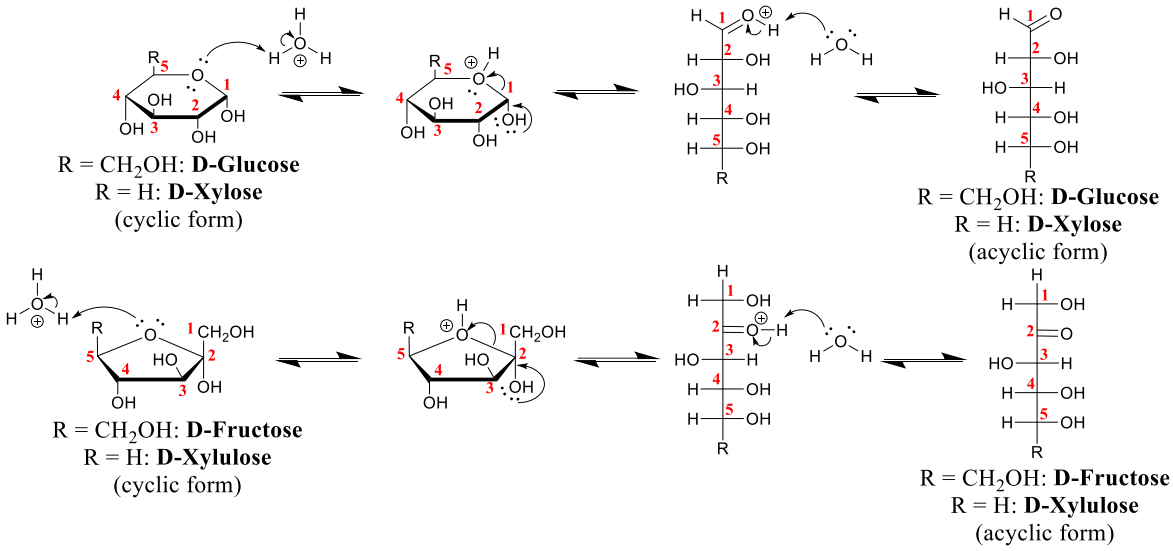

FIGURE 1.7 – Cyclic and acyclic form of the aldoses glucose and xylose, as well as of their respective ketose isomers fructose and xylulose.

The acyclic mechanism (FIGURE 1.8) involves an intramolecular hydride shift, producing their respective isomers fructose and xylulose [24], which are then dehydrate to their platform molecules. This mechanism is supported by tritium labelling of glucose and xylose at the C2 position. After the treatment of glucose-2-^{3}H in sulfuric acid under reflux during 16 h, fructose-1-^{3}H is obtained [27], as well as, xylulose-1-^{3}H was observed from the treatment of xylose-2-^{3}H in sulfuric acid at 100 °C during 3 h [28].

However, numerous cyclic reaction pathways are supported by Density Functional Theory (DFT) calculations and gas phase studies [24]. The most widely accepted pathway involves pyranose ring contraction via O_2H attack on C5 [25] (FIGURE 1.8), a theory substantiated by an experiment utilizing ^{18}O-labelled xylose (where the label is on the ring oxygen) in aqueous HCl (at 140 °C,

50 mM). According to this study, 69 % of the resultant furfural contains ^{18}O in the ring, while 31 % exhibits ^{18}O at the aldehyde moiety. In the presence of NaCl (5 M), 48 % of the ^{18}O was found at the C=O group [29]. This oxygen transfer from the xylose ring to the furfural aldehyde group aligns with the cyclic mechanism illustrated in FIGURE 1.8.

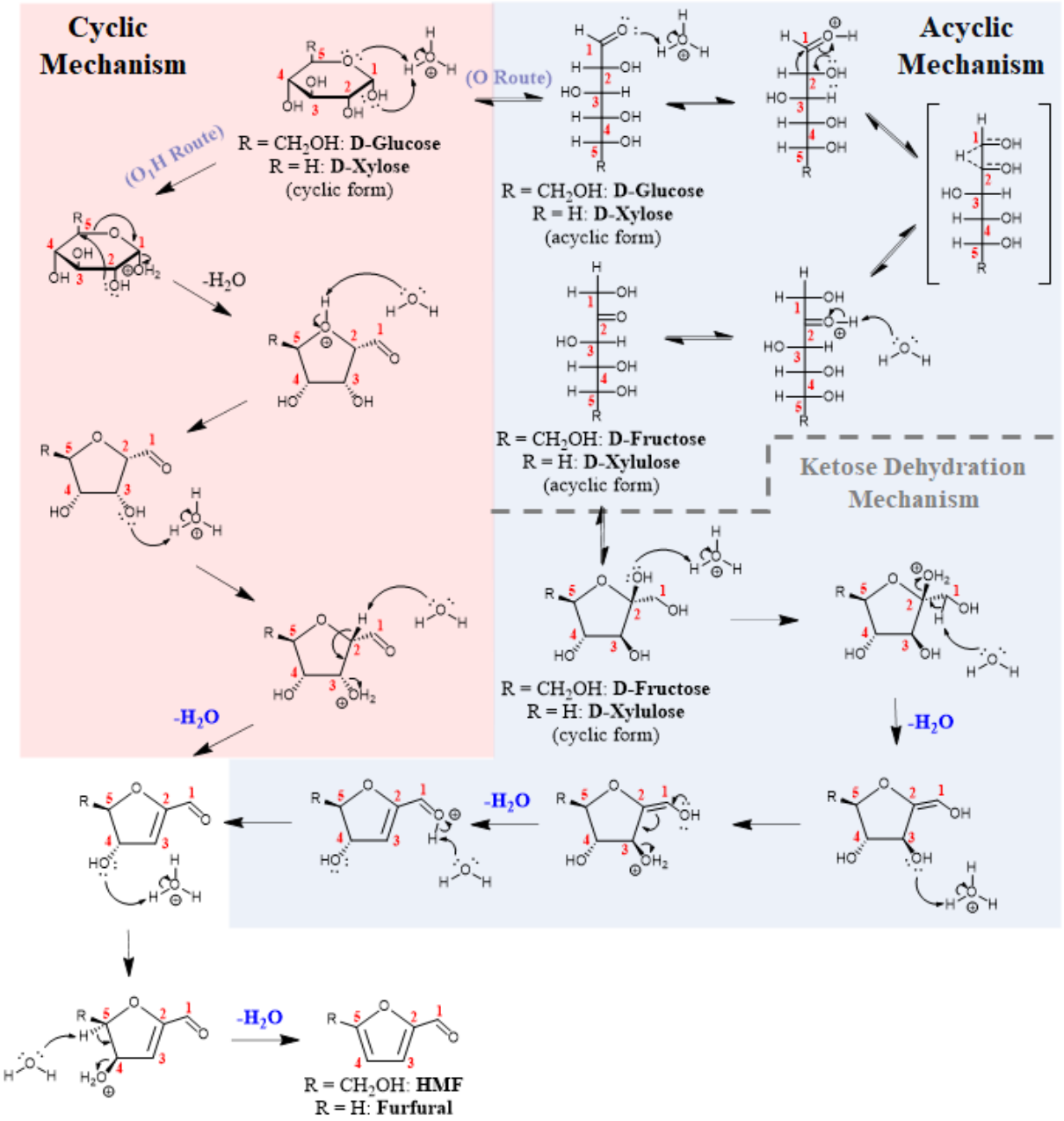

FIGURE 1.8 – Cyclic and acyclic mechanisms of the dehydration of glucose and xylose into HMF and furfural, respectively, in Brønsted acidic media.

According to literature, xylose exhibits significantly higher reactivity and selectivity towards furfural compared to glucose's conversion to HMF in aqueous Brønsted acid solutions. For instance, in hydrochloric acid solution (5.20 mol L^{-1}) at 107 °C, a furfural yield of 93 % was achieved, and 69 % yield was obtained using sulfuric acid solution (3.75 mol L^{-1}) at 106 °C from xylose [30]. In contrast, only 44 % of HMF was obtained from glucose using HCl (pH = 2.5) at 240 °C, or 30 % using phosphoric acid (pH = 2.0) at 240 °C [31]. This lower activity and selectivity of glucose towards HMF production are supported by the cyclic mechanism shown in FIGURE 1.8: glucose, being more substituted at C5 compared to xylose (CH_2OH group and H atom, respectively), may sterically hinder O_2H attack on C5.

Furthermore, DFT studies have indicated that in the dehydration of glucose under acidic conditions, protonation of O_1H or O_4H promotes pathways leading to either the self-polymerization of glucose or the cross-condensation of glucose, HMF, and intermediates into insoluble polymers known as humins [26]. This also explains its lower selectivity to HMF compared to xylose dehydration to furfural. Experimental results corroborate those pathways; for instance, a 1 mol L^{-1} solution of glucose containing sulfuric acid (0.01 M) can yield insoluble humins up to 35 wt. % after 6 hours at 180 °C [32]. For this reason, new routes for HMF production must be researched.

An effective strategy to overcome this challenge involves employing bifunctional catalysts with both Lewis and Brønsted acidity. These catalysts first catalyze the isomerization of glucose into fructose at Lewis acid sites, producing a more reactive intermediate that readily dehydrates into HMF at Brønsted acid sites [33]. For example, when employing Amberlyst-70, a pure Brønsted acid catalyst, in the dehydration of glucose to HMF at 130°C, a yield of 30 % HMF was achieved. However, when the same Brønsted acid catalyst was combined with Sn-β, a Lewis acid catalyst, the HMF yield increased significantly to 63 % [34].

In a general case using Lewis acid catalysts, the isomerization mechanism starts with the coordination of oxygen of the glucose carbonyl group in the Lewis acid center (such as metallic cations of Al, Fe, Sn, Sc, Cu, Yb, Nb, Cr, etc. [35–38]) (FIGURE 1.9). Simultaneously, an adjacent hydroxyl group of the same catalyst or its support interacts with the proton of the second hydroxyl group of the glucose, facilitating the hydride shift between C2 to C1 (rate-determining step) and the production of the acyclic form of fructose [39]. One can ask whether the isomerization process using Brønsted acid catalysts (FIGURE 1.8) is comparable to using a Lewis acid catalyst (FIGURE 1.9). The answer is no. This distinction arises because the Lewis acid center more effectively withdraws electron density from the carbonyl moiety than the proton does, rendering its carbon more electrophilic and thus more susceptible to hydride attack [39]. For example, the production of fructose from glucose using sulfuric acid is barely detectable [40], whereas employing Sn-containing MCM-41 (with 3.0 % metal loading) achieves a selectivity of 70 % at 20 % glucose conversion and 110 °C [36].

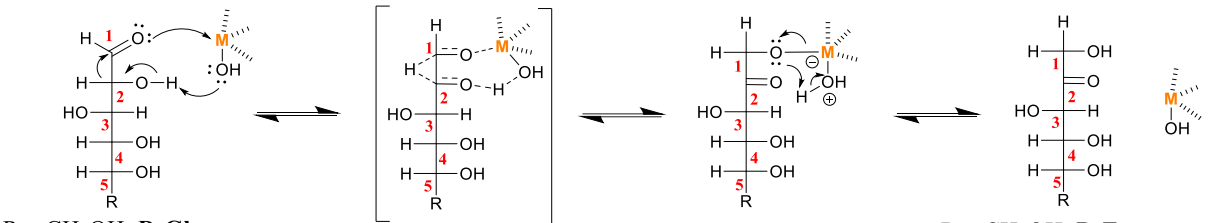

FIGURE 1.9 – Aldose isomerization mechanism to ketose using a general Lewis acid center "*M*" with an adjacent hydroxyl group.

After the production of fructose, the dehydration mechanism in the Brønsted acid sites initiates with a protonation at the O_2H hydroxyl group (FIGURE 1.8), which is the most favorable site due to the stability of the resulting carbocation. The subsequent three consecutive dehydrations are

thermodynamically favored, with a ΔG of - 163 kJ mol^{-1} [26]. Furthermore, the overall free energy of this pathway is more favorable compared to that leading to reverse products and insoluble humins, thus explaining the observed higher activity and selectivity relative to glucose. For example, fructose dehydration using sulfonic carbons achieved a HMF selectivity of 70 % at 65 % fructose conversion at 130 °C [41].

However, the utilization of bifunctional catalysts offers advantages not only for the conversion of glucose into HMF but also for the conversion of xylose into furfural. In this case, Lewis acid sites provide the isomerization of this aldose to xylulose, a more reactive intermediate that is dehydrated to furfural by Brønsted acid sites at higher reaction rates [33]. A study reported elsewhere demonstrated that both sulfuric acid (0.02 mol L^{-1}) and H-β (a bifunctional Lewis and Brønsted catalyst) yielded approximately 75 % furfural at 175 °C. However, the former catalyst exhibited a *TOF* (Turnover Frequency) for furfural of 8.4 s, whereas the latter showed a significantly higher TOF of 41.5 s, nearly five times higher [42].

The isomerization mechanism of xylose into xylulose is very similar to that of glucose into fructose in Lewis acid sites, also presenting the hydride shift between C2 to C1 as a rate-determining step [43] (FIGURE 1.9). To our knowledge, no detailed mechanistic insights have been provided for xylulose dehydration, but it is likely to be analogous to the dehydration of fructose to HMF (FIGURE 1.8). However, several studies have demonstrated the higher reactivity of xylulose compared to xylose [44,45]. For example, after 45 minutes at 145 °C in an aqueous solution of HCl (pH = 1), 66 % of xylulose is converted to furfural, whereas under the same conditions, xylose only yields 29 % [45]. One possible explanation for this improved result is based on theoretical studies, which have shown that the energy barrier for xylulose dehydration is lower (23 kcal mol^{-1}) than the energy barrier for xylose dehydration (30 – 32 kcal mol^{-1}) [45].

In summary, it can be concluded that the most effective methods for obtaining HMF and furfural from biomass involve the conversion of glucose and xylose, respectively, using bifunctional catalysts with both Lewis and Brønsted acidity. However, it is worth noting that the dehydration of fructose and xylose using only Brønsted acidic catalysts also presents itself as an alternative method.

1.5 - Important Parameters for the Dehydration of Monosaccharides into HMF and Furfural Using Acidic Catalysts

The first important parameter is the catalyst employed. Nowadays, many studies have been selecting solid catalysts rather than liquids; i.e., heterogeneous catalysts over homogeneous ones because they are easier to recycle from the product stream and do not corrode the reactor [46]. Additionally, solid catalysts with mesoporosity (pore diameters higher than 2 nm) are preferred over microporous catalysts (pore diameters lower than 2 nm), in order to avoid intraparticle transport effects, which can block either the entrance of the reactants into the active acid sites within the pores or the exit of the products already formed into the pores, favoring their polymerization into insoluble humins [47].

Besides, the catalyst must be a single solid, in order to catalyze the reactions in the same reactor, minimizing the number of separation procedures [15]. This is in contrast to using a single Lewis solid acid catalyst in one reactor and a single Brønsted acid catalyst in another, for example. Moreover, both acid sites in a single solid bifunctional catalyst must be well distributed so that the isomer formed in a Lewis acid center can readily meet an adjacent Brønsted acid site to be dehydrated into furan. On one hand, if the catalyst have more Lewis acid sites than Brønsted, the isomer formed can undergo self-polymerization or cross condensation in the same Lewis acid site, producing humins [48,49]. On the other hand, if the catalyst have more Brønsted acid sites than Lewis, the yield of the reaction (for glucose to HMF) or the rate of the reaction (for xylose to furfural)

can decrease substantially [34,42]. In short, the bifunctional catalyst must have a good balance and distribution of Lewis and Brønsted acid sites to better produce platform molecules.

Additionally, depending on the nature of Lewis or Brønsted acid sites, alternative by-product routes can be favored. For example, in addition to catalyzing the isomerization reactions of glucose and xylose into fructose and xylulose, respectively, Lewis acid sites also promote the epimerization of these reactants into mannose and lyxose [33] (FIGURE 1.10). In this context, the reaction mechanism can occur either via C2 to C1 hydride transfer to the isomer, followed by a reverse hydride transfer to the epimer; or via the Bilik mechanism, which involves a direct C1 to C2 intramolecular carbon shift between the reactant and the epimer [50]. Studies have suggested that trivalent lanthanides with an optimum radius of ~ 1 Å are more likely to mediate the Bilik reaction, whereas smaller cations such as chromium and aluminum prefer the pathway through the isomer intermediate [50]. The formation of those epimers is undesirable because mannose and lyxose are dehydrated to platform molecules similarly to glucose and xylose, resulting in low selectivity for HMF and furfural production at low reaction rates, respectively [24]. Therefore, it is crucial for the Lewis acid center to exhibit selectivity majority to the isomerization.

The nature of the Brønsted acid site, particularly its strength, is more crucial for the production of HMF than for the production of furfural [33], despite in both cases the production of humins is favored in very strong acidic media [40,51]. Studies have demonstrated that high yields of 5-HMF can be achieved within a pH range of 1.5 to 1.9; however, no HMF is obtained when the pH is above 3.9. Furthermore, at pH levels below 1.5, the selectivity for HMF decreases due to its hydrolysis, producing levulinic acid and formic acid [22,52] (FIGURE 1.10). In summary, a stronger Brønsted acid site leads to lower selectivity for HMF due to its propensity for hydrolysis, resulting in the formation of levulinic

acid.

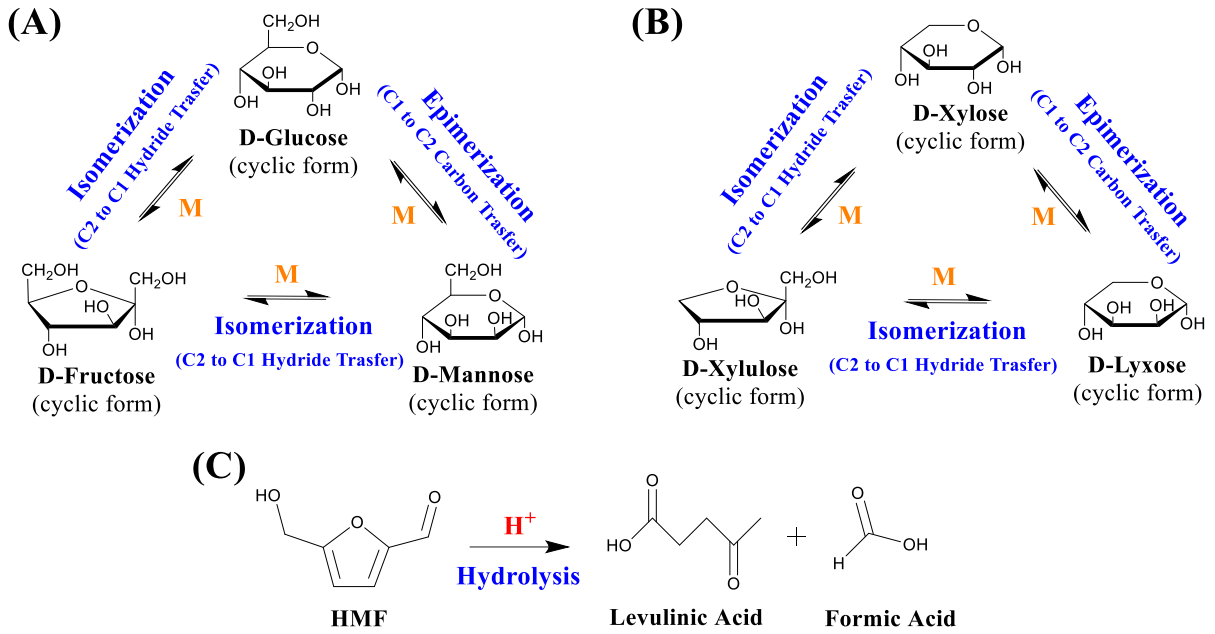

FIGURE 1.10 – The products derived from glucose (A) and xylose (B) under Lewis acid catalysis, and the by-products obtained from HMF under stronger Brønsted acid catalysis (C).

Another crucial parameter is the choice of the solvent. Solvent selection is important not only for dissolving the substrates into the reaction medium but also for stabilizing substrates, intermediates, and products to enhance thermodynamic equilibrium for higher yields [53]. Additionally, the solvent must be stable in the reaction medium, meaning it should not react with the catalyst. Otherwise, the active sites of the catalysts may be poisoned by reacting with the solvent, and any derivatives produced in this process must be separated from the main products during downstream processing.

While water is often the primary choice, it provides platform molecules at relatively low yields. For example, when using fructose as a reactant, HMF yields are typically lower than 30 % [54]. This is primarily due to the increased solvation of the acidic proton by water molecules (ΔG = - 1113 kJ mol^{-1}), which reduces monosaccharide reactivity in this medium [55]. Furthermore, a

pure water solvent system also promotes hydrolysis reactions that lead to the formation of humin intermediates [22]. To overcome these limitations, aprotic solvents such as tetrahydrofuran (THF), γ-valerolactone (GVL), acetone, methyl isobutyl ketone (MIBK) or dimethyl sulfoxide (DMSO) are often combined with water. These solvents enhance platform molecule yields by reducing the solvation energy of the acidic proton and protecting the furan aldehyde moiety from polymerization and condensation reactions that lead to humin formation [15,24,53,55,56].

Some studies have employed a biphasic solvent system consisting of an aqueous and an aprotic organic extracting layer [57]. In this setup, the dehydration reaction occurs within the aqueous layer, and the platform molecule formed is subsequently extracted into the organic layer, where it is protected from degradation. However, this system presents several drawbacks: (i) efficient stirring is required to ensure proper mixing of both phases, and (ii) the aqueous phase needs the addition of salt to prevent mixing with the organic layer, rendering the catalysis in this layer homogeneous [15].

Another approach involves creating a monophasic system by combining water with an aprotic organic solvent. Studies have shown that employing a monophasic system of GVL or THF with 10 – 20 % water as a co-solvent provides the highest HMF yield at 130 °C from fructose (higher than 70 %) [54]. Similarly, it has been found that using a monophasic mixture of GVL and water instead of pure water, the reaction rate for furfural production from xylose increases more than the reaction rates for formation of undesirable byproducts (31 and 8 times, respectively), explaining the higher furfural yields observed [55]. Both GVL and THF are aprotic solvents derived from biomass; however, due to its lower cost, THF is often preferred for creating a monophasic solvent system with 10 – 20 % water to convert monosaccharides into platform molecules.

The last two crucial parameters for favoring the dehydration of

glucose and xylose into platform molecules are monosaccharide loading and reaction temperature. It is well-established in the literature that monosaccharide loadings above 3 % tend to promote self-condensation into disaccharides or polymerization to humins [22,58]. Kinetic studies indicate that the reaction partial order of glucose into condensation products is higher than that towards dehydration into HMF (1.30 and 1.09, respectively), demonstrating that high monosaccharide loading favors condensation reactions over dehydration [40]. Furthermore, furfural selectivity of 80 % was achieved from 2.4 wt. % of xylose at 170 °C using GVL as a solvent and a sulfonic acid carbon catalyst, whereas under the same conditions, only 20 % furfural selectivity was achieved from 9.6 wt. % xylose [58]. Therefore, monosaccharide loadings lower than 3 % are preferred to promote platform molecule production over condensation reactions.

The reaction temperature significantly influences the yield of platform molecules. Generally, reactions leading to humins production exhibit higher activation energies compared to isomerization or dehydration into platform molecules. Thus, higher reaction temperatures typically result in increased humins production [22,51,59]. A kinetic study on the conversion of glucose to HMF using a bifunctional $HCl/CrCl_3$ catalyst showed activation energies of 100 kJ mol^{-1} for glucose to fructose isomerization in Lewis acid sites and 127 kJ mol^{-1} for fructose to HMF dehydration in Brønsted acid sites. Conversely, the activation energies for fructose conversion to humins were found to be 114 kJ mol^{-1} in Lewis acid sites and 133 kJ mol^{-1} in Brønsted acid sites [59]. The optimal temperature identified in this study, as well as in other literature [33], was 130 °C. For xylose, the activation energy for xylose dehydration to furfural in formic acid solution was 152 kJ mol^{-1}, while for xylose polymerization to humins was 161 kJ mol^{-1} [51]. The literature suggests that the dehydration of xylose to furfural using either a pure Brønsted acid catalyst or a bifunctional catalyst with Brønsted and Lewis acidity can be achieved at reaction temperatures between 130 °C and 160 °C

[33,60].

In conclusion, the successful conversion of monosaccharides into platform molecules depends on several key parameters. Employing a mesoporous catalyst is crucial, with single solid catalysts preferred over liquids due to easier recyclability and reduced need for separation procedures. The balance, distribution, and nature of the catalyst acid sites are vital to prevent undesired side reactions, such as self-condensation to disaccharides and polymerization to humins, epimerization to mannose and lyxose, and HMF hydrolysis to levulinic acid. Additionally, solvent selection is pivotal, with aprotic solvents like THF, in combination with 10 – 20 % water in a monophasic system, offering the highest platform molecule yields. Furthermore, controlling monosaccharide loading and reaction temperature within optimal ranges below 3 % and between 130 °C to 160 °C, respectively, is essential for favoring platform molecule production over undesired by-products like humins. Understanding and optimizing these parameters are critical for achieving efficient and selective conversion of glucose and xylose into valuable platform molecules.

1.6 - Motivation and Objectives

Much more than just producing a highly efficient catalyst for the HMF and furfural production from monosaccharides, in this thesis, we are more interested in understanding how the composition and surface acidity (balance, distribution, and nature of acid sites) of the catalyst can correlate with the production of platform molecules. Therefore, the main objective of this thesis is to synthetize mesoporous acidic catalysts for the dehydration of monosaccharides into HMF and furfural with the aim of studying their composition and surface acidity and their effect on the catalytic performance.

This thesis has three chapters. In the first chapter, we synthesize niobium phosphates, an inherent bifunctional catalyst, for dehydrating glucose

and xylose into HMF and furfural, respectively. This study generated the paper "Niobium Phosphates as Bifunctional Catalysts for the Conversion of Biomass-Derived Monosaccharides," published in Applied Catalysis A, General [61] (Impact Factor of 4.7). This chapter will show the pivotal role of the ratio between Lewis and Brønsted acid sites (*L/B* ratio) in driving the dehydration of glucose and xylose into HMF and furfural.

Based on that, we synthesize a controlled mesoporous bifunctional carbon catalyst, to produce in an easier way a catalyst with a *L/B* ratio for platform molecule production. First, we prepared sulfonated carbons with only Brønsted acidity and applied them for the dehydration of fructose and xylose to HMF and furfural (Chapter 2). This study generated the paper "The Impact of the Ratio Between Stronger and Weaker Acid Sites on the Production of 5-Hydroxymethylfurfural and Furfural from Monosaccharides," published in ChemCatChem [62] (Impact Factor 3.8). Finally, some sulfonated carbons from this study were selected to undergo partial ion exchange with different metallic cations with Lewis acidity, to produce the expected controlled bifunctional carbon catalyst (Chapter 3).

As mentioned earlier, in order to optimize the production of platform molecules instead of by-products, in all chapters, the monophasic solvent system of THF in combination with 10 – 20 % of water was selected, with a monosaccharide loading of 2 wt. % and reaction temperatures between 130 °C and 160 °C.

2 - CHAPTER 1: NIOBIUM PHOSPHATES AS BIFUNCTIONAL CATALYSTS FOR THE CONVERSION OF BIOMASS-DERIVED MONOSACCHARIDES (APPLIED CATALYSIS A, GENERAL – IMPACT FACTOR 4.7)

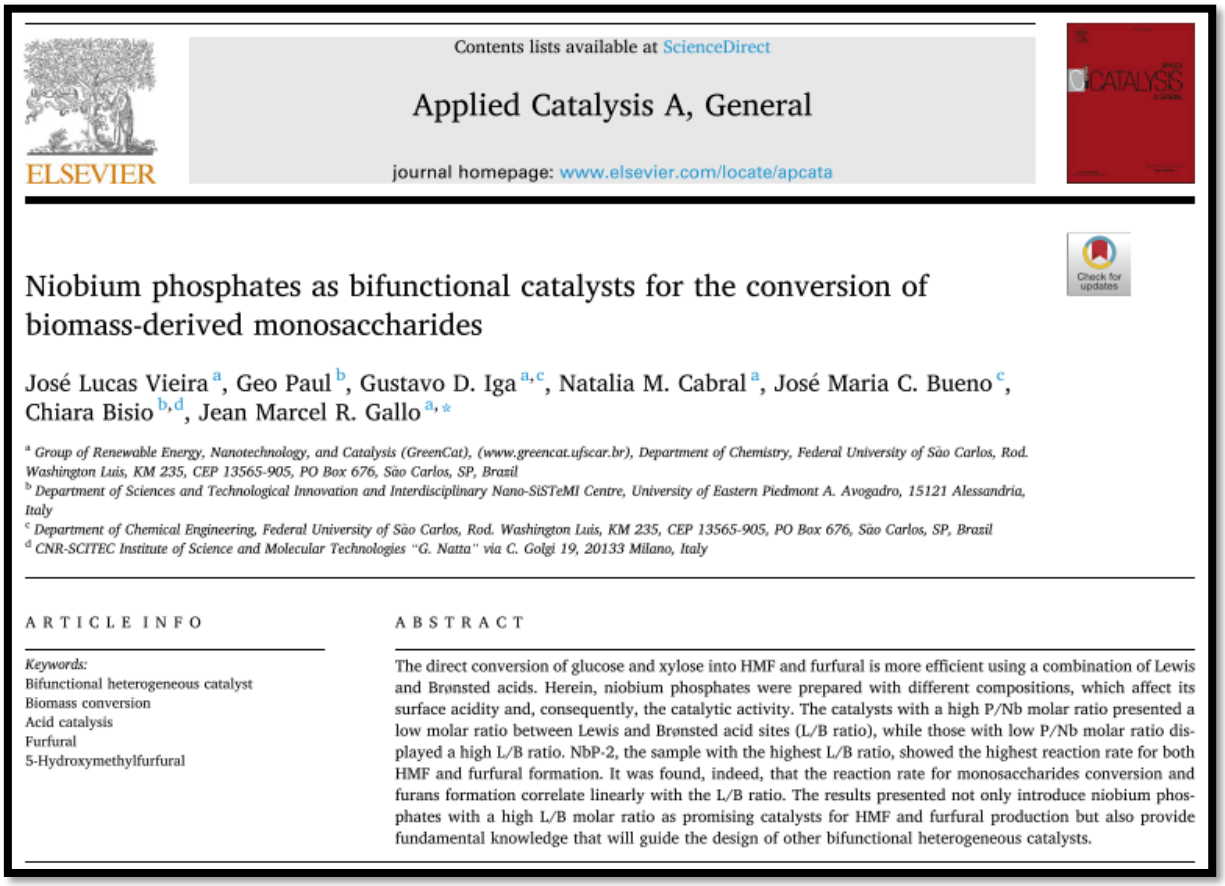

Contents lists available at ScienceDirect

Applied Catalysis A, General

journal homepage: www.elsevier.com/locate/apcata

Niobium phosphates as bifunctional catalysts for the conversion of biomass-derived monosaccharides

José Lucas Vieira [a], Geo Paul [b], Gustavo D. Iga [a,c], Natalia M. Cabral [a], José Maria C. Bueno [c], Chiara Bisio [b,d], Jean Marcel R. Gallo [a,*]

[a] Group of Renewable Energy, Nanotechnology, and Catalysis (GreenCat), (www.greencat.ufscar.br), Department of Chemistry, Federal University of São Carlos, Rod. Washington Luis, KM 235, CEP 13565-905, PO Box 676, São Carlos, SP, Brazil
[b] Department of Sciences and Technological Innovation and Interdisciplinary Nano-SiSTeMI Centre, University of Eastern Piedmont A. Avogadro, 15121 Alessandria, Italy
[c] Department of Chemical Engineering, Federal University of São Carlos, Rod. Washington Luis, KM 235, CEP 13565-905, PO Box 676, São Carlos, SP, Brazil
[d] CNR-SCITEC Institute of Science and Molecular Technologies "G. Natta" via C. Golgi 19, 20133 Milano, Italy

ARTICLE INFO

Keywords:
Bifunctional heterogeneous catalyst
Biomass conversion
Acid catalysis
Furfural
5-Hydroxymethylfurfural

ABSTRACT

The direct conversion of glucose and xylose into HMF and furfural is more efficient using a combination of Lewis and Brønsted acids. Herein, niobium phosphates were prepared with different compositions, which affect its surface acidity and, consequently, the catalytic activity. The catalysts with a high P/Nb molar ratio presented a low molar ratio between Lewis and Brønsted acid sites (L/B ratio), while those with low P/Nb molar ratio displayed a high L/B ratio. NbP-2, the sample with the highest L/B ratio, showed the highest reaction rate for both HMF and furfural formation. It was found, indeed, that the reaction rate for monosaccharides conversion and furans formation correlate linearly with the L/B ratio. The results presented not only introduce niobium phosphates with a high L/B molar ratio as promising catalysts for HMF and furfural production but also provide fundamental knowledge that will guide the design of other bifunctional heterogeneous catalysts.

2.1 - Introduction

Petroleum is currently the main carbon source to produce fuels and chemical compounds. However, as a non-renewable feedstock, the global reserves are expected to last 70 – 130 years [15]. Also, the oil-based industry plays a big role in the production of greenhouse gases (GHG). For instance, the petroleum well-to-refinery GHG emissions were estimated at approximately 1.7 Gt of CO_2 eq. in 2015, 42 % higher than the previously anticipated by the International Association of Oil and Gas Producers [63].

Hence, lignocellulosic biomass appears as an alternative and renewable source of carbon, capable of delivering fuels and chemicals through processes with reduced CO_2 emission [15,64]. This source of biomass is composed of approximately 40 – 50 % of cellulose, a crystalline polymer of the monosaccharide glucose; 2 5 – 30 % of hemicellulose, a polymer formed mainly by the monosaccharide xylose, and 15 – 30 % of lignin, a polymer composed of phenolic units [15]. Therefore, monosaccharides account for 60 – 80 % of the lignocellulosic composition, and their use is strategic for the success of the potential biorefinery.

As for the chemical conversion, glucose and xylose can be converted by acid catalysis to 5-hydroxymethylfurfural (HMF) and furfural, respectively. These compounds, indicated among the most important biomass-derived molecules [64–66], are key intermediates in a biorefinery to obtain a broad range of chemicals, monomers to polymers, and fuels [15].

The direct conversion of glucose to HMF in high yields depends on a combination of a Lewis acid catalyst and a Brønsted acid catalyst [34,67–69]. The former is responsible for isomerizing glucose to fructose, which is then efficiently dehydrated to HMF catalyzed by the Brønsted acid. Furfural can be directly obtained from xylose with high yields using only a mineral acid or zeolite [42], however, it was shown that using a combination of Lewis and Brønsted acid

catalysts, the product formation TOF increases by 5-8 times [70].

H-Beta zeolite [70], $CrCl_3$/HCl [45], and Nb_2O_5/Amberlyst have been studied as bifunctional systems for the conversion of xylose to furfural [33,71], As for the direct conversion of glucose to HMF, catalytic systems based on $AlCl_3$/HCl [69], (Sn-Beta or Sn-SBA-15)/HCl [67,72], and (Sn-Beta or Sn-SBA-15)/Amberlyst [34,72] have been used. It is interesting to note that bifunctional catalytic systems that are efficient for the conversion of one of the monosaccharides, might not be to the other. For instance, Sn-Beta/Amberlyst reached high product yields only for glucose conversion [34,73], while H-Beta only for xylose conversion [70].

The direct conversion of glucose to HMF mainly relies on the combination of two catalysts, however, using a single bifunctional catalyst would be ideal since lower diffusion issues and higher reaction rates are expected when both catalytic sites are nearby in the surface. In this respect, developing a bifunctional heterogeneous Lewis and Brønsted acid catalyst is one of the major challenges in the conversion of biomass-derived saccharides into platform molecules [15].

Due to their inherently bifunctional nature [74], niobium oxide has been applied as catalysts for the transformation of saccharides in recent studies [75–83]. For the conversion of xylose, Nb_2O_5 acts as an efficient bifunctional catalyst using as solvent both THF (with 20 wt. % of water) or pure water. The catalyst was shown to promote the isomerization of xylose to xylulose followed by dehydration to furfural, reaching selectivities between 42 and 47 %.

As for the conversion of glucose in THF/H_2O, Nb_2O_5 promoted efficiently the Lewis acid-catalyzed isomerization to fructose, whereas it displayed very low activity towards its subsequent dehydration, indicating that the Brønsted acid sites are not effective for this reaction. Hence, for glucose conversion, niobium oxide should be treated as a Lewis acid catalyst, instead of a

bifunctional catalyst [33,71].

In this context, niobium oxyphosphate (also commonly referred to as niobium phosphates and herein named NbP) appears as a water-tolerant bifunctional catalyst [84] and, hence, an alternative to niobium oxide. The surface phosphate groups should be responsible for providing the Brønsted acidity, while the Lewis acid sites are still on the top of pentacoordinated Nb sites [33,85].

Recently, niobium phosphate has been suggested as a catalyst for the conversion of monosaccharides. For instance, commercial niobium phosphate (NbP-C) was combined with Nb_2O_5 (both from CBMM-Brazil) for the direct conversion of glucose to HMF, in which the former acts as Brønsted acid and the latter as Lewis acid [76,86]. In these catalytic systems, moderate yields for HMF (between 30 – 35 %) were obtained. Comparable yields were also obtained in a biphasic solvent system using a laboratory prepared NbP [87] and in water using a mesoporous niobium phosphate [88]. NbP-C was also studied for the conversion of cellobiose and glucose was obtained as a major product [84]. Low selectivity to fructose was obtained (< 3 %) suggesting the inefficiency of the Lewis acidity, and consequently, HMF selectivity was also low (< 10 %) [84]. As for the conversion of xylose to furfural, NbP led to *ca.* 45 % yield in a biphasic solvent system [89].

In this work, niobium phosphates were prepared by different simple methodologies to obtain efficient bifunctional catalysts for direct conversion of glucose and xylose to HMF and furfural using monophasic solvent systems, which are more suitable for industrial application [34,54]. Structure and surface properties of the most promising catalysts were also studies seeking to correlate their properties and catalytic activities.

2.2 - Materials and Methods

2.2.1 - Synthesis of the catalysts

Neutral and anionic surfactants have been previously used for producing porous niobium oxyphosphates and [90–92], herein, we adapted these methodologies to obtain NbP by eight different methodologies, as described in the Annex and summarized in TABLE 2.1. The NbP samples were used in preliminary catalytic activity studies for the conversion of glucose (as discussed in section 2.3.1) and the most relevant catalysts (hereafter named NbP-1, NbP-2, and NbP-3) were characterized and further studied as for their catalytic activity. For the sake of comparison, a commercial niobium phosphate provided by CBMM-Brazil was also studied (sample hereafter coded NbP-C).

TABLE 2.1 – Synthetic parameters in the synthesis of NbPs.

Samples	Water volume for $NbCl_5$[a] hydrolysis (mL)	H_3PO_4 concentration (g L^{-1})	Surfactant	Surfactant concentration (g L^{-1})	Aging temperature (°C)	Soxhlet extraction	Calcination temperature (°C)
NbP-1	50	46[b]	Hexadecylamine	145[d]	65	No	550
NbP-2	50	46[b]	Sodium Dodecyl Sulfate (SDS)	195[e]	65	Yes	550
NbP-3	50	46[b]	Hexadecylamine	145[f]	90	No	550
NbP-4	50	46[b]	Hexadecylamine	145[f]	65	No	450
NbP-5	50	46[b]	Hexadecylamine	145[f]	65	No	550
NbP-6	50	46[b]	Hexadecylamine	145[f]	65	Yes	550
NbP-7	100	Concentrated[c]	Hexadecylamine	145[d]	65	Yes	550
NbP-8	50	46[b]	Hexadecylamine	145[f]	90	Yes	550

[a] $NbCl_5$ mass of 2.73 g.

[b] H_3PO_4 mass of 2.30 g in 50 mL of water.

[c] H_3PO_4 mass of 2.30 g.

[d] Surfactant mass of 2.90 g in 20 mL of water.

[e] Surfactant mass of 3.90 g in 20 mL of water.

[f] Surfactant mass of 1.45 g in 10 mL of water.

The NbP-1 sample was prepared by the addition of 50.0 mL of

deionized water in 2.73 g of $NbCl_5$ under stirring, then 2.30 g of H_3PO_4 (85 wt. % in water) and 50.0 mL of deionized water were added under vigorous stirring. The mixture was stirred for 30 min, followed by adjusting the pH to 2.60 with NH_4OH (27 wt. % in water). After, stirring for 5 more minutes, the white precipitate formed was separated by filtration, washed with 1.5 L of deionized water, and transferred (still wet due to the filtration process) to a 50 mL Beaker containing a solution of 2.90 g of hexadecylamine in 20.0 mL of deionized water. The dispersion was stirred for 30 min, the pH adjusted to 4.00 with concentrated H_3PO_4 and the solution stirred for another 30 min. The mixture was transferred to an autoclave and aged for 48 h at 65 °C. Finally, the white solid was filtered out and washed with 2.0 L of deionized water, dried overnight at room temperature, and calcined under air flow for 6 h at 550 °C (1 °C min^{-1}).

The NbP-2 sample was synthesized as described for NbP-1 except that sodium dodecyl sulfate (SDS) was used instead of hexadecylamine. Furthermore, before the calcination process, the sample underwent a Soxhlet extraction process with a 0.10 mol L^{-1} HCl ethanolic solution.

The synthesis of NbP-3 was similar to the one described for the NbP-1 sample, with two modifications: (i) niobium chloride was added to a mixture of 10.0 mL of deionized water and 1.45 g of hexadecylamine, instead of 2.90 g of hexadecylamine and 20.0 mL of deionized water; (ii) the aging process in an autoclave was performed at 90 °C, instead of 65 °C.

2.2.2 - Characterizations

The powder X-ray diffraction (XRD) analyses were performed using a Shimadzu XRD 6000, with CuK_α radiation, a voltage of 30 kV, and a current of 30 mA using a scan speed of 1.5° min^{-1}. X-ray fluorescence (XRF) analyses were carried out in a Thermo Scientific ARL PERFORM'X, with a rhodium tube source.

^{31}P solid state nuclear magnetic resonance (^{31}P ssNMR) spectra were obtained on a Bruker Advance III 500 spectrometer with a wide-bore magnet of 11.75 T using a ^{31}P operating frequency of 202.45 MHz. Before the analyses, the samples were pretreated under vacuum (1 x 10^{-4} mbar) at 150 °C for 2 h. A triple resonance 4 mm probe, in double resonance mode, with magic angle spinning (MAS) was employed in all experiments and the samples were placed in a Zirconia rotor and spun at a rate of 15 kHz. The magnitude of the ^{31}P RF field (μ_{rf}) used was 83 kHz and the repetition time between the accumulations was 30 s. During the acquisition, high-power proton decoupling was applied while no decoupling was done on ^{93}Nb. Chemical shifts are reported on δ scale and were externally referenced to H_3PO_4 (85%). ^{31}P MAS NMR spectra were fitted with DMFIT functions for quantitative deconvolution of the overlapping peaks [93].

Nitrogen physisorption at -196 °C was carried out in an Autosorb 1. The surface area was calculated by the BET equation and the pore size distribution by DFT method using the adsorption branch and the plot went through smoothing. Pore volume was calculated at PP_0^{-1} of 0.9. The presence of micropores was ruled out according to the t-plot method.

2.2.3 - Study of the surface properties of solids by adsorption of probe molecules followed by FTIR spectroscopy

FTIR analyses were performed using a Bruker Equinox 55 spectrophotometer equipped with a pyroelectric detector (DTGS) using a resolution of 4 cm^{-1}. The samples, reduced under the form of self-supported pellets (pressed at 3 ton cm^{-2}) with density between 4 and 8 mg cm^{-2}, were placed inside of an infrared cell equipped with KBr windows permanently connected to a vacuum line. Before the adsorption/desorption experiments, the samples were dried at 150 °C (5 °C min^{-1}) under vacuum (1 x 10^{-4} mbar) for 2 h.

Ammonia, pyridine, or acetonitrile was adsorbed on the catalysts at

room temperature with a maximum pressure of 50, 25, and 130 mbar, respectively, for 1 h to warrant the saturation of adsorbed molecules in the catalyst surface. The desorption of the probe molecules was performed under vacuum conditions (1 x 10^{-4} mbar) at 100°C for pyridine and acetonitrile and room temperature for ammonia.

Analyses of ammonia and pyridine were used for quantification of the Lewis and Brønsted acid sites using the methodology reported elsewhere [94,95]. The spectra were normalized as described in these previous works.

2.2.4 - Catalytic studies

The catalytic reactions were performed in thick-glass reactors at 130 °C. The reactors were loaded with 2.0 g of a solution of 2 wt. % of glucose or xylose in tetrahydrofuran (THF) containing 20 wt. % of water (THF/H_2O = 4/1) or pure water. For reactions using HCl as co-catalyst, the acid was introduced in the reaction mixture with a concentration of 0.18 mol L^{-1}. The reactions were stopped at different reaction times by cooling down the reaction in an ice bath. Identification and quantification of the products were performed by High-Performance Liquid Chromatography (HPLC) using standards. For the analyses, a Shimadzu HPLC LC-10AD was coupled to a Bio-Rad Aminex® HPX-87H column of 300.0 mm x 7.8 mm (0.005 mol L^{-1} of aqueous H_2SO_4 was used as mobile phase) and to detectors of refraction index (Shimadzu RI20A) and diode array (Shimadzu SP10A).

The conversion, selectivity, reaction rates, and mass balances were calculated using the equations below:

$$Conversion = \left(\frac{mol\ precursor_{initial} - mol\ precursor_{final}}{mol\ precursor_{initial}}\right) * 100$$

$$Selectivity = \left(\frac{mol\ product_{final}}{mol\ precursor_{initial} - mol\ precursor_{final}}\right) * 100$$

$$Reaction\ rate_{Precursor\ conversion} = \frac{mol\ precursor_{initial} - mol\ precursor_{final}}{(catalyst\ weight)*(reaction\ time)}$$

$$Reaction\ rate_{Furan\ formation} = \frac{mol\ furan_{final}}{(catalyst\ weight)*(reaction\ time)}$$

$$Mass\ balance_{Glucose\ conversion} = \left(\frac{mass\ glucose_{final} + mass\ fructose_{final} + mass\ HMF_{final} + mass\ LA_{final}}{mass\ glucose_{initial}}\right) * 100$$

$$Mass\ balance_{Xylose\ conversion} = \left(\frac{mass\ xylose_{final} + mass\ xylulose_{final} + mass\ furfural_{final}}{mass\ xylose_{initial}}\right) * 100$$

2.3 - Results and Discussion

2.3.1 - Catalytic screening

The chemical composition of the niobium oxyphosphate samples (NbP) was determined by X-ray fluorescence (XRF) analyses, revealing that the preparation method affects the phosphorous loading and, consequently, the sample composition (TABLE 2.2). A rationalization of the chemical composition and the synthesis method is present in the Annex. The stoichiometric niobium oxyphosphate [$NbO(PO_4)$] is expected to have a *P/Nb* molar ratio of 1.0, whereas, according to the literature, this class of compounds is typically formed with *P/Nb* molar ratios between 0.80 and 1.00 [96–98]. Hence, NbP-1, NbP-3, NbP-5, NbP-7, NbP-8 obtained a composition similar to the expected for niobium oxyphosphate (TABLE 2.2). Lower *P/Nb* ratios indicate the presence of niobium oxide and, indeed, the *P/Nb* molar ratio for a phosphated niobium oxide was found to be 0.5 (Nb_2O_5-PO_4, TABLE 2.2). Interestingly, NbP-2, NbP-4, and NbP-C displayed *P/Nb* similar to the phosphated niobium oxide (TABLE 2.2), suggesting that these syntheses methodologies led to a high degree of Nb-O-Nb condensation. Based on the P and Nb loading, a molecular formula was proposed for the NbP samples (TABLE 2.2).

TABLE 2.2 – Quantification of niobium and phosphorus on the NbP by X-ray fluorescence.

Samples	*P/Nb* molar ratio	Formula[a]
NbP-1	0.9	$(NbO_{1.15})_{10}(PO_4)_9$
NbP-2	0.5	$(NbO_{1.75})_2(PO_4)$
NbP-3	1.0	$NbO(PO_4)$
NbP-4	0.6	$(NbO_{1.60})_5(PO_4)_3$
NbP-5	0.8	$(NbO_{1.30})_5(PO_4)_4$
NbP-6	0.7	$(NbO_{1.45})_{10}(PO_4)_7$
NbP-7	1.0	$NbO(PO_4)$
NbP-8	0.9	$(NbO_{1.15})_{10}(PO_4)_9$
NbP-C	0.4	$(NbO_{1.90})_5(PO_4)_2$
Nb_2O_5-PO_4	0.5	$(NbO_{1.75})_2(PO_4)$

[a] Proposed based on the *P/Nb* molar ratio, considering Nb(IV) and that P is present as phosphate species.

To identify if the catalysts were active in the direct conversion of glucose to HMF, a first screening was performed and as shown in FIGURE 2.1A, as glucose is converted, both fructose and 5-hydroxymethylfurfural (HMF) are formed. SCHEME 2.1 shows a typical reaction roadmap for glucose conversion in the presence of a combination of Brønsted and Lewis acids. Fructose is formed from the Lewis acid-catalyzed isomerization of glucose, while HMF is obtained from the Brønsted acid-catalyzed dehydration of fructose [34,69]. These results suggest that the NbP catalysts are indeed bifunctional.

The catalytic performance among the NbPs is significantly different which could be associated with their composition. Indeed, by plotting the *P/Nb* ratio of the different materials as a function of the reaction rate value obtained from the data in FIGURE 2.1A, a clear trend is observed: reaction rate for HMF formation increases as the *P/Nb* ratio decreases (FIGURE 2.1B). In particular, NbP-2 and NbP-C, the catalysts with the lowest *P/Nb* ratio, displayed the highest

reaction rate for HMF formation.

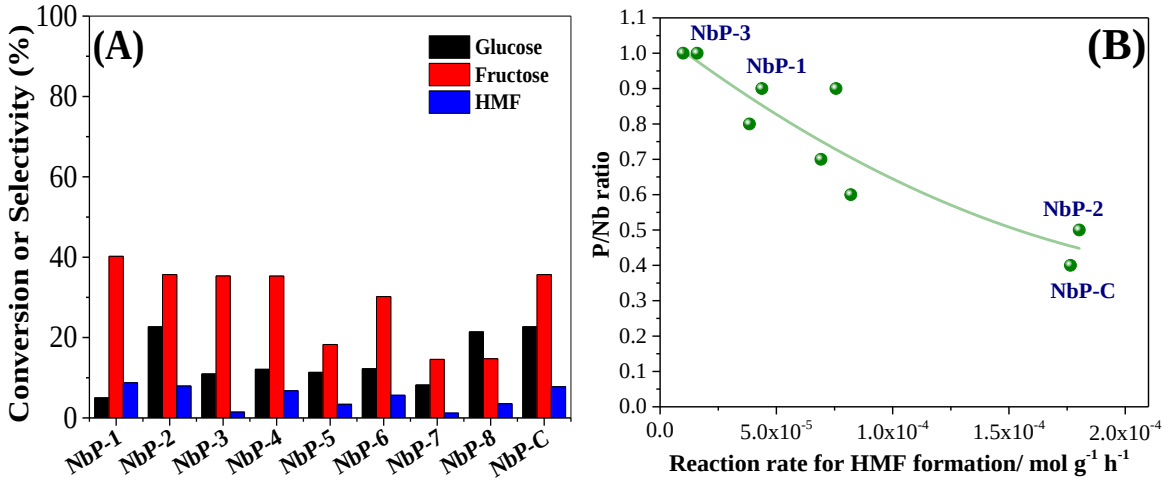

FIGURE 2.1 – (A) Catalytic tests with 0.020g of the NbP samples (catalyst/substrate mass ratio = 0.50) in THF/H_2O = 4/1 for 1 h at 130 °C and (B) Correlation between *P/Nb* molar ratio and reaction rate for HMF formation at 1h of reaction.

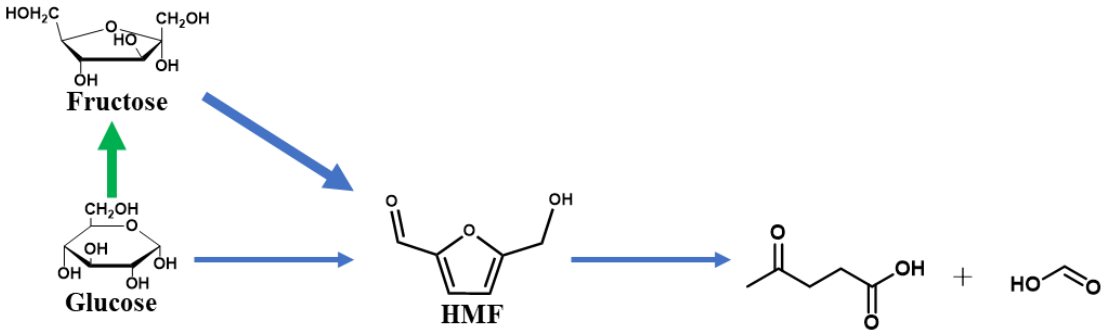

SCHEME 2.1 – Conversion of glucose with a combination of Brønsted and Lewis acids. Thicker arrows indicate the preferential routes. Green and blue arrows indicate the reaction steps catalyzed by Lewis and Brønsted acid sites, respectively.

NbP-2 and NbP-C samples were selected for further characterization and catalytic studies since they are the most promising samples for the direct conversion of glucose to HMF. For sake of comparison, NbPs with different compositions, such as NbP-1 and NbP-3, were also chosen for further studies.

2.3.2 - Psychochemical characterization of selected solids

X-ray diffraction analyses (FIGURE A1.1) suggest that the prepared samples and the commercial NbP-C are amorphous. Nevertheless, analyses performed at a low angle ($2\theta < 3°$), displays poorly defined diffraction peaks, which could indicate the formation of mesopores, for both NbP-2 and NbP-C samples (FIGURE A1.1B).

The textural properties, such as specific surface area and porosity, were determined by nitrogen physisorption at -196 °C and the results are shown in FIGURE 2.2 and TABLE 2.3. NbP-2, NbP-3, and NbP-C present Type-IV isotherms (FIGURE 2.2A), typical for mesoporous materials, endorsing that the XRD pattern observed at a low angle (FIGURE A1.1B) could be due to poorly organized mesopores. Isotherm for NbP-1 presents low adsorption, typical of non-porous material, while DFT (FIGURE 2.2B) reveals the presence of mesopores. Hence, this isotherm type could be an intermediate between Type II and Type IV, i.e., a predominantly non-porous material with some contribution of mesopores. The pore size distribution (FIGURE 2.2B) reveals well-defined families of mesopores with a broad distribution. In particular, NbP-1 and NbP-3, both synthesized with hexadecylamine, presented a maximum in the pore size distribution at 3.9 nm, which was similar to the commercial NbP-C. NbP-2, prepared with sodium dodecyl sulfate as a structure-directing agent presented larger pores, with a maximum at 4.7 nm.

NbP-C is the sample with the highest surface area (366 $m^2\ g^{-1}$), followed by NbP-2 and NbP-3, both with similar surface areas (231 and 244 $m^2\ g^{-1}$, respectively) (TABLE 2.3). NbP-1 presented a surface area significantly lower than the other samples (44 $m^2\ g^{-1}$), as a consequence of the low porosity. The materials did not present a microporous surface area according to the t-plot. The total pore volume was calculated at a partial pressure of 0.9 and followed the same tendency of the surface area.

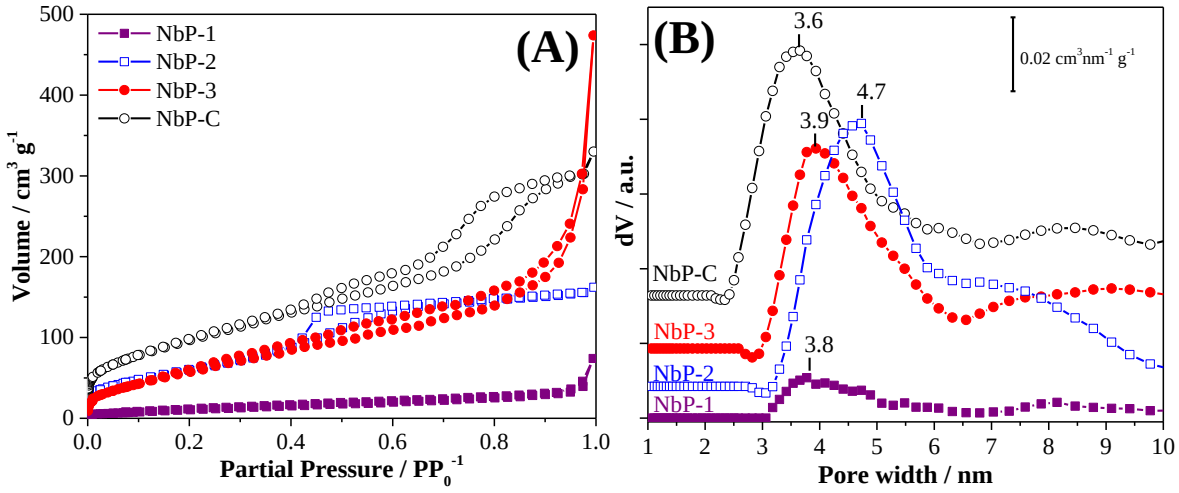

FIGURE 2.2 – (A) Nitrogen physisorption isotherm at -196 °C and (B) smoothed pore width distribution obtained by the DFT method.

TABLE 2.3 – Textural properties obtained by N_2 physisorption at -196 °C and the relative proportion of the population distribution of phosphorus species in the NbP samples as estimated by ^{31}P MAS NMR analysis.

Samples	Textural properties			^{31}P NMR relative contribution / wt. %			
	S_{BET}[a] (m^2g^{-1})	D_p[b] (nm)	V_P[c] (cm^3g^{-1})	H_3PO_4	$H_2PO_4^-$	HPO_4^{2-}	PO_4^{3-}
NbP-1	44	3.8	0.05	1	27	29	43
NbP-2	231	4.7	0.23	1	34	38	27
NbP-3	244	3.9	0.27	1	21	34	44
NbP-C	366	3.6	0.44	2	36	42	20

[a] Specific surface area calculated by the BET equation;

[b] pore size distribution calculated by DFT method;

[c] total pore volume calculated at a partial pressure of 0.9.

Since XRF analyses indicate the different compositions of the samples, solid state nuclear magnetic resonance analyses of ^{31}P (^{31}P ssNMR) were carried out seeking an understanding of the P species formed (FIGURE 2.3). As a general feature, NMR bands in the ranges -18 – -27, -11 – -17, and -4 – -10 ppm are due to, respectively, phosphate groups (PO_4^{3-}) in the bulk of the material,

surface hydrogenphosphate (HPO_4^{2-}), and surface dihydrogenphosphate ($H_2PO_4^-$) [99,100]. Moreover, a very weak band at 2 − 0 ppm is also visible and can be attributed to hydrolyzed phosphate groups [98].

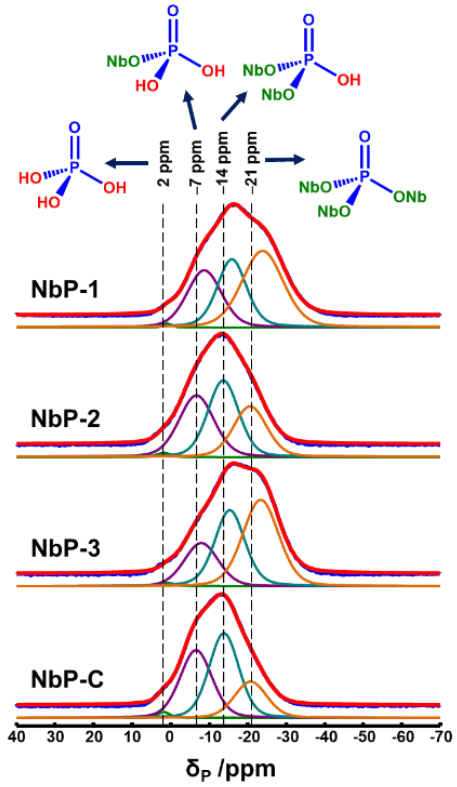

FIGURE 2.3 – ^{31}P MAS NMR spectra of the NbP samples at 11.74 tesla after thermal treatment at 150 °C for 2 h. A MAS rate of 15 kHz and high-power proton decoupling was applied during the acquisition.

The relative area of the bands observed for the different samples is shown in TABLE 2.3. NbP-1 and NbP-3 are the samples with the highest contribution of PO_4^{3-} (and similar between the two materials), in accordance with the XRF results shown in TABLE 2.2. These samples, however, differ on the composition of the surface species, i.e., NbP-3 is richer HPO_4^{2-}, while NbP-1 surface displays a larger contribution of $H_2PO_4^-$ species (TABLE 2.3). Interestingly, in the ^{31}P ssNMR spectra of NbP-1 and NbP-3, an up-field shift of the resonance peaks towards more negative chemical shift values has been

observed. This shift might indicate the presence of more internal phosphate groups that do not interact with surface OH groups or adsorbed water [101,102]. NbP-2 and NbP-C are characterized by a large predominance of surface HPO_4^{2-} and $H_2PO_4^-$ species, and the relative concentrations of these species are similar in both samples. This confirms a high degree of Nb-O-Nb condensation in the bulk, which is characteristic of phosphated niobium oxide-like catalysts. NbP-2, however, displays a slightly higher concentration of bulk PO_4^{3-} (27 % against 20 % for the NbP-C). It is outstanding to observe that the relative concentration of the P species obtained by ^{31}P ssNMR and the *P/Nb* molar ratio calculated from the XRF appear to correlate, as shown in FIGURE A1.2.

2.3.3 - Surface characterization by FTIR spectroscopy

Different surface acidity of the samples can be expected based on the different structural and chemical compositions of the NbP samples. Therefore, the overall concentration of Brønsted and Lewis acid species was determined by using Fourier-transform infrared spectroscopy (FTIR) spectroscopy of adsorbed pyridine and ammonia. The use of pyridine is well-established in the literature for the quantification of acid sites in different types of materials, while ammonia is considerably less employed due to a lack of consensus on the extinction coefficient. Furthermore, NH_3 interacting with Lewis acid sites have a low FTIR extinction coefficient which can lead to analytical error [103]. Hence, herein, quantification of the acid sites was performed using pyridine as a probe molecule, while the results obtained with ammonia adoption should be taken with parsimony and were used for the calculation of the *L/B* molar ratio for sake of comparison.

Lewis acidity in niobium oxyphosphates and phosphated niobium oxide arise from low coordination surface niobium sites, similarly to found for niobium oxide [74]. The Brønsted acid sites, as previously discussed, are provided by the hydrogenphosphate and dihydrogenphosphate groups already

characterized by ^{31}P ssNMR (FIGURE 2.3).

Upon adsorption of pyridine in the NbP samples (FIGURE 2.4A), eight bands are present in the 1700 – 1400 cm^{-1} range. According to the literature, the bands at 1637 and 1540 cm^{-1} are due to the ring vibration of pyridinium ion formed by the interaction of pyridine and the Brønsted acid sites, the bands at 1598 and 1437 cm^{-1} related to pyridine hydrogen bond to terminal hydroxyls, and the absorptions at 1609, 1580 and 1446 cm^{-1} are due to molecular pyridine bond to Lewis acid sites [84,104–106]. Finally, the formation of the band at 1489 cm^{-1} is assigned to both pyridine and pyridinium species. The area of bands at 1446 and 1540 cm^{-1} were used to quantify the concentrations of both Lewis and Brønsted acid sites (TABLE 2.4), respectively, using the molar absorption coefficients and according to the methodology described elsewhere [94]. A schematic view of the interaction between pyridine with both Lewis and Brønsted acid sites on the NbPs surface is reported in FIGURE 2.4A.

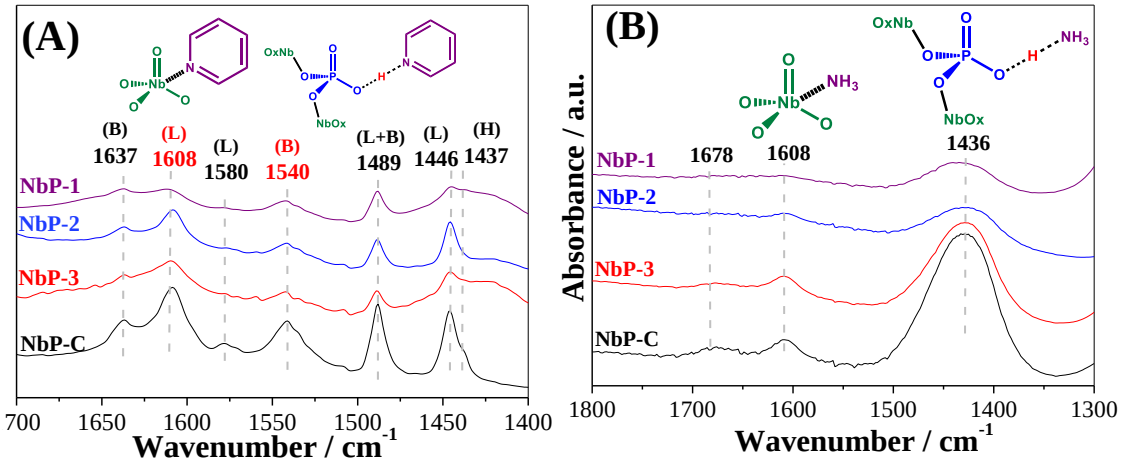

FIGURE 2.4 – Normalized FTIR spectra of the samples adsorbing (A) pyridine and (B) ammonia after desorption (10^{-4} mbar) at 100 °C and room temperature, respectively. In the figure on the left, *B* stands for pyridine bonded to Brønsted acid sites, *L* for pyridine bonded to Lewis acid sites, and *H* for pyridine hydrogen-bonded to terminal hydroxyls.

As for adsorption of ammonia monitored by FTIR (FIGURE 2.4B),

in the range between 1800 and 1300 cm^{-1}, it is possible to observe the formation of three bands located at 1678, 1608, and 1436 cm^{-1}. As it is well known, the absorptions at 1678 and 1436 cm^{-1} are characteristics of the asymmetric and symmetric bending modes, respectively, of the ammonium ion (NH_4^+) formed in the presence of surface Brønsted acid sites [107]. The band at 1608 cm^{-1} is related to the asymmetric bending mode of the ammonia coordinated with Lewis acid sites [107]. From the intensity of the IR bands formed contacting the NbP samples with NH_3 and then evacuating the probe molecule at room temperature [103], it is possible to notice that the NbP samples contain a different amount of both Brønsted and Lewis acid sites. The integrated intensity of the bands at 1608 and 1436 cm^{-1} (related to the presence of Lewis and Brønsted acid sites, respectively) and an extinction coefficient previously reported [95] were used to calculate the *L/B* molar ratio (TABLE 2.4).

TABLE 2.4 – Quantification of the Lewis and Brønsted acid sites by ammonia and pyridine adsorption monitored by FTIR spectroscopy.

Sample	Ammonia	Pyridine				
	***L/B* ratio**	**Concentration / µmol g^{-1}**		***L/B* ratio**	**Normalized concentration of acid sites (µmol m^{-2})**	
		Brønsted	**Lewis**		**Brønsted**	**Lewis**
NbP-1	0.15	182	31	0.17	4.14	0.70
NbP-2	0.38	172	155	0.90	0.74	0.67
NbP-3	0.26	134	54	0.40	0.55	0.22
NbP-C	0.34	484	314	0.65	1.32	0.86

As shown in TABLE 2.4, NbP-C is the sample with the largest overall loading of Lewis and Brønsted acid sites, followed by NbP-2. Interestingly, although NbP-1 presents a specific surface area significantly lower than the other NbPs, the concentration of Brønsted acid sites is comparable, thus indicating a higher Brønsted acid site concentration by the unit of area (TABLE 2.4). The *L/B*

molar ratios obtained by pyridine or ammonia adsorption differ in absolute value, however, there is a fairly good linear correlation between them (FIGURE A1.4). This observation is extremely important since it suggests that although the absolute values may differ, the trend is validated by using the two probe molecules.

Interestingly, the two samples with the highest *L/B* ratio (NbP-2 and NbP-C) are the ones previously shown to have predominantly surface HPO_4^{-2} and $H_2PO_4^-$ groups (TABLE 2.3). Contrarily, for NbP-1 and NbP-3, structures with nearly stoichiometric niobium oxyphosphate compositions display a higher relative concentration of Brønsted acid sites (lower *L/B* ratio), suggesting that the stoichiometric niobium oxyphosphate structure [(NbO)(PO_4)] shall present a low loading of low coordination Nb sites.

Since the presence of Lewis acidity is crucial for an efficient conversion of glucose, these sites were further studied by acetonitrile adsorption monitored by FTIR spectroscopy (FIGURE 2.5). After adsorption of 130 mbar (FIGURE 2.5A), the following bands are observed in the 2450 – 2100 cm^{-1} range: (i) a triplet at 2315, 2294, and 2269 cm^{-1} resulting from the overlap of two doublets related to the Fermi resonance between the stretching of the C≡N and the combination mode υ(C-C) + δ(CH_3), wherein the doublet with lower wavenumbers (2269 and 2294 cm^{-1}) is related to weak hydrogen bonds between the acetonitrile and terminal hydroxyls and the doublet with higher wavenumbers (2294 and 2315 cm^{-1}), related to the interaction of acetonitrile with Lewis acid sites with medium strength; (ii) a doublet at 2294 and 2254 cm^{-1} related to acetonitrile weakly physisorbed on the surface of the catalysts [85].

Upon desorption of the excess of acetonitrile by evacuation at 100 °C (FIGURE 2.5B), the bands related to physisorbed molecules disappear and the other bands decrease in intensity. When acetonitrile interacts with the Lewis acid sites, a blueshift is observed in respect to its original band, due to the interaction

with electron-withdrawing surface centers. Hence, the higher the Lewis acidic strength, the greater the shift. The analysis of the IR bands (FIGURE 2.5B) reveals the presence of two families of strong Lewis acid sites due to the bands at 2315 and 2340 cm^{-1}, representing shifts of *ca.* 20 and 45 cm^{-1}, respectively. The former is present for all samples, while the latter, a stronger site [85], is present for NbP-1 (FIGURE 2.5B) [108]. The presence of stronger Lewis acid sites is not necessarily an advantage since these sites not only catalyze the isomerization of glucose but can also promote the decomposition of fructose [59].

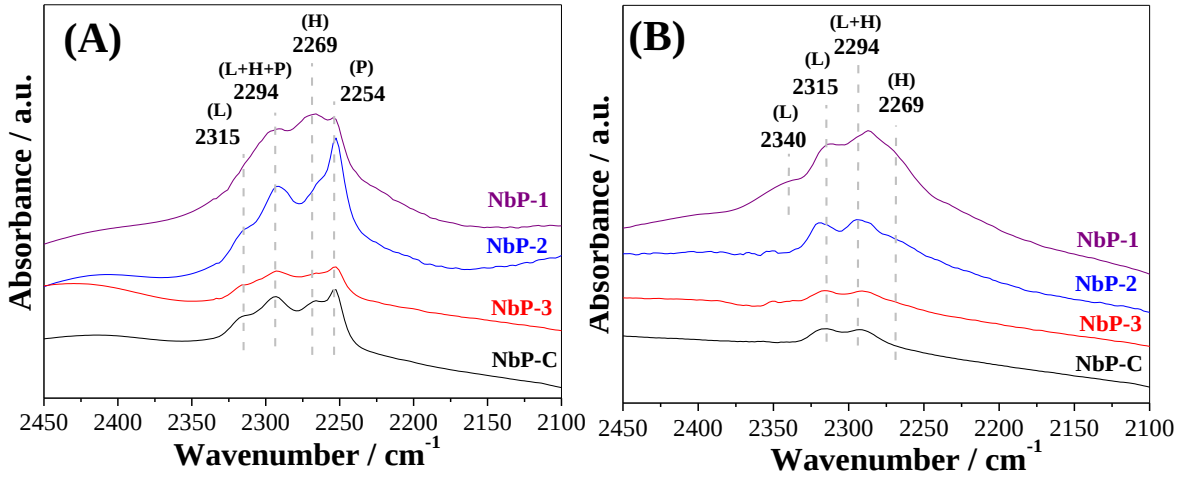

FIGURE 2.5 – FTIR of the samples (A) after adsorption of 130 mbar of acetonitrile at room temperature and (B) after subsequent desorption at 100 °C under vacuum (10^{-4} mbar). In the figures, *L* stands for acetonitrile bonded to Lewis acid sites, *H* for acetonitrile hydrogen-bonded to terminal hydroxyls, and *P* for acetonitrile weakly physisorbed on the surface of the catalysts.

2.3.4 - Glucose direct conversion to HMF

As mentioned before, the motivation for developing niobium oxyphosphate catalysis was based on our previous work [33], in which we report that niobium oxide Brønsted acid exhibits poor performance in dehydrating fructose. Hence, in NbP, phosphates would provide the Brønsted acidity necessary for the reaction [33,34]. Indeed, previous studies show that phosphates provide stronger Brønsted acids than the ones found in niobium oxide [109]. As for the

reaction media, it has been already shown that pure water leads to a high decomposition of the formed HMF [33,110], hence, monophasic solvent systems composed of THF or GVL containing 10 – 20 wt. % of water as co-solvent has gained attention due to its compatibility with industry requirements [33,34,54,110].

Therefore, using the reaction conditions previously established by our and other groups [33,34,54], NbP-1, NbP-2, NbP-3, and NbP-C were studied, as a function of time, for direct conversion of glucose to HMF using THF containing 20 wt. % of water (THF/H_2O = 4/1), as shown in FIGURE 2.6. It is important to note that NbP-1 and NbP-3 samples are significantly less active, and hence, for the reaction, it was used twice the amount of catalyst relative to NbP-2 and NbP-C.

As expected, the glucose conversion increases along with the reaction time, except for NbP-1 which achieves a plateau after the second hour of reaction. In the first hour of reaction, the formation of fructose by the isomerization of glucose promoted by Lewis acids is observed. The concentration of fructose along the reaction is higher for reaction promoted by the catalysts with a higher Lewis/Brønsted sites ratio (TABLE 2.4), *i.e*. NbP-2 and NbP-C. All the catalysts were able to convert fructose to HMF and after 5 h of reaction, the selectivities for HMF was *ca.* 40 % for NbP-1 and *ca.* 50 % for NbP-2, NbP-3, and NbP-C. The highest HMF yield was obtained for NbP-2 (*ca.* 42.5 %), followed by NbP-3 and NbP-C (*ca.* 38 %), and NbP-1 reached the lowest catalyst yield (*ca.* 21.6 %).

The mass balance for the reactions is shown in FIGURE A1.5. The acid-catalyzed conversion of glucose or xylose commonly leads to the low mass balance due to the formation of humins [111], condensation reactions, degradation, and/or decomposition [33]. Importantly, the Lewis acid sites necessary to isomerize glucose are also active in the decomposition of the reaction

products [59]. Overall, the NbPs presented a similar mass balance, except for the NbP-1 when used to convert glucose FIGURE A1.5**.** Hence, developing bifunctional catalysts for the conversion of glucose (and xylose) which leads to high furan yield and high carbon balance in water or aprotic solvents is an important challenge in the field.

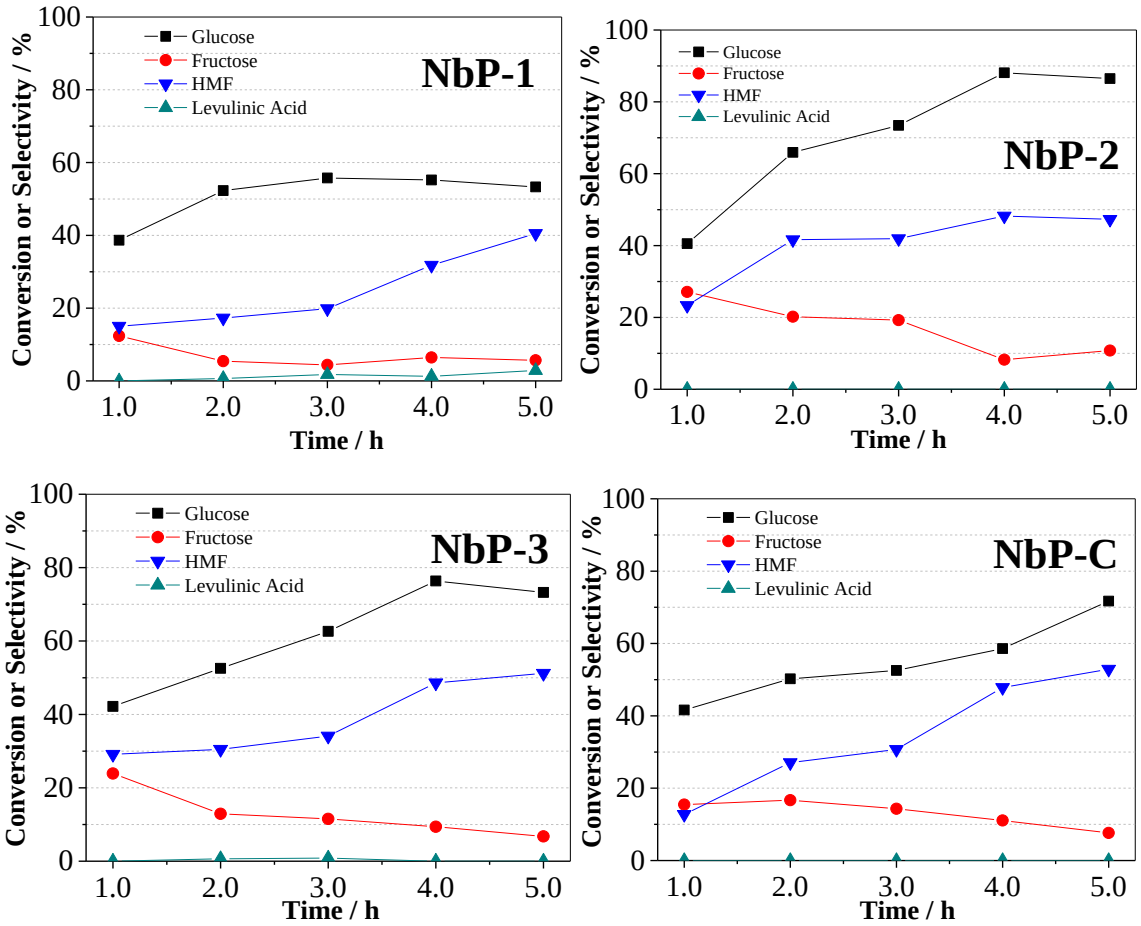

FIGURE 2.6 – Conversion of glucose catalyzed by NbPs as a function of reaction time at 130 °C using THF/H_2O = 4/1 as a solvent system. For NbP-C and NbP-2, it was used 0.080 g of catalyst (catalyst/substrate mass ratio = 2.00) and for the others, 0.160 g (catalyst/substrate mass ratio = 4.00). Mass balance is shown in FIGURE A1.5.

NbP-1 is noticeably the catalyst that leads to the lowest HMF selectivity and yield. According to the acetonitrile adsorption analysis by FTIR, this sample was the only one to display an important contribution of strong Lewis

acid sites (FIGURE 2.5B), which could be responsible for the poor performance of this catalyst. It is known that for some catalysts the Lewis acid sites can also catalyze the decomposition of fructose, as observed for niobium oxide and other systems [33,59]. It is rather difficult to correlate the concentration of the active sites and the activity for Lewis/Brønsted bifunctional catalysts because the nature of these sites can be, sometimes, more important than the concentration. For instance, the Brønsted acid sites on niobium oxide showed to be effective in the dehydration of xylose but not for fructose [33], while the Lewis acid sites on Al-Beta Zeolite are active in isomerizing xylose, but not for glucose isomerization [70].

Nonetheless, previous studies for homogeneous catalysts have shown the importance of controlling the ratio of Lewis and Brønsted acid sites for glucose conversion to HMF [59]. It is shown that if the Lewis acid concentration is too high compared to the concentration of the Brønsted acid, fructose degradation to humins can take place, while if it is too low, isomerization becomes the rate-limiting step [59].

Indeed, for the NbP catalysts, it appears that the catalytic activity is directly controlled by the Lewis/Brønsted acid sites (*L/B*) ratio and as shown in FIGURE 2.7, the reaction rate for both glucose conversion and HMF formation increases along with the *L/B* ratio. Importantly, this trend is valid for niobium phosphate-type catalysts. Furthermore, it cannot be extrapolated, otherwise one could conclude that the best activity would be reached when only Lewis acid sites are present. Herein, we used catalysts with borderline compositions, i.e., stoichiometric niobium oxyphosphate (NbP-3) and (phosphated niobium oxide)-like (NbP-C) as well as catalysts with an intermediate composition (NbP-1 and NbP-2), and the correlation observed in FIGURE 2.7 is valid for this range.

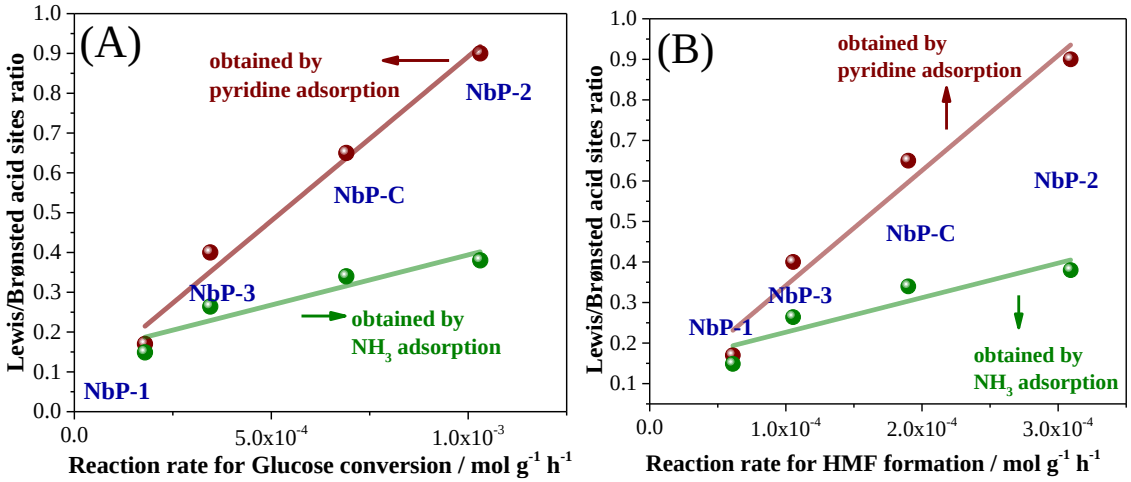

FIGURE 2.7 – Correlation between Lewis/Brønsted acid sites ratio and reaction rate for (A) Glucose conversion and (B) HMF formation. Reaction rate calculated at *ca.* 50 % conversion from the data in FIGURE 2.6.

The stability of NbP-2 and NbP-C, the catalysts with the best reaction rate for HMF formation, were studied by reusing the catalysts, as shown in FIGURE A1.6. NbP-2 is stable for reuse but after the 4th use, the selectivity to HMF reduces. NbP-C, instead, was shown to be stable for all five uses. It is interesting to mention that the activity of NbP-C increases along with the number of uses, although the standard deviation for the conversion is pronounced and one could argue that the activities are comparable. After the first use, NbP-2 and NbP-C were characterized by XRD (FIGURE A1.7), XRF, and ^{31}P ss-NMR (FIGURE A1.8). The spent samples presented a similar XRD pattern compared to the fresh ones, confirming that no crystallization or phase transformation took place. XRF analyses revealed that the spend samples presented a reduction of 1.87 and 4.07 mol % of the phosphorous content (based on the total amount of P and Nb), respectively. The phosphate leaching was also confirmed by ^{31}P ss-NMR, which identified leaching of the dihydrogenphosphate (H_2PO^{4-}) species (FIGURE A1.8). The NMR spectra of the spent NbP-2 and NbP-C present a slight decrease in the band due to dihydrogenphosphates species (*ca.* 2 and -7 ppm, respectively) compared to the fresh samples. For NbP-2, these species could also be partially

condensing with the structure, since an increase of the band at -14 ppm due to hydrogenphosphate is observed Although phosphate leaching is observed, it appears to be small enough not to affect significantly the catalytic activity of the catalysts since both NbP-2 and NbP-C were shown to be successfully reused (FIGURE A1.6).

Previous studies in the literature report that combining Nb_2O_5 with an additional Brønsted acid catalyst can increase the HMF productivity [33]. In order to compare NbP with the Nb_2O_5-HCl catalytic system, experiments combining NbP and HCl (0.18 mol L^{-1}) were performed (FIGURE A1.9), however, it was observed a decrease in the HMF yield compared to the reaction catalyzed by neat NbP (*ca.* 29, 39, 28, and 31 %, respectively, for NbP-1, NbP-2, NbP-3, and NbP-C). Therefore, NbP-2 and NP-C were shown to be efficient bifunctional catalysts able to achieve HMF yields comparable to the combination of Nb_2O_5/HCl. NbPs, however, are purely heterogeneous and easy to prepare, in accordance with industrial requirements.

2.3.5 - Xylose conversion to furfural

Xylose conversion to furfural was performed in THF/H_2O = 4/1 as the solvent system and revealed that xylose is first isomerized to xylulose and then dehydrated to furfural (SCHEME 2.2). In this case, there is a competitive dehydration between xylose and xylulose, but the reaction is faster for xylulose [33,45,59,70]. NbP-2 is the catalyst with the highest reaction rate and the reaction is nearly completed after 2 h (FIGURE 2.8). The highest furfural yields obtained after 5 h of the reaction were *ca.* 28, 49, 37, and 50 %, respectively, for NbP-1, NbP-2, NbP-3, and NbP-C. Interestingly, NbP-2 presented product yield comparable to NbP-C, whereas, with a higher reaction rate. Compared with previous works, it seems that Nb_2O_5 is not less efficient in producing furfural from xylose through the isomerization/dehydration route [33], but NbP-C, NbP-2

appears as valid alternative.

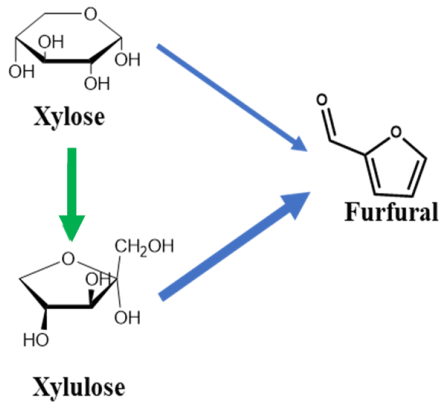

SCHEME 2.2 – Conversion of xylose with a combination of Brønsted and Lewis acids. The thicker arrow indicates the preferential route. Green and blue arrows indicate the reaction steps catalyzed by Lewis and Brønsted acid sites, respectively.

As for the effect of the surface properties in the reaction rate, a similar trend to the observed for glucose is also present in the conversion of xylose. The reaction rate for xylose conversion (FIGURE 2.9A) and furfural formation (FIGURE 2.9B) increases along with the Lewis/Brønsted acid sites ratio acids [70]. This confirms the previous findings that state that the reaction rate for xylose conversion to furfural increases when combining Lewis and Brønsted. Interestingly, although NbP-2 and NbP-C have *L/B* molar ratios significantly different, they display similar reaction rates for furfural formation (FIGURE 2.9B). To verify if the strength of the Brønsted acids is responsible for this behavior, the samples were characterized by CO adsorption at -176 °C monitored by FTIR. As shown in FIGURE A1.10, upon adsorption of CO in the samples (followed by subtraction of the spectra before adsorption) it is observed a negative band at 3665 cm^{-1}, corresponding to the O-H stretching of the hydrogen phosphate terminals group (P-OH). The negative band indicates that this species was consumed due to its interaction with CO, leading to a broad band between 3600 and 3400 cm^{-1}. The relative strength of the Brønsted acid site is proportional to

the shift of this band relative to the original band of P-OH (at 3665 cm^{-1}) [112]. The shifts ($\Delta\nu_{OH}$) observed for NbP-2 and NbP-C were 175 and 198 cm^{-1}, respectively, suggesting comparable acid site strength [112]. For sake of comparison, the difference of $\Delta\nu_{OH}$ for a weak acid such as silica and a medium strength acid such as Al-SBA-15 is higher than 100 cm^{-1} and the difference in $\Delta\nu_{OH}$ for Al-SBA-15 and a strong Brønsted acid, such as a Zeolite, is of at least 70 cm^{-1} [112]. Hence, due to the small difference between the acid strength of NbP-2 and NbP-C, we were unable to confirm if this parameter is responsible for the results observed in FIGURE 2.9B, yet, this cannot be completely ruled out.

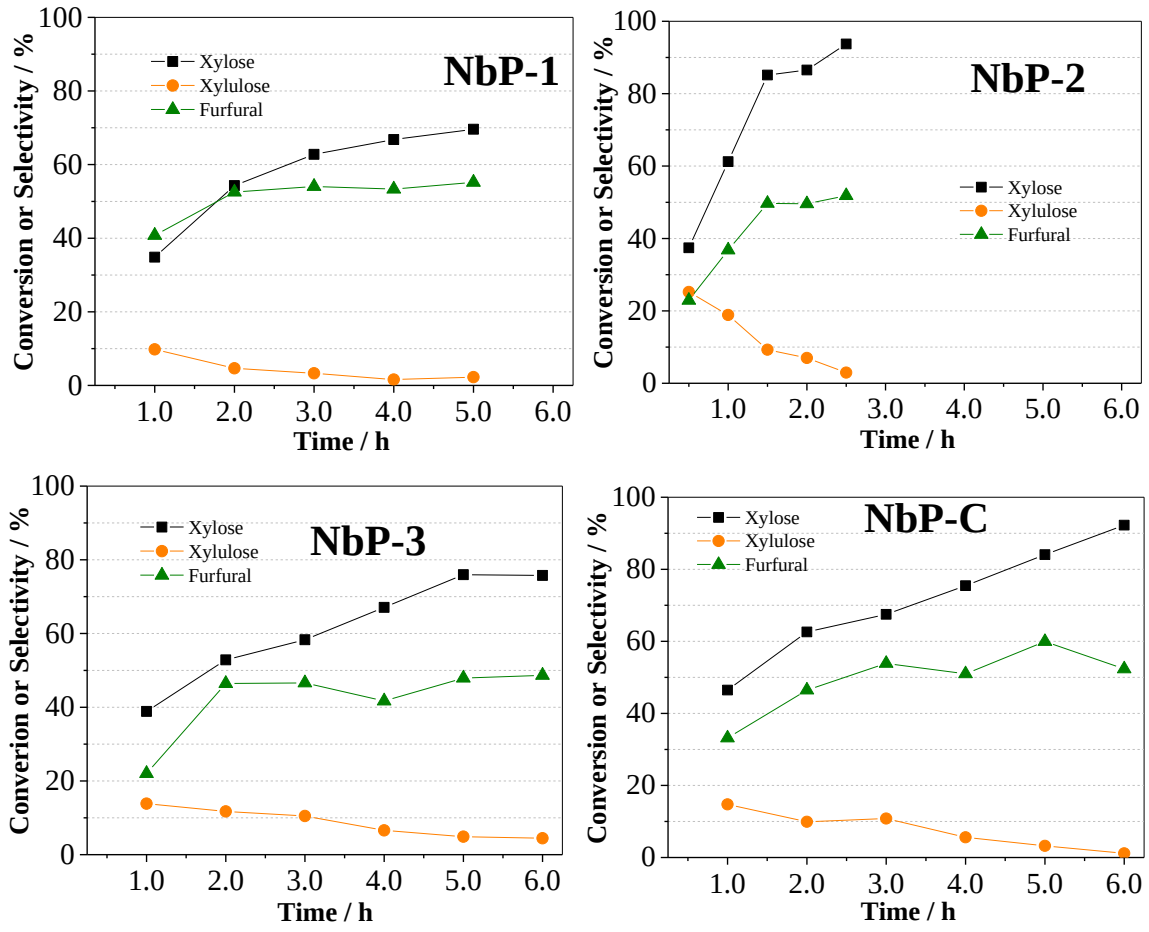

FIGURE 2.8 – Conversion of xylose catalyzed by NbPs as a function of reaction time at 130 °C using THF/H_2O = 4/1 as a solvent system. It was used 0.080 g of catalyst (catalyst/substrate mass ratio = 2.00), except for NbP-1, with a mass of 0.160 g (catalyst/substrate mass ratio = 4.00). Mass balance is shown in FIGURE A1.5.

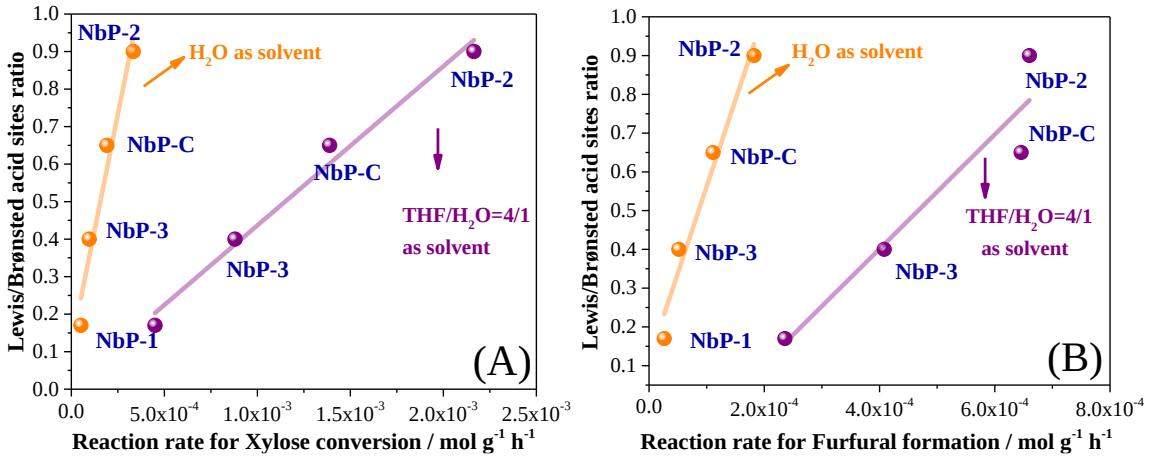

FIGURE 2.9 – Correlation between Lewis/Brønsted acid sites ratio (obtained by pyridine adsorption) and reaction rate for (A) xylose conversion and (B) furfural formation. Reaction rate calculated at *ca.* 50 % conversion from the data in FIGURE 2.8 and FIGURE 2.10.

Different from glucose, xylose can be efficiently converted to furfural using pure water as a solvent for niobium-based catalysts [33]. For Nb_2O_5, for instance, the product yields in water tend to be slightly lower than in THF/H_2O, but still comparable [33]. Pure water also tends to be inadequate for phosphate and sulfates catalysts due to hydrolysis and leaching of the inorganic anions, however, seeking a comparison to the previously reported niobium oxide system [33], NbPs performance in xylose conversion as a function of reaction time were also studies in pure water (FIGURE 2.10). NbP-C and NbP-3 appear to lose activity after a few hours of reaction, which was not observed in THF/H_2O = 4/1. NbP-2, once again, displayed the highest reaction rate (although lower than in THF/H_2O = 4/1) since the reaction was nearly completed after 5 h.

FIGURE 2.9 shows that, overall, the reaction rates are significantly lower in water than in THF/H_2O = 4/1, however, the trend of activity per sample, as well as the effect of Lewis/Brønsted acid sites in the catalytic performance is similar.

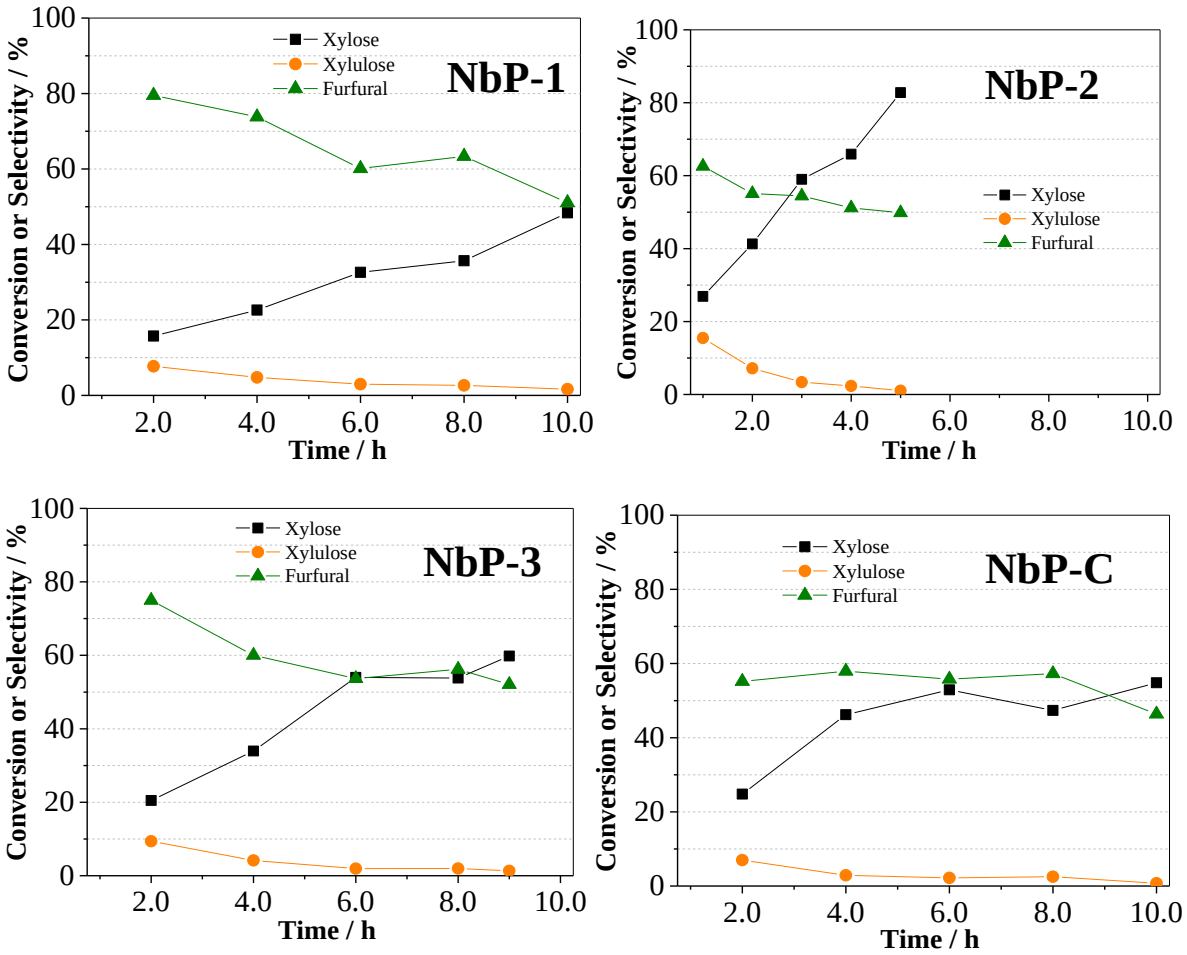

FIGURE 2.10 – Conversion of xylose catalyzed by NbPs as a function of reaction time at 130 °C using pure water as the solvent system. It was used 0,160 g of NbP-C or NbP-2 (catalyst/substrate mass ratio = 4.00) and 0.250 g of NbP-1 or NbP-3 (catalyst/substrate mass ratio = 6.25). Mass balance is shown in FIGURE A1.5.

2.4 - Conclusions

By modifying synthesis parameters such as type and concentration of the surfactant, temperature, and post-reaction treatment, niobium phosphates were prepared with different compositions. It was obtained from materials with the composition of stoichiometric niobium oxyphosphate [(NbO)(PO_4)] until those that resemble a phosphated niobium oxides. The overall composition affected the surface composition and, consequently, the surface acidity.

The catalysts with a high *P/Nb* molar ratio (composition similar to niobium oxyphosphate) presented a low molar ratio between Lewis and Brønsted

acid sites (*L/B* ratio), while those with low *P/Nb* molar ratio displayed a high *L/B* ratio. The trend of the *L/B* ratio obtained from adsorption of ammonia or pyridine monitored by FTIR was NbP-1 < NbP-3 < NbP-C < NbP-2. Acetonitrile adsorption monitored by FTIR revealed that the samples have predominantly the same strength of Lewis acidity, however, NbP-1 and NbP-3 also present a small contribution of a family of stronger Lewis acid sites.

NbP-2, the sample with the highest *L/B* ratio, presented the highest reaction rate for both HMF and furfural formation. It was found, indeed, that the reaction rate for monosaccharides conversion and for furans formation correlate linearly with the *L/B* ratio. The importance of the *L/B* ratio has been previously observed for homogeneous catalysts, whereas, to the best of our knowledge, it is the first time that a direct and linear correlation between the *L/B* ratio and the reaction rate is found.

The results presented herein not only introduce niobium phosphates with a low *L/B* molar ratio as highly promising catalysts for HMF and furfural production but also provides fundamental knowledge that will guide the design of other bifunctional heterogeneous catalysts.

2.5 - Acknowledgments

This work has been funded by the FAPESP Young Research Award (Process # 2016/02128-2). J.M.R.G thanks the Alexander von Humboldt Foundation for Return Fellowship and the Conselho Nacional de Desenvolvimento Científico e Tecnológico (CNPq) for the productivity fellowship (303640/2019-7). J.M.R.G also thanks to the Department of Sciences and Technological Innovation at the University of Eastern Piedmont for the visiting professorship. J.M.C.B thanks FAPESP for the funding (2018/01258-5). G.D.I thanks FAPESP for the fellowship (2020/15949-0). J.L.V thanks FAPESP for the fellowship (2017/17042-9, 2018/10536-9, 2019/02132-8, and 2020/04109-

0) and Dr. Diana F. Olivas Olivera for the helpful discussions. The authors thank CBMM Brazil for providing the samples of niobium phosphate among others.

3 - CHAPTER 2: THE IMPACT OF THE RATIO BETWEEN STRONGER AND WEAKER ACID SITES ON THE PRODUCTION OF 5-HYDROXYMETHYLFURFURAL AND FURFURAL FROM MONOSACCHARIDES (CHEMCATCHEM – IMPACT FACTOR 3.8)

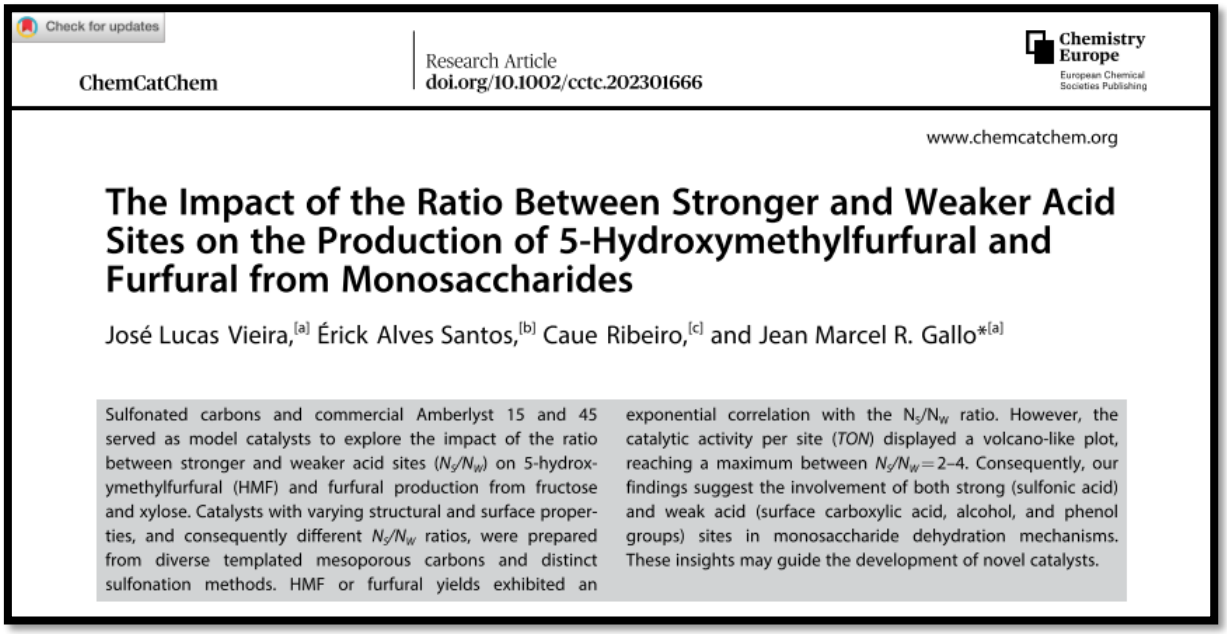

Check for updates

ChemCatChem

Research Article
doi.org/10.1002/cctc.202301666

Chemistry Europe
European Chemical Societies Publishing

www.chemcatchem.org

The Impact of the Ratio Between Stronger and Weaker Acid Sites on the Production of 5-Hydroxymethylfurfural and Furfural from Monosaccharides

José Lucas Vieira,[a] Érick Alves Santos,[b] Caue Ribeiro,[c] and Jean Marcel R. Gallo*[a]

Sulfonated carbons and commercial Amberlyst 15 and 45 served as model catalysts to explore the impact of the ratio between stronger and weaker acid sites (N_S/N_W) on 5-hydroxymethylfurfural (HMF) and furfural production from fructose and xylose. Catalysts with varying structural and surface properties, and consequently different N_S/N_W ratios, were prepared from diverse templated mesoporous carbons and distinct sulfonation methods. HMF or furfural yields exhibited an exponential correlation with the N_S/N_W ratio. However, the catalytic activity per site (*TON*) displayed a volcano-like plot, reaching a maximum between $N_S/N_W = 2–4$. Consequently, our findings suggest the involvement of both strong (sulfonic acid) and weak acid (surface carboxylic acid, alcohol, and phenol groups) sites in monosaccharide dehydration mechanisms. These insights may guide the development of novel catalysts.

3.1 - Introduction

The imperative to replace oil as a source of chemicals and fuels arises from the high levels of associated greenhouse gas emissions [8]. Lignocellulosic biomass emerges as a promising alternative source of carbon to fossil fuels. This feedstock primarily comprises cellulose and hemicellulose, which can be hydrolyzed into glucose and xylose [15,64]. These monosaccharides are precursors for important platform molecules such as 5-hydroxymethylfurfural (HMF) and furfural, pivotal in the synthesis of various chemicals and fuels [15].

Fructose (an isomer of glucose) and xylose can be selectively dehydrated to HMF and furfural using Brønsted acid catalysts. While metal oxides and zeolites are commonly used as heterogeneous catalysts in the chemical industry [113], they often exhibit limited performance or low stability in monosaccharide dehydration [114–116]. For instance, aluminum oxide demonstrates low selectivity to the synthesis of HMF or furfural [42,117]. Zeolites and niobium oxide are promising for xylose dehydration; however, their effectiveness in converting fructose to HMF is poor [33,42,70,118–120]. Moreover, in the presence of water (a typical solvent in biomass conversion), approximately 1 – 2 wt. % of zeolite catalysts dissolve in the aqueous-phase dehydration of fructose to HMF at 130 °C. This results in a solution of aluminosilicate species that can catalyze side reactions of fructose and HMF to undesirable products [121].

Sulfonated solid catalysts have often displayed outstanding performance in fructose and xylose dehydration to furan; however, several of these catalysts suffer from deactivation [15,42,122–124]. In contrast, sulfonated carbons emerge as a highly stable catalyst class for monosaccharide dehydration, even in the presence of water [41,125–128]. Studies indicate that these catalysts exhibit 8 to 60 times lower deactivation rates than those of sulfonated silicas for fructose dehydration at 130 °C with tetrahydrofuran containing 20 wt. % water

[41].

A systematic study has shown that SBA-15-propylsulfonic acid and sulfonated carbons can achieve similar HMF selectivity at the same fructose conversion [41]. However, the activity per site significantly differs among the carbon-based catalysts but is higher than that obtained from SBA-15. Furthermore, the activity of the carbons is especially influenced by the sulfonation methodology. For instance, the activity per site of CMK-3 functionalized with naphthalene sulfonic acid (NSA) is 1.9 times higher than the same structure sulfonated with fuming sulfuric acid [41]. It is worth mentioning that different functionalization methodologies require distinct pretreatments in the carbon support. For example, functionalization with NSA is performed on carbon with low surface oxygen, while sulfonation with sulfuric acid is only effective on carbons pyrolyzed at low temperatures. Hence, the difference in catalytic activity [41] could be attributed to the carbon structure, pyrolysis temperature, or functionalization methodology.

The pyrolysis temperature also affects the degree of surface functionalization of the carbon [129] and these functional groups can play a role in the catalytic activity. Studies have proposed that the phenol and carboxylic acid groups present in the support surface, when adjacent to the sulfonic acid group, can play a role in converting monosaccharides into furans [130–136]. For instance, phthalic acid [135] and hydroxybenzoic acid [136] were shown to be more active when the two functional groups were in the ortho position rather than meta or para. Additionally, fructose dehydration activity was compared using glycolic acid, acetic acid, o-hydroxy-benzoic acid, and benzoic acid. A higher HMF carbon yield was achieved with glycolic acid and o-hydroxy-benzoic acid, suggesting a synergistic effect between -COOH and adjacent -OH groups in fructose dehydration [131]. These studies provide solid evidence of the relevance of the synergy in adjacent groups. Furthermore, DFT calculations [136] suggest

that weaker acid sites adjacent to the strong acid sites offer additional hydrogen bonds that increase fructose adsorption, stabilize the intermediate transition states, and decrease the activation energy of the rate-determining step.

On the field of heterogeneous catalysis, sulfated cyclopentanone–formaldehyde condensate resins containing adjacent SO_3H and OH groups have shown higher performance in the dehydration of fructose to HMF than Amberlyst-15, Amberlyst-36, and Nafion-212, commercial resins with no selective presence of adjacent groups [135]. Similarly, lignosulfonate-based resins have shown to be more selective to HMF from fructose compared to typical commercial resins, which was attributed to a synergism effect of the adjacent -SO_3H, -COOH, and phenolic -OH functional groups [131]. To support this claim, the authors evaluated the activity of the combination of acetic acid and Amberlyst-15, which led to a noticeable increase in the HMF selectivity compared to the resin alone.

Sulfonated graphene quantum dots were also shown to take advantage of the synergistic collaboration between Brønsted acid sites (-SO_3H groups) and hydroxyl groups in the production of HMF [132]. Regarding carbon-based catalysts, a systematic study has been carried out with sulfonated carbons prepared by carbonizing lignin and polyvinyl chloride at different temperatures. The yield for furfural obtained from the xylose dehydration correlates with the total number of acid sites (weak + strong) rather than with the acid sites derived from sulfonic groups [133].

Although the synergistic effect of adjacent sites has been proposed in different catalytic systems [130–136], there is a lack of understanding of the optimal ratio between these sites for the catalyst activity. Furthermore, previous studies have been carried out predominantly in low surface area carbons [133] or resins where the swelling effect could play a role and was not considered.

Addressing the essential hurdles in catalyst design involves considerations related to the availability, performance, and durability of acid sites.

Sulfonated mesoporous carbon, distinguished by its elevated concentration of robust SO_3H acidic groups, meticulously arranged mesoporous structure, distinctive surface affinity, and exceptional hydrothermal stability, emerges as a prospective candidate for facilitating biomass conversions in the liquid phase [137]. Therefore, periodic mesoporous carbons are reliable model catalysts due to the high surface area (> 500 m^2 g^{-1}) and efficient infusibility of large substrates due to the mesoporosity.

This study used different methodologies to sulfonate periodic mesoporous carbons (CMK-3, CMK-5, and CMK-8) and a nonperiodic carbon derived from chitosan. These catalysts, in addition to commercial Amberlyst 15 and Amberlyst 45, offered a wide range of ratios between strong and weak acid sites (Ns/Nw). This diversity allowed us to rationalize the collaborative effect between Ns/Nw ratios and catalytic activity in the dehydration of monosaccharides derived from biomass.

3.2 - Materials and Methods

3.2.1 - Synthesis: carbons derived from chitosan

The carbon C-Chi was synthesized from the non-periodic silica colloid LUDOX® AS-40. In this case, 2.00 g of chitosan was firstly dissolved in a solution of 197.92 g of water with 2.08 g acetic acid for 1 h under stirring. The solution was then heated to 35 °C and stirred for 1 h. After that, 8.75 g of the silica LUDOX® AS-40 were added dropwise, and the resulting slurry was stirred at the same temperature until evaporation of the solvent. The gel obtained was further dried under air for 24 h, resulting in a semi-transparent film [138]. The film was pyrolyzed under argon flow at either 550 °C for 6 h or 1000 °C for 5 h (3.25 °C min^{-1}). The silica template was removed using 50 % w/w HF by mixing 0.175 g of the composite with 1 mL of HF for 10 minutes at room temperature (CAUTION: this step is highly exothermic). The resulting carbons were named

C-Chi-X, where X refers to the pyrolysis temperature (either 550 °C or 1000 °C).

3.2.2 - Synthesis: carbons CMK-3 and CMK-5

For the synthesis of the carbons CMK-3 and CMK-5, the periodic silica SBA-15 was used as a silica template, and its synthesis was reported elsewhere [139]. For the preparation of CMK-3, 4.00 g of SBA-15 were impregnated with a solution of 5.00 g of sucrose, 20.00 g of deionized water, and 0.56 g of sulfuric acid. The slurry was heated at 100 °C for 6 h and 160 °C for 6 h. The impregnation step was repeated with a solution containing 3.20 g of sucrose, 20.00 g of deionized water, and 0.36 g of sulfuric acid [140]. The final brown composite was pyrolyzed under argon flow at either 550 °C for 6 h or 1000 °C for 5 h (3.25 °C min^{-1}). The silica template was removed using 50 % w/w HF by mixing 0.175 g of the composite with 1 mL of HF for 10 minutes at room temperature (CAUTION: this step is highly exothermic). The resulting carbons were named CMK-3-X, where X refers to the pyrolysis temperature (either 550 °C or 1000 °C).

For the synthesis of CMK-5, it was first necessary to aluminate SBA-15 to produce a Brønsted acid material to catalyze the polymerization of the carbon precursor. Thus, 4.00 g of SBA-15, previously dried at 150 °C for 3 h, was impregnated with 25 mL of an aqueous solution of 0.8037 g of aluminum chloride hexahydrate. The slurry was stirred for 30 min at room temperature and dried at 80 °C for 3 h. The final white solid was calcined for 10 h at 550 °C (1.00 $^{o}C\ min^{-1}$) under oxygen flow, producing Al-SBA-15 [141]. For the carbon synthesis, 1.00 g of Al-SBA-15 was impregnated with 2.50·g of furfuryl alcohol and heated at 80 °C for 2 h and 150 °C for 8 h [142]. The unreacted furfuryl alcohol was removed under vacuum at 80 °C for 2 h. The final brown composite was pyrolyzed under argon flow at either 550 °C for 6 h or 1000 °C for 5 h (3.25 °C min^{-1}). The silica template was removed using 50 % w/w HF by mixing 0.175 g of the composite

with 1 mL of HF for 10 minutes at room temperature (CAUTION: this step is highly exothermic). The resulting carbons were named CMK-5-X, where X refers to the pyrolysis temperature (either 550 °C or 1000 °C).

3.2.3 - Synthesis: carbons CMK-8 and S-CMK-8

The carbons CMK-8 and S-CMK-8 were prepared from the periodic silica template KIT-6, which was synthesized based on a method reported elsewhere [143].

The carbon CMK-8 was synthesized with the same methodology employed for CMK-3 but KIT-6 as a silica template. The final brown composite was pyrolyzed under argon flow at either 550 °C for 6 h or 1000 °C for 5 h (3.25 °C min^{-1}). The silica template was removed using 50 % w/w HF by mixing 0.175 g of the composite with 1 mL of HF for 10 minutes at room temperature (CAUTION: this step is highly exothermic). The resulting carbons were named CMK-8-X, where X refers to the pyrolysis temperature (either 550 °C or 1000 °C).

For synthesizing the carbon S-CMK-8, 2.00 g of KIT-6 were impregnated with 25 mL of a 0.5 mol L^{-1} ρ-toluenesulfonic acid ethanolic solution and stirred for 1 h at room temperature. The product was filtered, washed with 10 mL of ethanol 70 %, and dried at 80 °C for 2 h. A second impregnation was performed using a solution of 1.80 g of 2-thiophenemetanol in 6.5 mL of acetone, followed by a thermal treatment at 100 °C for 16 h [144]. The final brown composite was pyrolyzed under argon flow at either 550 °C for 6 h or 1000 °C for 5 h (3.25 °C min^{-1}). The silica template was removed using 50 % w/w HF by mixing 0.175 g of the composite with 1 mL of HF for 10 minutes at room temperature (CAUTION: this step is highly exothermic). The resulting carbons were named S-CMK-8-X, where X refers to the pyrolysis temperature (either 550 °C or 1000 °C).

3.2.4 - Sulfonation method: fuming sulfuric acid

This sulfonation was performed in templated carbons pyrolyzed at 550 °C. At room temperature and under an argon atmosphere, 1.00 g of carbon support was added under stirring to 50 mL of fuming sulfuric acid (20 wt. % SO_3). The mixture was stirred for 15 h at 150 °C and then slowly added to 1 L of water at 3 °C (CAUTION: this step is highly exothermic). The solid was separated by filtration, washed with water until neutral, and dried at 100 °C for 3 h [145]. The catalysts were named using the suffix SA, i.e., CMK-3-SA, CMK-5-SA, CMK-8-SA, S-CMK-8-SA, and C-Chi-SA.

3.2.5 - Sulfonation method: diazonium salt method

This sulfonation was performed in templated carbons pyrolyzed at 1000 °C. For the preparation of the diazonium salt, 13.12 g of sulfanilic acid was dispersed in 750 mL of HCl 1.00 mol L^{-1} under vigorous stirring for 1 h at room temperature. This dispersion was cooled to 3 °C, and 82.5 mL of $NaNO_2$ 1.00 mol L^{-1} was added dropwise, producing a white suspension that remained stirring for 1 h at the same temperature. The white solid was filtered, washed with 20 ml of water at 3 °C, and dried at room temperature overnight. The wet solid was dissolved in a mixture of 200 mL of water with 200 mL of ethanol at room temperature under stirring. After that, 1.20 g of carbon support was added to the mixture, and the system was cooled to 3 °C. Subsequently, 200 mL of 50 wt. % H_3PO_2 aqueous solution was added, and the mixture was stirred for 30 min, followed by another 200 mL of H_3PO_2 aqueous solution and 30 min of stirring, still at 3 °C. The final suspension was filtered and washed with distilled water until the pH neutralization, and the solid was dried at 80 °C for 3 h [146]. The catalysts were named using the suffix PSA, i.e., CMK-3-PSA, CMK-5-PSA, CMK-8-PSA, S-CMK-8-PSA, and C-Chi-PSA.

3.2.6 - Characterizations

Various analytical techniques were employed in this study. Powder X-ray diffraction (XRD) analysis utilized a Bruker AXS X-ray Diffraction Instrument with a Cu-k_α source, operating at 25 mA current and 40 kV voltage. Scanning Electron Microscopy (SEM) was conducted using Hitachi S-3400N equipment. Nitrogen physisorption measurements were recorded at 77 K using a Micro 100 series Surface Area and Pore Size Analyzer from JWGB Sci & Tech, with an outgassing process of the powders at 413 K for 5 hours before the reactions. Raman spectra were acquired using a Renishaw in Via spectrometer with a 633 nm excitation wavelength (10 % laser intensity, 3 accumulations, and 10 seconds exposure time). Infrared spectroscopy (FTIR) was carried out using a Prestige-21 infrared spectrometer with a mercury-cadmium-telluride (MCT) detector. The samples (300 mg of KBr + 1 mg of the sample) were pressed at 5 tons into self-supported pellets. For X-Ray Photoelectron Spectroscopy (XPS), a Thermo Fisher Scientific K-alpha photoelectron spectrometer was employed under Ultra High Vacuum (UHV) conditions (~ 6×10^{-9} mbar) with monochromatic Al-K_α radiation (1486.68 eV) and a spot size of 400 μm, using an energy step size of 0.05 eV and a constant pass energy of 50 eV. Elemental analysis was conducted using a PerkinElmer® 2400 Series II CHNS/O Elemental Analyzer. Thermogravimetric Analysis (TGA) was carried out in a TGA Q500 V20.13 Build 39, with an airflow of 60.0 mL min^{-1} and a ramp rate of 5.00 °C min^{-1}.

Potentiometric titration was performed utilizing a Metrohm 827 pH Lab pH meter. In this method, 200 mg of the acidic templated carbons or 40 mg of the sulfonated carbons were mixed with 35 mL of a 1.00 x 10^{-1} mol L^{-1} $NaNO_3$ solution and stirred for 5 minutes. After that, the mixture still under stirring was titrated with a standard solution of NaOH (9.18 x 10^{-3} mol L^{-1}/1.00 x 10^{-1} mol L^{-1} $NaNO_3$). Since the respective pH meter does not measure the data automatically,

each point was manually noted after adding 0.2 mL of titrant and 30 seconds of mixture stabilization.

For the quantification of active acid sites, the inflection points were determined by the maximum center value of Gaussian deconvoluted curves in the first derivative potentiometric titration curve (FIGURE A2.14-17). Thus, the following formulas were used to calculate the concentration of stronger (N_S), weaker (N_W), and total acid sites (N_T), respectively:

$$N_S = \frac{C_{NaOH} * V_{NaOH,1°IP} * 1000}{m}$$

$$N_W = \frac{C_{NaOH} * (V_{NaOH,2°IP} - V_{NaOH,1°IP}) * 1000}{m}$$

$$N_T = \frac{C_{NaOH} * V_{NaOH,2°IP} * 1000}{m}$$

Where C_{NaOH} stands for the concentration of NaOH (mol L^{-1}), $V_{NaOH,1°IP}$ for the volume of NaOH at the first inflection point (mL), $V_{NaOH,2°IP}$ for the volume of NaOH at the second inflection point (mL), and m for the mass of material (g).

3.2.7 - Catalytic studies

Catalytic tests were carried out in 15 mL thick-glass reactors, each containing 2.00 g of a solution comprising 2 wt. % fructose or xylose in tetrahydrofuran with 20 wt. % water (THF/H_2O = 4/1), along with the catalyst. The reactors were placed in an oil bath preheated to 130 °C or 160 °C for fructose or xylose dehydration, respectively, and stirred at 300 rpm for varying reaction times. The reactions were quenched by cooling the reactors in an ice bath. Product identification and quantification were accomplished using High-Performance Liquid Chromatography (HPLC) with standards. Shimadzu HPLC LC-10AD was coupled to a Bio-Rad Aminex® HPX-87H column (300.0 mm x 7.8 mm) using 0.005 mol L^{-1} aqueous H_2SO_4 as mobile phase and equipped with refractive index detector (Shimadzu RI20A) and diode array detector (Shimadzu SP10A) for

analysis.

The conversion, selectivity, yield, turnover number of platform molecule production (TON_{Furan}), and mass balances were calculated by the equations:

$$Conversion = \left(\frac{mol\ precursor_{initial} - mol\ precursor_{final}}{mol\ precursor_{initial}}\right) * 100$$

$$Selectivity = \left(\frac{mol\ product_{final}}{mol\ precursor_{initial} - mol\ precursor_{final}}\right) * 100$$

$$Yield = \frac{(Conversion) * (Selectivity)}{100}$$

$$TON_{Furan} = \frac{mol\ furan_{final}}{mol\ of\ total\ acid\ sites}$$

$$Mass\ balance_{Fructose\ conversion} = \left(\frac{mass\ fructose_{final} + mass\ HMF_{final} + mass\ LA_{final}}{mass\ fructose_{initial}}\right) * 100$$

$$Mass\ balance_{Xylose\ conversion} = \left(\frac{mass\ xylose_{final} + mass\ xylulose_{final} + mass\ furfural_{final}}{mass\ xylose_{initial}}\right) * 100$$

3.3 - Results and Discussion

3.3.1 - Characterization: structural and textural properties

Periodic mesoporous carbon CMK-3, CMK-5, CMK-8, and S-CMK-8 (ρ-toluenesulfonic acid and 2-thiophenemethanol were used as carbon source for the latter) and a carbon sample derived from chitosan were prepared as reported elsewhere [138–144]. These supports were pyrolyzed at 550 or 1000 °C and named according to the pyrolysis temperature. Carbon-550 was sulfonated with sulfonic acid, yielding Carbon-SA [145]. Carbon-1000 was functionalized with phenylsulfonic acid species and named Carbon-PSA [146].

As expected for SBA-15 replicas, CMK-5-550, CMK-3-1000, and CMK-5-1000 (FIGURE A2.1A) display X-ray diffraction (XRD) patterns with the three expected peaks assigned to the Miller index (100), (110) and (200), which are characteristic of the hexagonal pores array in the *P6mm* symmetry [147]. The XRD pattern for CMK-3-550 exhibits only the first peak, suggesting a

lack of long-range ordering of the mesopores [145].

CMK-8 and S-CMK-8 are negative replicas of KIT-6 and, hence, are expected to display similar XRD patterns. As observed in FIGURE A2.1B, S-CMK-8 and KIT-6 have typical diffractograms with peaks at 0.98° and 1.14° due to the plans (211), (200), and a series of overlapped peaks between 1.70° – 2.10° which can be assigned to the Miller index (321), (400), (420), (322), (422) and (431) [143]. The XRD pattern for CMK-8 did not show the group of overlapped peaks, indicating a lower long-range organization of the mesopores.

After the sulfonation (FIGURE 3.1A), CMK-5-PSA still displays the characteristic XRD peaks, suggesting the structure was stable during the functionalization procedure. On the contrary, no peak was observed in the XRD patterns for CMK-3-SA and CMK-5-SA, indicating a loss in the periodicity in the mesopores' organization. The CMK-8 samples were less affected by the sulfonation methodology, particularly the S-CMK-8-PSA (FIGURE 3.1B). Interestingly, previous studies have shown a deterioration or severe collapse in carbon mesostructure after sulfonation with fuming sulfuric acid [138,148].

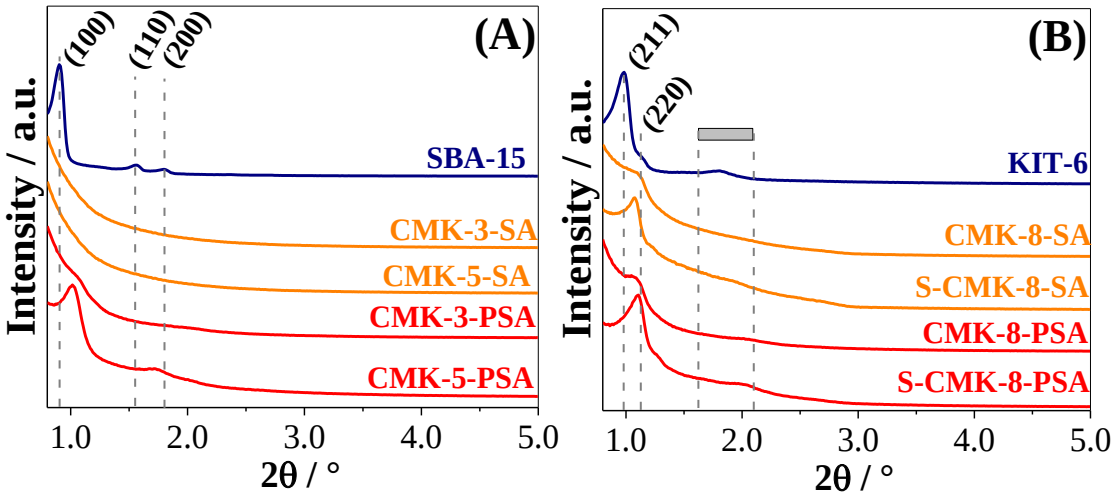

FIGURE 3.1 – XRD diffractograms of the sulfonated carbons derived from the (A) silica SBA-15 and (B) KIT-6.

The Scanning Electron Microscopy (SEM) of the templated carbons

revealed similar morphologies for the samples pyrolyzed at 550 or 1000 ºC (FIGURE A2.2 and FIGURE A2.3). C-Chi carbons exhibit rough surfaces with abundant honeycomb-like mesopores between 10 – 25 nm. CMK-3 and CMK-5 display aggregates of worm-like morphology with lengths of 319 (± 41) and 512 (± 45) nm, respectively. CMK-8 and S-CMK-8 show aggregates without well-defined morphology. After the sulfonation (FIGURE 3.2 and FIGURE 3.3), the morphology remained similar, except for CMK-5-SA (FIGURE 3.2C) and CMK-5-PSA (FIGURE 3.3C), which lost their well-defined morphology. This is particularly interesting, considering that CMK-5-PSA is the only among the CMK-3 and CMK-5 catalysts that retained the periodicity of the mesopores organization.

The textural properties of the templated carbons and sulfonated carbons were studied by nitrogen physisorption at - 196 ºC (FIGURE A2.4 and TABLE 3.1). In general, the surface areas (S_{BET}) of the carbon supports are higher when pyrolyzed at 1000 ºC (except for carbons C-Chi and CMK-8). CMK-5-1000 displayed the highest surface area (1431 $m^2\ g^{-1}$). Among the samples pyrolyzed at 550 ºC, CMK-8-550 achieved the highest S_{BET} (982 $m^2\ g^{-1}$). C-Chi-550 and C-Chi-1000 display the lowest S_{BET} (540 and 391 $m^2\ g^{-1}$, respectively), which is expected since they were prepared from a non-periodic silica template.

The functionalization of Carbon-1000 with PSA led to approximately a 40 % reduction in the S_{BET}, except for CMK-5-PSA, which exhibited a 61 % reduction. As discussed earlier, for this sample, functionalization also resulted in a loosening of the morphology of the particles, although it maintained a well-organized arrangement of micropores in a hexagonal array.

The sulfonation of Carbon-550 led either to *ca.* 45 % increase in S_{BET} (CMK-3-SA and CMK-8-SA) or a decrease of 13 – 32 % (C-Chi-SA, CMK-5-SA, and S-CMK-8-SA).

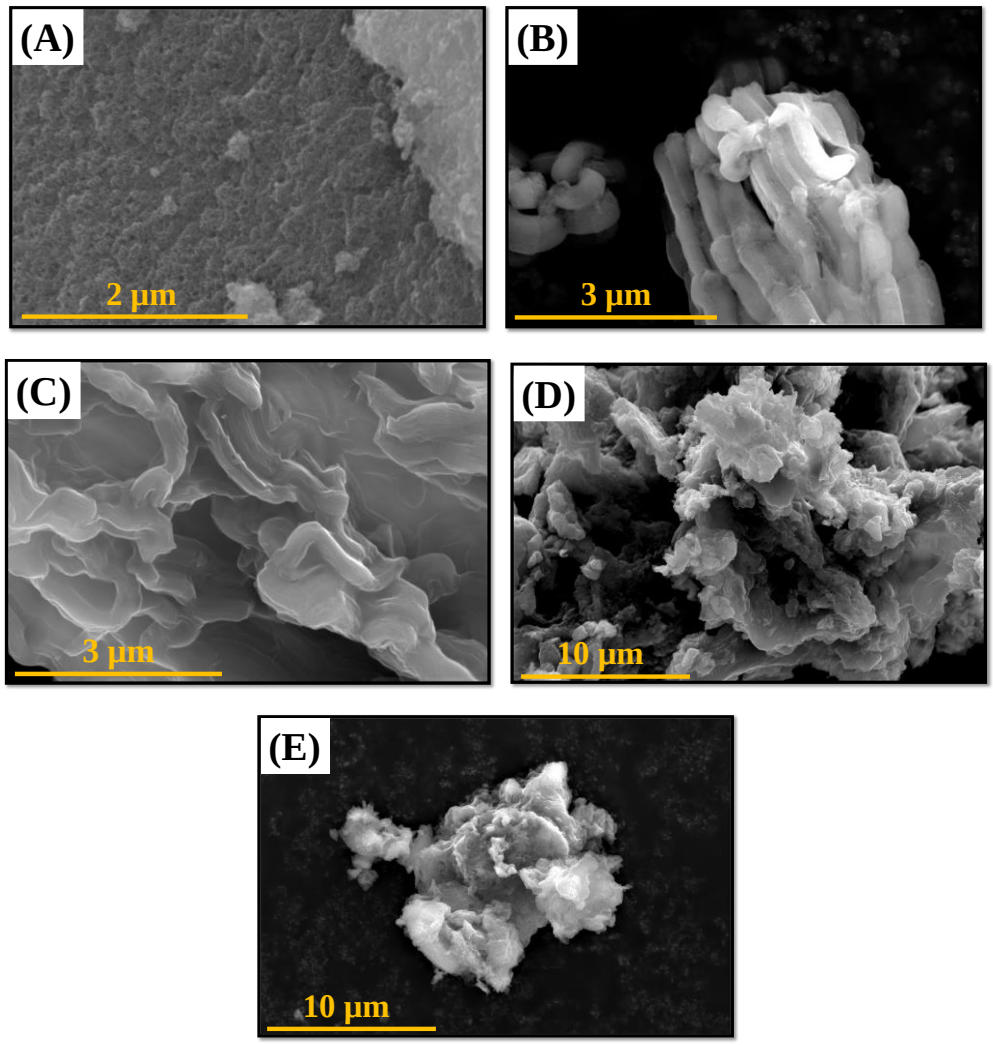

FIGURE 3.2 – SEM micrographs of the sulfonated carbons (A) C-Chi-SA, (B) CMK-3-SA, (C) CMK-5-SA, (D) CMK-8-SA, and (E) S-CMK-8-SA.

The samples from the C-Chi group display a broad pore size distribution ranging from *ca.* 3.5 – 27.0 nm (FIGURE A2.5A), which is expected considering that they were obtained from a silica matrix without periodic organization of the pores. For the CMK carbons (FIGURE A2.5B-D), the pyrolysis temperature had little effect on the pore sizes, and CMK-3 and CMK-5 present higher pore sizes than CMK-8 and S-CMK-8. In most cases, the functionalization led to less than 13 % change in the pore sizes (for more or less), except for C-Chi-550, in which the pore reduction was almost 40 % compared to C-Chi-SA. For C-Chi-1000, CMK-3-550, and CMK-3-1000, no significant

change in pore size was observed upon functionalization.

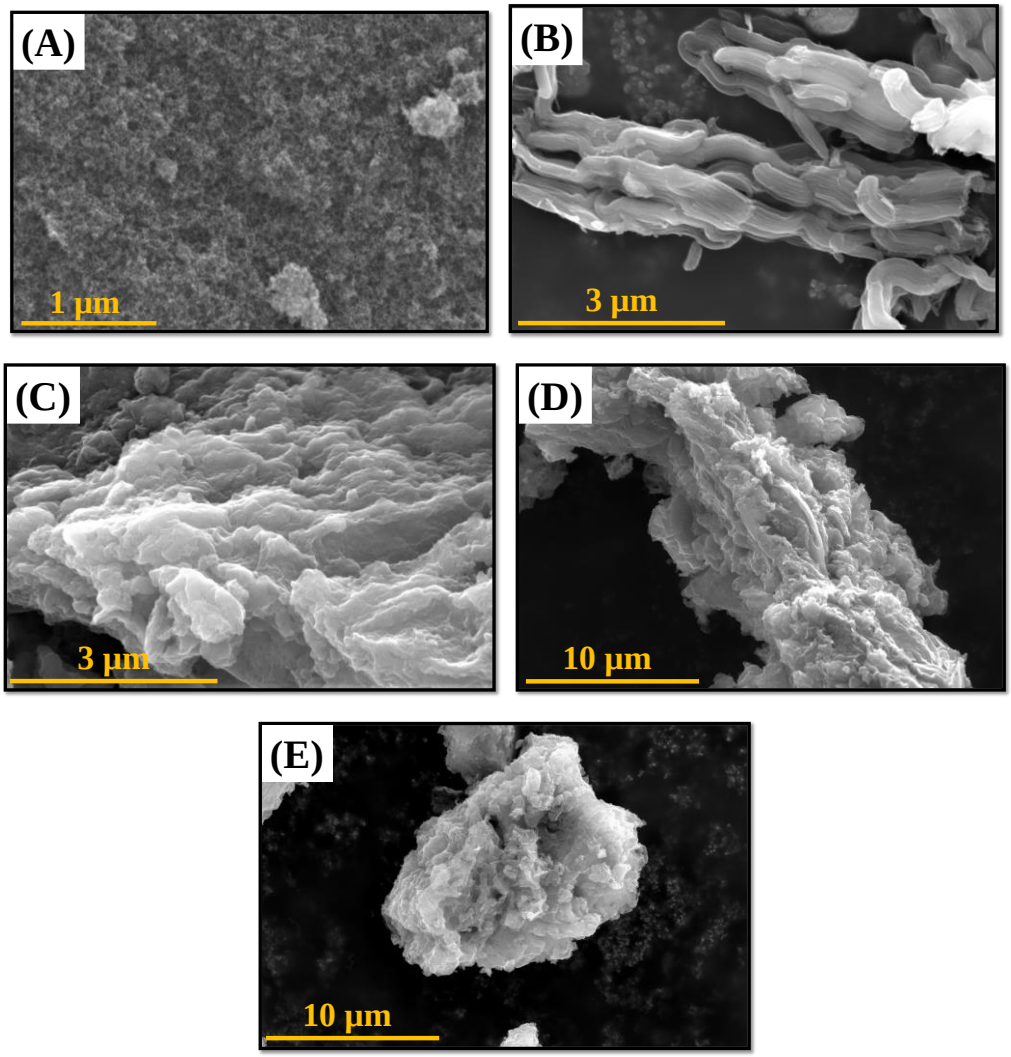

FIGURE 3.3 – SEM micrographs of the sulfonated carbons (A) C-Chi-PSA, (B) CMK-3-PSA, (C) CMK-5-PSA, (D) CMK-8-PSA and (E) S-CMK-8-PSA.

Raman deconvoluted spectra of the templated carbons (FIGURE A2.6) and sulfonated carbons (FIGURE 3.4) display the D*-band at 1230 cm^{-1}, related to defect-rich short carbon layers; the band between 1320 – 1350 cm^{-1}, due to defective graphene layers; the $D^{\#}$-band at 1500 cm^{-1}, associated to oxidized functional groups on the carbon surface; and finally the G-band between 1580 – 1600 cm^{-1}, related to ordered graphene layers [149,150].

TABLE 3.1 – Textural properties and relative intensity of Raman bands for the templated and sulfonated carbons.

Samples	Textural properties			Relative intensity of Raman bands		
	S_{BET} ($m^2\ g^{-1}$)[a]	V_{Total} ($cm^3\ g^{-1}$)[b]	D_P (nm)[c]	I_G/I_D	I_{D*}/I_D	$I_{D\#}/I_D$
C-Chi-550	540	2.30	18.8	0.88	0.48	0.73
C-Chi-SA	471	1.14	11.4	0.98	0.46	0.76
C-Chi-1000	391	1.84	19.7	0.95	0.23	0.41
C-Chi-PSA	228	1.05	19.6	0.93	0.18	0.32
CMK-3-550	956	0.85	4.2	1.31	0.36	0.33
CMK-3-SA	508	0.34	4.2	1.24	0.28	0.38
CMK-3-1000	1021	1.22	4.2	0.95	0.23	0.22
CMK-3-PSA	572	0.47	4.1	0.91	0.17	0.25
CMK-5-550	837	0.69	4.0	1.35	0.35	0.28
CMK-5-SA	626	0.39	4.5	1.28	0.23	0.30
CMK-5-1000	1431	1.40	4.2	0.96	0.20	0.19
CMK-5-PSA	555	0.43	3.9	0.91	0.14	0.20
CMK-8-550	982	0.98	3.6	1.26	0.37	0.35
CMK-8-SA	549	0.48	3.5	1.26	0.24	0.30
CMK-8-1000	909	1.06	3.4	1.00	0.19	0.19
CMK-8-PSA	534	0.54	3.7	0.95	0.14	0.22
S-CMK-8-550	743	0.91	3.2	0.95	0.20	0.52
S-CMK-8-SA	503	0.52	3.4	0.99	0.36	0.87
S-CMK-8-1000	870	1.11	3.4	0.92	0.18	0.22
S-CMK-8-PSA	519	0.56	3.0	0.81	0.17	0.24

[a] BET surface area. It was evaluated using adsorption data in a relative pressure range from 0.04 to 0.2.

[b] Total pore volume. It was estimated from the amount adsorbed at a relative pressure of about 0.99.

[c] Pore diameter.

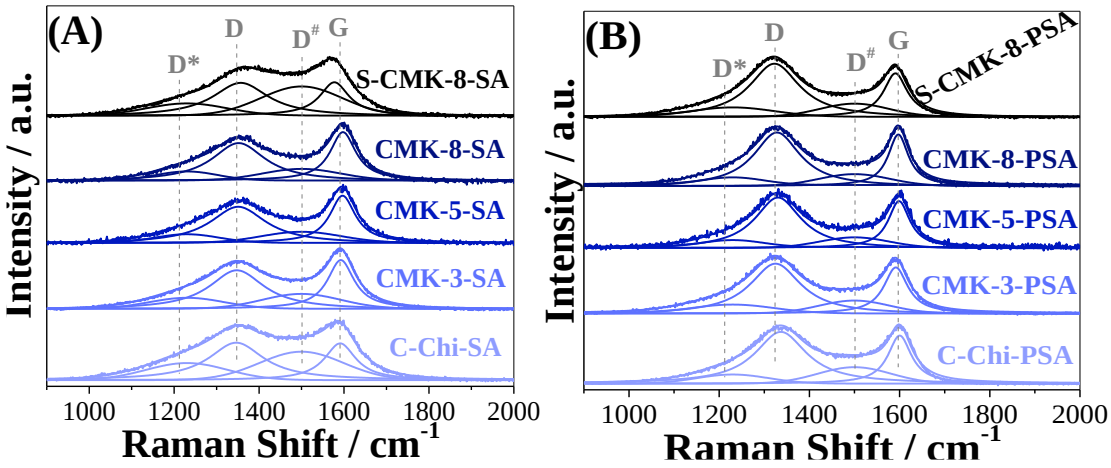

FIGURE 3.4 – Raman deconvoluted spectra of the sulfonated carbons functionalized with (A) SA and (B) PSA.

As shown in TABLE 3.1, the graphitization degree, given by the I_G/I_D ratio, decreases along with the increase in the pyrolysis temperature (except for C-Chi-1000). However, the concomitant reduction in the I_{D*}/I_D ratio suggests a favored aromatization of short carbon layers. In addition, increasing the pyrolysis temperature also leads to a less O-functionalized surface, as evidenced by the lowering of the Raman $I_{D\#}/I_D$ ratio and the CHNOS results in TABLE A2.2. Therefore, at higher pyrolysis temperatures, deoxygenation and the aromatization of short carbon layers occur. Yet, large carbonaceous structures may break down into smaller structures [148].

After the functionalization with sulfonic acid groups, the Raman of most samples indicates that the I_D*/I_D ratio decreases while the $I_{D\#}/I_D$ ratio increases. This suggests that sulfonation favored the production of longer graphene layers and increased the amount of oxidized functional groups, which is expected due to the grafting of sulfonic and phenylsulfonic acid species. The graphitization degrees for the Carbons-PSA decreased, while this parameter only decreased for CMK-3-SA, CMK-5-SA, and CMK-8-SA.

3.3.2 - Characterization: surface and composition

FTIR spectra of the templated carbons (FIGURE A2.7) reveal the presence of alcohols and carboxylic acid functionalities. In the case of C-Chi carbons, prepared by the pyrolysis of the nitrogen-based chitosan, a band at 1550 cm^{-1} and 1350 cm^{-1} assigned to pyridinic and graphitic groups, respectively, are present [151]. For S-CMK-8 carbons, prepared by the pyrolysis of the sulfur-based 2-thiophenemetanol, the FTIR analyses exhibit the presence of C-S stretching of the thiophene ring in the at 850 cm^{-1} [152] and sulfonic acid groups (bands at 1380 cm^{-1}, 1120 cm^{-1} and 1080 cm^{-1}) [58,153,154], indicating an intrinsic acidity in these materials. The templated carbons pyrolyzed at 1000 °C (FIGURE A2.7B) present a reduced amount of oxygen surface functionality compared to the samples pyrolyzed at 550 °C (FIGURE A2.7A), in alignment with the Raman (TABLE 3.1) and CNHOS (TABLE A2.2) results.

The effectiveness of the sulfonation with sulfuric acid was confirmed by FTIR (FIGURE 3.5A), evidenced by the band at *ca.* 1040 cm^{-1} due to sulfonic acid groups. Furthermore, bands due to O-H and C=O increased in intensity, while the band due to C-O signals became narrower. For the PSA functionalized carbon (FIGURE 3.5B), typical FTIR bands for phenylsulfonic acid were observed (1180 cm^{-1}, 1035 cm^{-1}, 1005 cm^{-1}, and 830 cm^{-1}) [155–157].

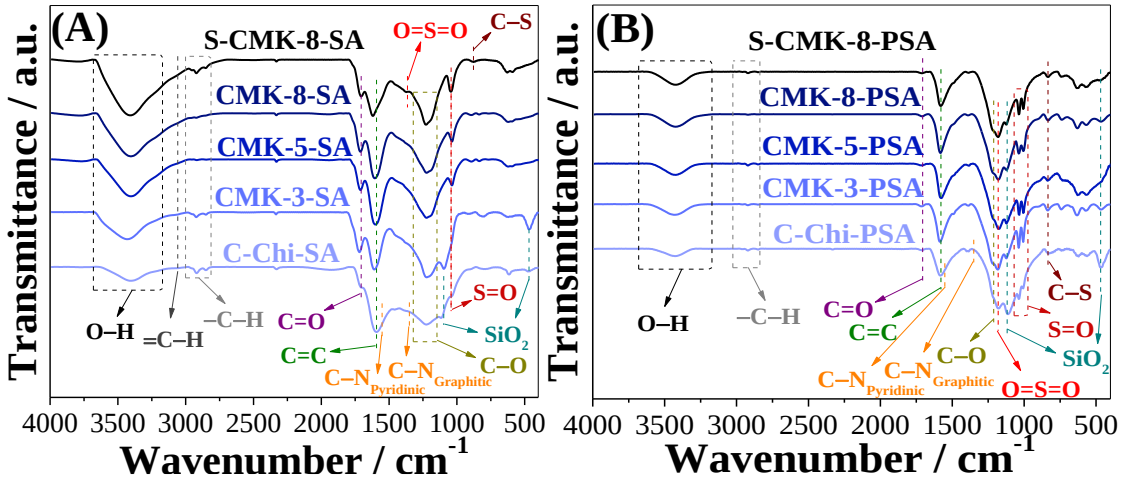

FIGURE 3.5 – FTIR spectra of the sulfonated carbons functionalized with (A) SA and (B) PSA.

The sulfur species on the functionalized samples were further studied by Sulfur XPS (FIGURE A2.8-10). Among the carbon supports, only S-CMK-8-550 and S-CMK-8-1000 displayed sulfur species before sulfonation, since ρ-toluenesulfonic acid and 2-thiophenemethanol were used as carbon sources for their synthesis. These samples predominantly exhibit the S 2p spectrum signal at 166 – 162 eV, attributed to thiol or thioether [144,158]. S-CMK-8-1000 also shows a signal at 168.0 – 170.0 eV, indicating the presence of sulfonic acid groups ($-SO_3H$) [159].

The sulfur XPS for Carbon-SA and Carbon-PSA (FIGURE A2.8-10) confirmed the presence of sulfonic acid groups (BE 168.0 – 170.0 eV) [159]. The deconvolution of the *S 2*$p_{3/2}$ and *S 2*$p_{1/2}$ signals provided a good fit for Carbon-PSA (FIGURE A2.9), while for Carbon-SA, the fit was only satisfactory. Further exploration of the deconvolution led us to seek additional bands (FIGURE A2.11-13). A better fit was achieved with the presence of bands in the ranges of BE 167.0 – 169.0 eV and 166.0 – 167.5 eV, typically attributed to sulfone (-C-(O=S=O)-C-) and sulfoxide species (-C-(S=O)-C-) [160]. Although the presence of these species is unlikely and has not been reported for sulfonated carbons, XPS suggests the potential existence of other sulfur-containing species that we could not properly identify using spectroscopic techniques.

The surface acidity of the acidic materials was evaluated by potentiometric titration (FIGURE A2.14-17). The Gaussian deconvoluted curves in the first derivative calculations reveal two different inflection points, indicating the presence of distinct families of acid sites. The first inflection point is due to the stronger acid sites, i.e., the sulfonic acid groups. In comparison, the second can be assigned to weaker acid sites, i.e., the surface carboxylic acid, alcohol, and phenol groups [160]. From those curves, the concentration of total (N_T), stronger (N_S), and weaker (N_W) acid sites, as well as the ratio between stronger and weaker acid sites (N_S/N_W), were calculated (FIGURE 3.6).

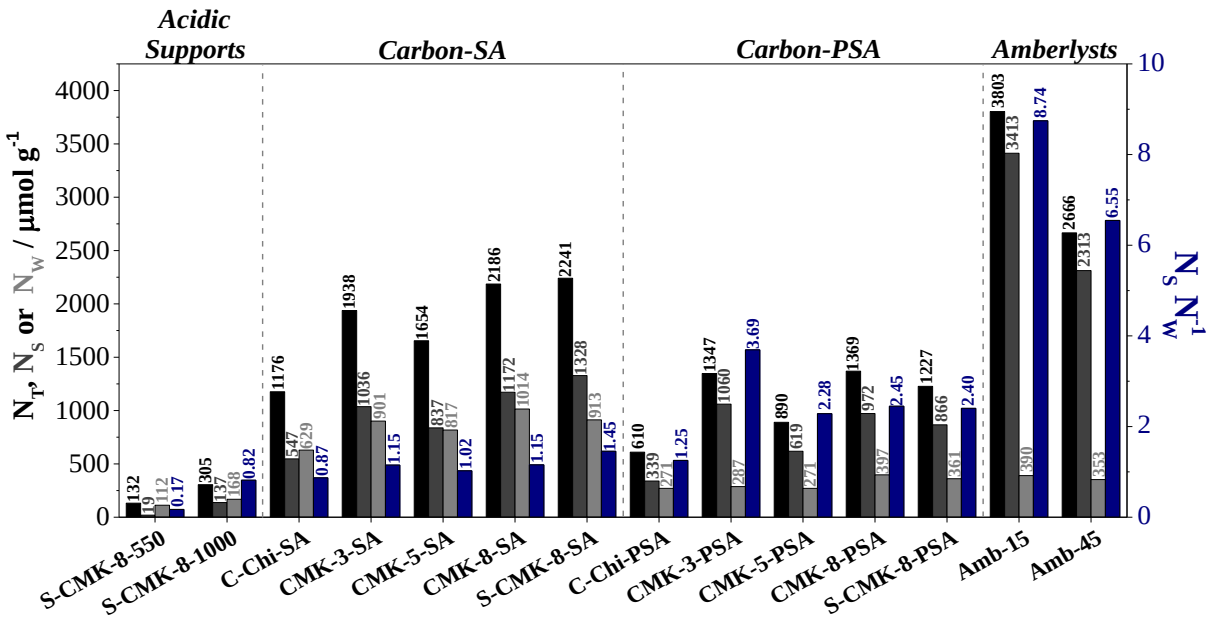

FIGURE 3.6 – Concentration of total (N_T), stronger (N_S), and weaker (N_W) acid sites and the ratio between stronger and weaker acid sites (N_S/N_W) for the acidic materials by potentiometric titration.

Among the templated carbons, strong acid sites are only observed for S-CMK-8-550 and S-CMK-8-1000 since p-toluenesulfonic acid as a carbon source for the synthesis of these materials.

Regarding the sulfonated carbons, strong acid sites (*Ns*) were found in all samples, and in general, comparing the same carbon structure, the sulfonation with fuming sulfuric acid was more efficient. As discussed above, the presence of weaker acid sites (*Nw*) arises from surface oxygenated species and is significantly higher in the Carbon-SA samples.

For the sake of comparison, the commercial resins Amberlyst-15 (Amb-15) and Amberlyst 45 (Amb-45) were also titrated, and the results display significantly higher acid site loading and concentration of stronger acid sites than the catalysts prepared herein. In any case, catalysts with different N_S/N_W ratios were observed in this study (FIGURE 3.6).

Normalizing the acid sites by the surface area (TABLE A2.1) reveals that the sulfonation with fuming sulfuric acid can lead to a higher concentration

of total and weaker acid sites per m^2. As for the density of *Ns*, they vary between 1.11 and 2.64 μmol m^{-2}. Among the sulfonated carbons, S-CMK-8-SA displays the highest and CMK-5-PSA the lowest concentration of acid sites per m^2.

The chemical composition of the templated carbons and sulfonated carbons was determined by a combination of CHN analysis, potentiometric titration, XPS spectra for *S 2*p, and thermogravimetric analysis (TGA) in an oxidant environment (TABLE A2.2). The quantification of the sulfonic acid groups by titration and the contribution of those groups determined by XPS allowed an estimation of the sulfur concentration in the samples. The remaining silica template was evaluated by TGA in an oxidant environment (FIGURE A2.18), granting the calculation of the silicon concentration (less than 6 wt. % in all samples).

3.3.3 - Catalytic studies

The unmodified templated carbons display low activity for converting fructose and xylose (FIGURE A2.20), except for S-CMK-8-550 and S-CMK-8-1000. For instance, S-CMK-8-1000 produced HMF and furfural with *ca*. 30 % of selectivity at *ca.* 30 % of conversion. It is noteworthy to mention that, although fructose and xylose are converted by the same type of active sites, previous studies have demonstrated that a catalyst efficient in converting one of the monosaccharides may not necessarily be effective for the other [33,61].

As a general trend, the Carbons-PSA have comparable performance to the Amberlysts and are more active and selective than the Carbons-SA for both dehydration of fructose and xylose (FIGURE 3.7).

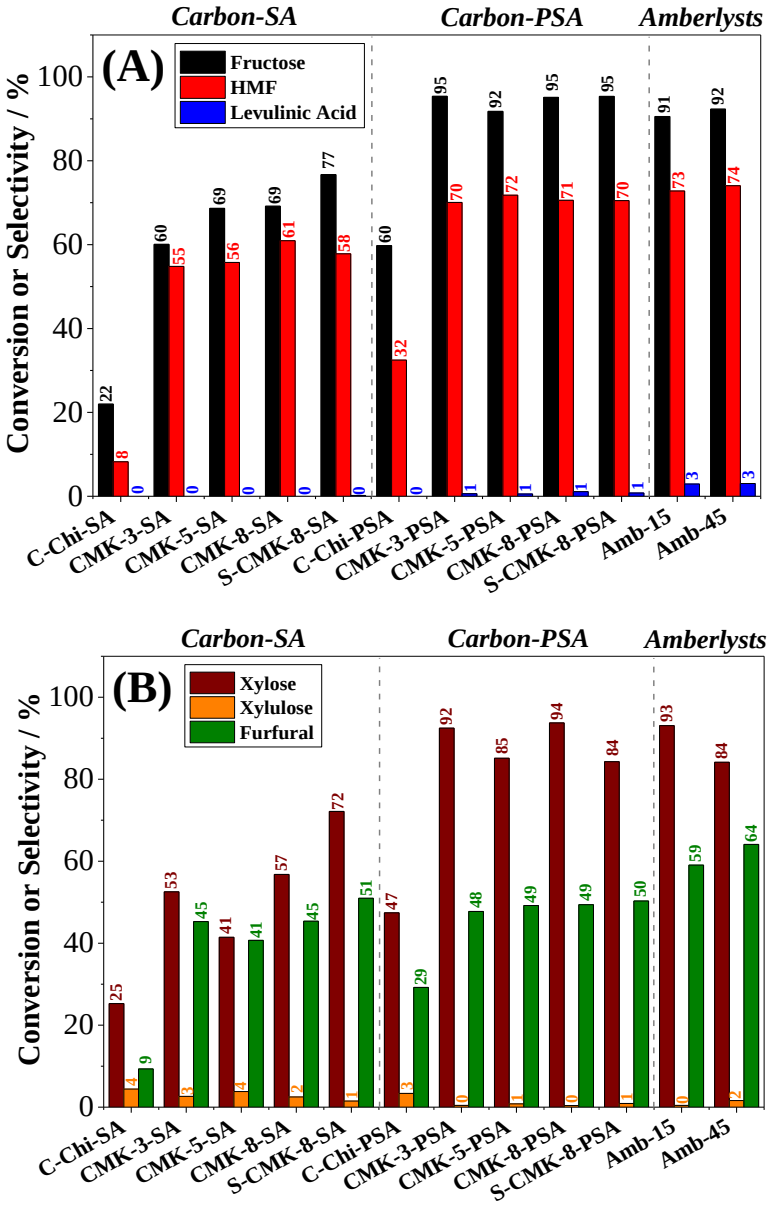

FIGURE 3.7 – Catalytic screening of the sulfonated carbons and Amberlysts for the conversion of (A) fructose into HMF and (B) xylose into furfural at 130 °C and 160 °C, respectively, in THF/H_2O = 4/1, 1 h of reaction and 50 mg of the catalyst (catalyst/substrate mass ratio = 1.25). Mass balance is shown in FIGURE A2.19.

FIGURE 3.8 shows a correlation between Furan Yield and the *Ns/Nw* ratio. The trend is particularly relevant since it comprises catalysts with different structures, porosity, surface areas, surface oxygen loadings, and chemical composition. The yield for HMF increases along with the *Ns/Nw* ratio, reaching a maximum at *ca.* 2 (FIGURE 3.8A), while the furfural yield increases along with

the *Ns/Nw*, but the effect is more pronounced at *Ns/Nw* < 2 (FIGURE 3.8B). Recent studies suggested a near-linear correlation between furfural yield and the total acid site loading (*Ns* + *Nw*) [133]. Our results show that such a correlation is only valid within a specific group of catalysts and cannot be considered general. As shown in FIGURE A2.21, a trend is found for Carbon-SA, and a separate trend is seen for Carbon-PSA.

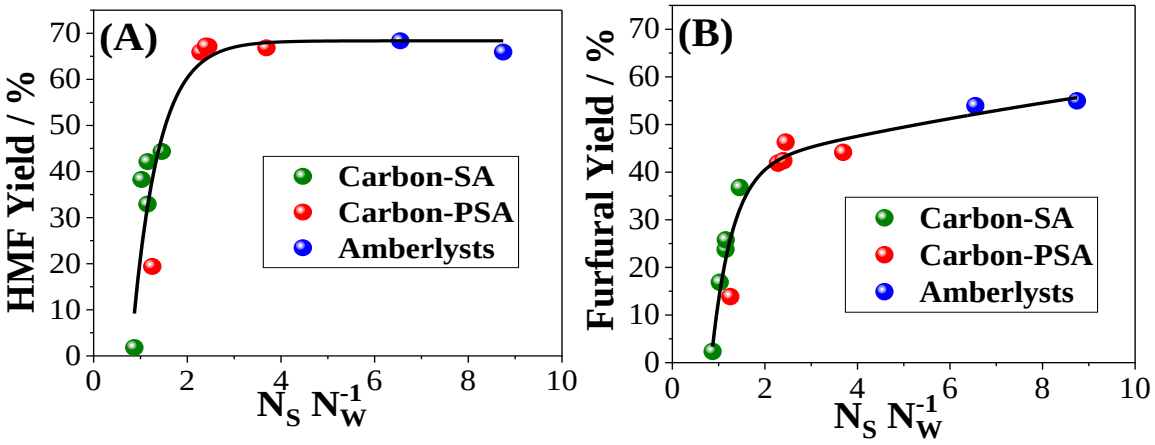

FIGURE 3.8 – Correlation of the ratio between stronger and weaker acid sites with the yields of (A) HMF and (B) furfural of the sulfonated carbons and Amberlysts.

Therefore, the correlation between Furan Yield and the ratio between strong and weak acid sites (*Ns/Nw*), in addition to previous DFT studies [136], suggests that the reaction occurs in the interfacial region between both sites. Indeed, previous studies for ethanol conversion suggest that for reactions taking place in the interface between sites, the effectiveness of the catalyst should correlate with the ratio between the two sites [161].

Further analyzing the activity per site revealed a volcano-like plot for the turnover number of furan (TON_{Furan}) as a function of the N_S/N_W ratio (FIGURE 3.9). For both HMF and furfural production, the highest TON_{Furan} is observed for catalysts with the ratio between stronger and weaker acid sites between 2 – 4, indicating that weaker acid sites should account for 20 – 33 % of the total acid

sites of the catalyst to optimize the production of platform molecules per acid site. Below these ratios, the lack of stronger acid sites, which are active in the dehydration, reduces the TON_{Furan}, as well as the absence of weaker acid sites at higher ratios, which are adjacent to stronger sites and assist with additional hydrogen bonds [136]. These results confirm the enhanced synergism between these sites in the production of furan per acid site.

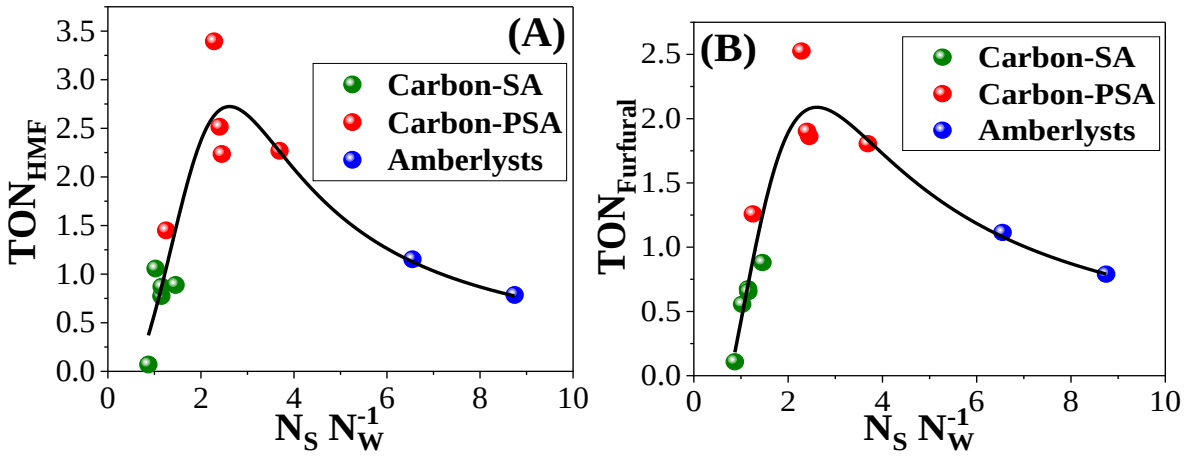

FIGURE 3.9 – Correlation of the ratio between stronger and weaker acid sites with the (A) TON_{HMF} and (B) $TON_{Furfural}$ of the sulfonated carbons and Amberlysts.

Combining the results from FIGURE 3.8 and FIGURE 3.9, one can conclude that $N_S/N_W < 2$ affects both furan yield and the activity per site (TON_{Furan}), while $N_S/N_W > 4$ has impacts predominantly on the TON_{Furan} (although in the xylose conversion the yield is also affected at a minor extent).

Our findings rationalize the empiric observations reported before claiming a collaborative (or synergistic) effect between the strong and weak acid sites for converting biomass-derived sugars into furans [130–132,135,136]. Previous studies have proposed that mainly phenol and carboxylic acids present on the surface of acid carbon and organic resins have a synergic effect when adjacent to the strong acid site [130–132,135,136]. Although the reaction mechanism requires further understanding, computation studies propose that the

weak acid sites mainly act to improve the energy of adsorption of the monosaccharide and the stability of reaction intermediates [136]. The results shown herein reveal the importance of the N_S/N_W ratio, and the quantitative analysis provided shall serve as a guide for future studies on the design of catalysts for these reactions.

3.4 - Conclusions

Sulfonated carbons were derived from various templated mesoporous carbons using distinct sulfonation methods, resulting in catalysts with varying concentrations of stronger acid sites (sulfonic acid groups) and weaker acid sites (surface carboxylic acid, alcohol, and phenol groups). These catalysts, alongside two commercial Amberlysts, were employed in producing 5-hydroxymethylfurfural (HMF) from fructose and furfural from xylose.

Our findings reveal a critical role of the ratio between stronger and weaker acid sites (N_S/N_W) in controlling catalytic performance. Notably, the yields of HMF and furfural exhibit an exponential increase with N_S/N_W. Moreover, a distinctive volcano-like plot emerges for the Turnover Number (*TON*) of product formation as a function of N_S/N_W, reaching a maximum between 2 – 4. These results provide experimental evidence supporting the involvement of weaker acid sites in the reaction mechanism of biomass-derived monosaccharides dehydration.

3.5 - Acknowledgments

This work has been funded by the FAPESP Young Investigator Award (2016/02128-2). J.M.R.G thanks CNPq for the productivity fellowship (303640/2019-7). J.L.V thanks FAPESP for the PhD fellowship (2019/02132-8 and 2020/04109-0). The authors also thank FAPESP (2018/01258-5 2016/02128-2, 2019/02132-8, 2020/04109-0, and 2022/02222-0), the Brazilian S&T&I

Ministry through SISNANO (CNPq 442575/2019-0), INCT Programs (CNPq 406925/2022-4), the Brazilian Renewable Energies (BRE) of UNICAMP (21/14442-1, 17/11986-5, 17/11958-1, 15/50093-0, 14/02163-7), the National Nanotechnology Laboratory (LNNano) and the National Center for Energy and Materials Research (CNPEM) (proposal # 20231022). The authors extend their thanks to Prof. Hudson Giovani Zanin for generously allowing the use of his facilities for material characterization, and to Manuel Jonathan Pinzón-Cárdenas for his valuable assistance with the XPS and N_2 physisorption analyses.

4 - CHAPTER 3: ION-EXCHANGED BIFUNCTIONAL CARBON ACIDS FOR THE DIRECT CONVERSION OF GLUCOSE AND XYLOSE INTO 5-HYDROXYMETHYLFURFURAL AND FURFURAL

4.1 - Introduction

In the first chapter of this thesis, we have demonstrated that the Lewis/Brønsted acid site ratio (*L/B*) drives the overall catalytic activity of HMF and furfural production from glucose and xylose, respectively. High *L/B* ratios exhibit a linear correlation with increased reaction rates for HMF and furfural production, highlighting the significance of balanced surface acidity [33]. A promising method for controlling the *L/B* ratio involves the partial ion-exchange of the Brønsted acid sites of a pure Brønsted acid catalyst with metallic cations, which exhibit good Lewis acidity for isomerization [35,37]. For example, in a study elsewhere [35], a partial ion-exchange of the Brønsted acid sites of Amberlyst-15 with Fe^{3+} was performed for the production of HMF from glucose. According to this study, the catalysts with 10 % of their Brønsted acid sites exchanged with Fe^{3+} (10%-Fe/AR) presented the optimal *L/B* ratio for the production of HMF (68 % HMF selectivity at 160 °C in a biphasic solvent system of water, THF, and NaCl). However, despite achieving promising results, this catalyst demonstrated low stability in catalytic reusability tests, likely due to the operational temperature of Amberlyst-15 being 120 °C, whereas the selected reaction temperature was 160 °C, suggesting degradation of the resin and consequent leaching of acid sites.

In the second chapter of this thesis, we prepared various sulfonated carbons with varying concentrations of stronger acid sites (sulfonic acid groups) and weaker acid sites (surface carboxylic acid, alcohol, and phenol groups) [62]. These catalysts, along with two commercial Amberlysts (15 and 45), were employed in the production of HMF and furfural from fructose and xylose,

respectively. Our findings reveal a critical role of the ratio between stronger and weaker acid sites (N_S/N_W) in these reactions. The main result of this study was a distinctive volcano-like plot for the Turnover Number (*TON*) of platform molecule formation as a function of N_S/N_W, reaching a maximum between 2 – 4, indicating that weaker acid sites should account for 20 – 33 % of the total acid sites of the catalyst to optimize the production of platform molecules per acid site. This range was achieved for four hand-made sulfonated carbons (CMK-3-PSA, CMK-5-PSA, CMK-8-PSA, and S-CMK-8-PSA), demonstrating superior performance compared to the Amberlysts studied. Consequently, it would be interesting to perform the previously mentioned partial ion-exchange technique using one of the best hand-made sulfonated carbons, as well as, for the sake of comparison, an Amberlyst catalyst with a higher operational temperature than Amberlyst-15, such as Amberlyst-45, which has an operational temperature of 170 °C.

In addition to the metallic cation Fe^{3+}, another promising metallic cations for isomerization will also be studied. For instance, Gallo *et al.* [36] proposed methodologies for the direct synthesis of Sn-containing mesoporous silicas with tin loadings between 1.5 and 4.5 % in the isomerization of glucose to fructose. The results obtained showed that the sample containing 3.0 % of Sn exhibited the highest selectivity to fructose (74 % at 20 % glucose conversion at 110 °C). For this reason, the Sn^{4+} cation will also be studied herein.

Another study [37] prepared various metal ion-exchanged montmorillonite catalysts for the conversion of glucose to methyl levulinate in methanol, a reaction dependent on both Lewis and Brønsted acid sites: the Lewis acid sites isomerize glucose into fructose, which is dehydrated to HMF and hydrolyzed to methyl levulinate and methyl formate by Brønsted acid sites. The results showed that the catalysts with the best balance between Lewis and Brønsted acid sites were Al^{3+} and Cu^{2+} exchanged montmorillonite (yielding

about 60 % methyl levulinate at 220 °C). Additionally, the aluminum catalyst exhibited very good stability, even after 5 cycles of reuse. Both metallic cations Al^{3+} and Cu^{2+} will also be studied herein.

Rare-earth metal triflates have been well established as potent environmentally-benign Lewis acid catalysts with good potential for isomerization reactions [38]. Computational studies showed that the rare-earth metallic cations with the highest oxophilicity, i.e., the better Lewis acidity, are Sc^{3+} and Yb^{3+} (2.37 and 2.09, respectively), mainly due to their small ionic radii. Both metallic cations will also be studied herein.

Therefore, the main objective of this work is to prepare ion-exchanged carbon acid catalysts with different *L/B* ratios by performing a partial ion-exchange of the Brønsted acid sites of a hand-made sulfonated carbon (CMK-8-PSA) and Amberlyst-45 (Amb-45) with the metallic cations Al^{3+}, Sc^{3+}, Fe^{3+}, Cu^{2+}, Sn^{4+}, and Yb^{3+} for the conversion of glucose and xylose into HMF and furfural, respectively.

4.2 - Materials and Methods

4.2.1 - Sulfonated carbon catalysts

The synthesis of CMK-8-PSA sulfonated carbon was detailed in section 3.2.3, while Amb-45 was bought at Sigma-Aldrich.

4.2.2 - Synthesis of the ion-exchanged carbon acid catalysts

The calculation of exchanged Brønsted acid sites of the Brønsted acid catalysts was based on the concentration of stronger acid sites determined by potentiometric titration (FIGURE 3.6). The synthesis of the ion-exchanged carbon acid catalysts involved a process conducted in a boiling flask containing a mixture of the metallic salt, the Brønsted acid catalyst, and an alcohol solvent (1 g of the Brønsted acid catalyst per 125 mL of alcohol solvent) under stirring and reflux

conditions for 24 hours. For the metallic cations Al^{3+} [from $AlCl_3 \cdot 6H_2O$], Sc^{3+} [from $Sc(SO_3CF_3)_3$], Fe^{3+} [from $FeCl_3 \cdot 6H_2O$], Cu^{2+} [from $Cu(NO_3)_2 \cdot 2.5H_2O$] and Sn^{4+} [from $SnCl_4 \cdot 5H_2O$], ethanol was used as alcohol solvent. For Yb^{3+} [from $Yb(SO_3CF_3)_3 \cdot XH_2O$], in turn, methanol was selected, since its salt was not well soluble in ethanol. Subsequently, the resulting product was filtered, washed with the respective alcohol solvent and water, and finally dried at 80 °C for 1.5 hours. The nomenclature of the bifunctional catalyst follows the format: "Percentage of exchanged Brønsted acid sites considering that 1 Brønsted acid site turns into 1 Lewis acid site (X) – Metallic cation (M) – Brønsted acid catalyst nomenclature".

4.2.3 - Characterizations

So far, we have only performed Scanning Electron Microscopy with Energy Dispersive X-Ray Spectroscopy (SEM-EDS). The instrument employed for this purpose was a MEV INSPECT EBSD with an operating voltage of 25.0 kV. Quantification was achieved using the EDAX PhiZAF Quantification method.

4.2.4 - Catalytic studies

Catalytic tests were carried out in 15 mL thick-glass reactors, each containing 2.00 g of a solution comprising 2 wt. % glucose or xylose in tetrahydrofuran with 20 wt. % water (THF/H_2O = 4/1), along with the catalyst. The reactors were placed in an oil bath preheated to 130 °C or 160 °C for glucose or xylose dehydration, respectively, and stirred at 300 rpm. The reactions were quenched by cooling the reactors in an ice bath. The reaction mixtures were analyzed by high-performance liquid chromatography (HPLC) in a Shimadzu LC-10/20 chromatograph equipped with either a Phenomenex Rezex RPM Monosaccharide (300 × 7.8 mm) column at 80 °C using H_2O as the mobile phase for the separation of glucose, mannose, fructose and HMF; or a Bio-Rad Aminex® HPX-87H column (300.0 mm x 7.8 mm) using 0.005 mol L^{-1} aqueous

H_2SO_4 as mobile phase for the separation of xylose, its isomers and epimers, and furfural. Quantification of the species was performed using calibration curves constructed with commercial standards. HMF and furfural was analyzed with a diode array detector at 254 nm and monosaccharides, using a refraction index detector operating at 40 °C.

The conversion, selectivity, and mass balances were calculated by the equations:

$$Conversion = \left(\frac{mol\ precursor_{initial} - mol\ precursor_{final}}{mol\ precursor_{initial}}\right) * 100$$

$$Selectivity = \left(\frac{mol\ product_{final}}{mol\ precursor_{initial} - mol\ precursor_{final}}\right) * 100$$

$$Mass\ balance_{Glucose\ conversion} = \left(\frac{mass\ glucose_{final} + mass\ mannose_{final} + mass\ fructose_{final} + mass\ HMF_{final}}{mass\ glucose_{initial}}\right) * 100$$

$$Mass\ balance_{Xylose\ conversion} = \left(\frac{mass\ xylose_{final} + mass\ xylulose/lyxose_{final} + mass\ arabinose/ribulose_{final} + mass\ furfural_{final}}{mass\ xylose_{initial}}\right) * 100$$

4.3 - Results and Discussion

4.3.1 - Catalytic screening

Considering that our goal is to produce catalysts with both Brønsted and Lewis acidity, we first decided to perform the partial ion exchange of 40 % of the Brønsted acid sites of CMK-8-PSA and Amb-45. Their catalytic screening in the conversion of glucose into HMF (FIGURE 4.1) initially showed 15 – 30 % glucose conversion and the production of fructose and HMF, as expected, along with mannose, an epimer of glucose that is produced by Lewis acid catalysis and is undesired for producing HMF in low yields [36]. On the other hand, for the conversion of xylose into furfural (FIGURE 4.2), the catalysts 40%-M-Amb-45 are more active than 40%-M-CMK-8-PSA (15 – 32 % and 18 – 45 % of xylose conversion, respectively). The products obtained were furfural and the isomers

xylulose + lyxose and arabinose + ribulose (our chromatography system does not separate them), which are produced by isomerization and/or epimerization of xylose by Lewis acid catalysis [39,162]. Unlike the glucose case, these isomers can be converted to furfural by Brønsted acid catalysis with similar selectivities. However, the reaction rates are higher for the ketopentoses xylulose and ribulose than for the aldoses xylose and arabinose [24].

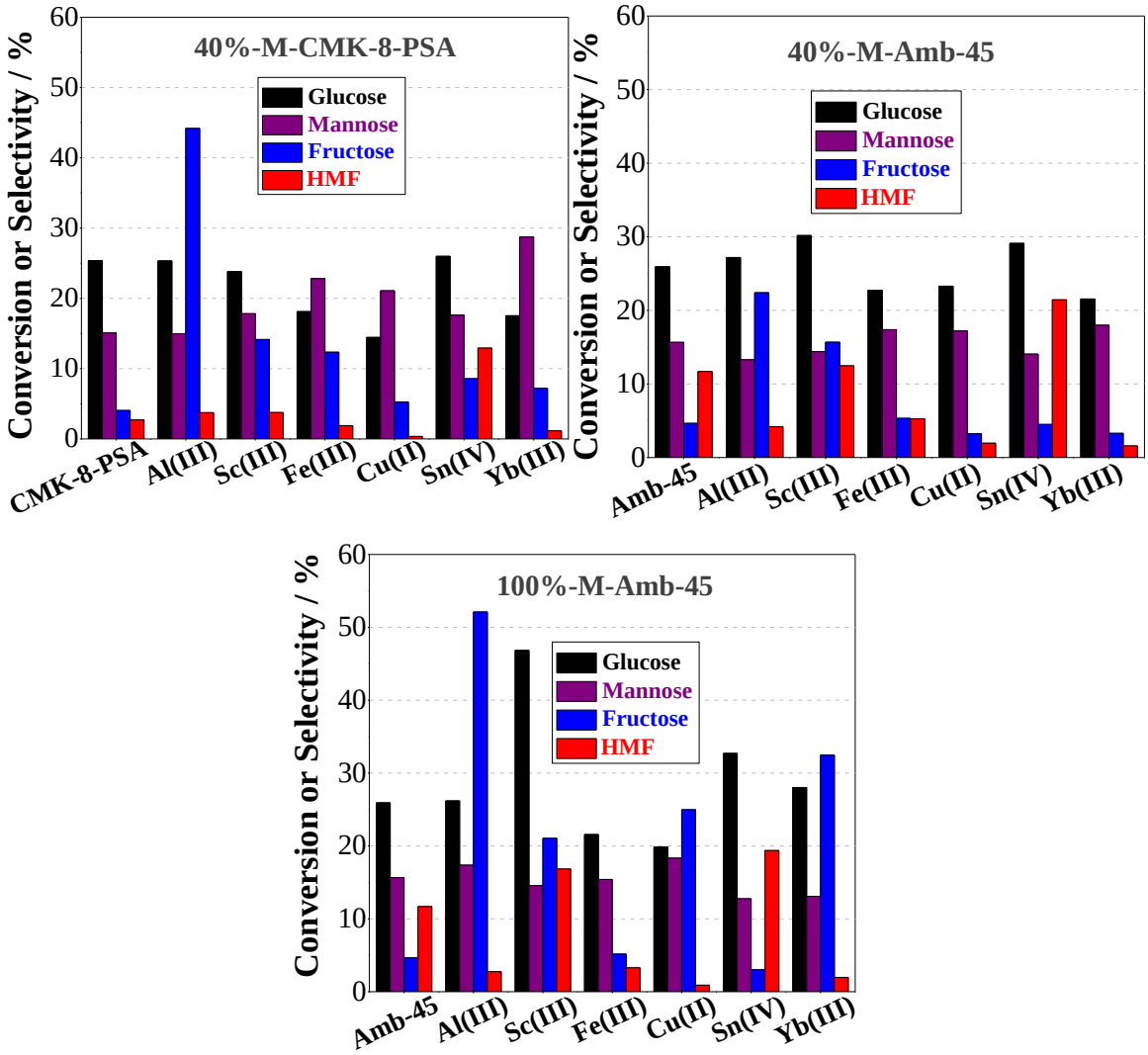

FIGURE 4.1 – Catalytic screening of the catalysts 40%-M-CMK-8-PSA, 40%-M-Amb-45, and 100%-M-Amb-45 in the conversion of glucose into HMF, at 130 °C, in THF/H_2O = 4/1, 2 h of reaction, and 20 mg of catalyst (catalyst/substrate mass ratio = 0.50).

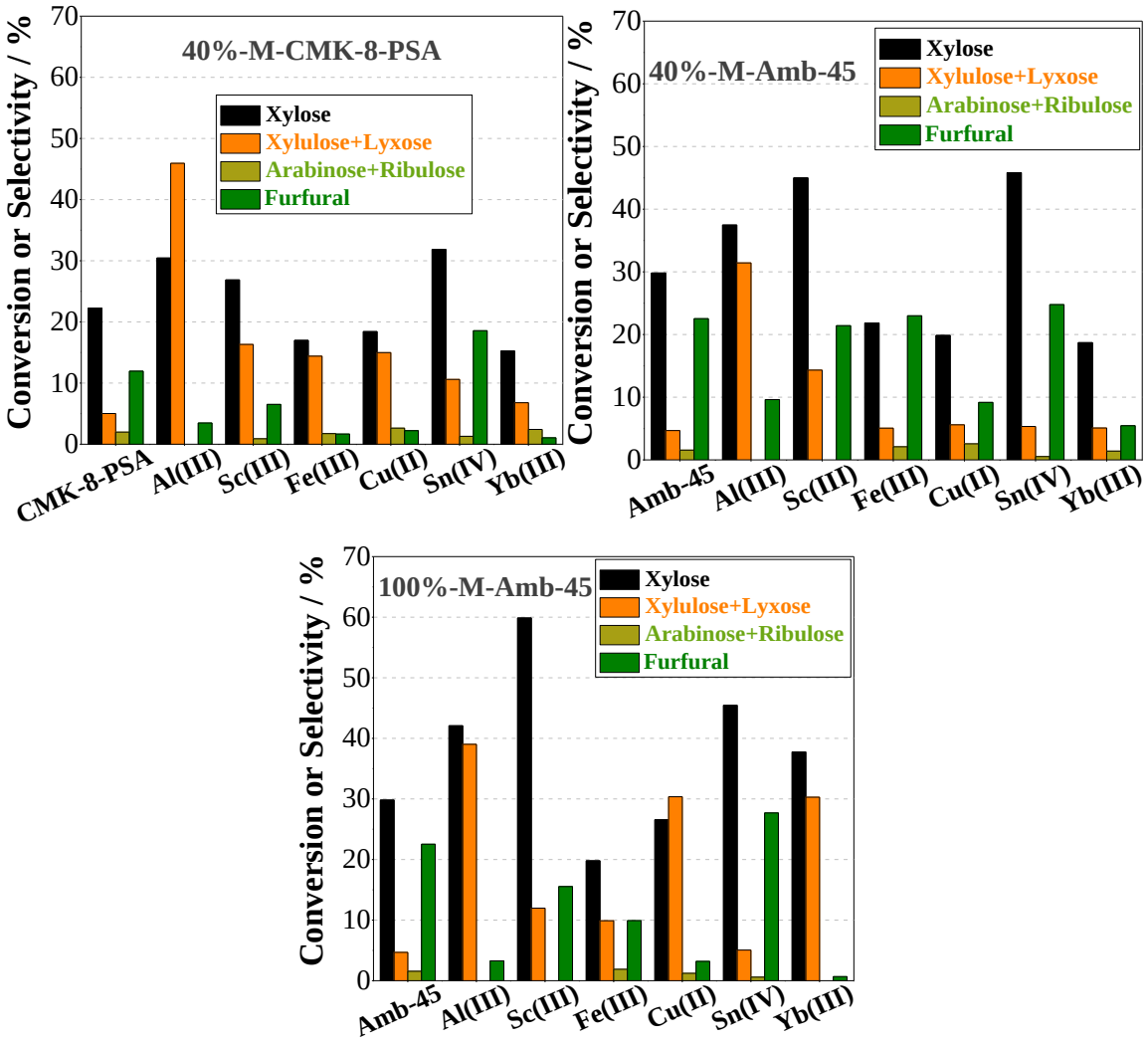

FIGURE 4.2 – Catalytic screening of the catalysts 40%-M-CMK-8-PSA, 40%-M-Amb-45, and 100%-M-Amb-45 in the conversion of xylose into furfural, at 160 °C, in THF/H_2O = 4/1, 30 min of reaction, and 10 mg of catalyst (catalyst/substrate mass ratio = 0.25).

Observing the effect of the metallic cations in both reactions, it is clear that the catalysts containing Fe^{3+}, Cu^{2+}, and Yb^{3+} exhibited the worst results compared to the pure CMK-8-PSA or Amb-45, showing lower monosaccharide conversion and platform molecule selectivity. On the other hand, the catalysts with Al^{3+} favored the production of the isomers fructose and xylulose + lyxose in equal or higher conversions than the pure Brønsted catalysts. In this case, 40%-Al(III)-CMK-8-PSA exhibited approximately 45 % selectivity for fructose and xylulose + lyxose, and 40%-Al(III)-Amb-45 exhibited 23 % and 32 % selectivity,

respectively. The catalysts with Sc^{3+} were highly active, producing both isomers and platform molecules in equal or higher conversions than the pure Brønsted catalysts. Lastly, the catalysts with Sn^{4+} were the best for the production of platform molecules, achieving HMF selectivities of 12 % and 21 % for 40%-Sn(IV)-CMK-8-PSA and 40%-Sn(IV)-Amb-45, and furfural selectivities of 18 % and 35 %, respectively. These results indicate that these materials present *L/B* ratio for platform molecule production, performing initially the isomerization, followed by the dehydration of the isomer into HMF and furfural.

As some metallic cations did not have any effect on the reaction with 40 % exchanged Brønsted acid sites, we decided to exchange 100 % of these sites. So far, this experiment was performed only for M-Amb-45 (FIGURES 4.1 and 4.2). Interestingly, the increase in the percentage of exchanged Brønsted acid sites did not change the conversion of glucose (with the exception of 100%-Sc(III)-Amb-45, achieving 47 % conversion); however, it enhanced the xylose conversions for the catalysts with Al^{3+} (42 %), Sc^{3+} (60 %), Cu^{2+} (27 %), and Yb^{3+} (38 %). It was also observed that the selectivity for fructose and xylulose + lyxose increased for the catalysts with Al^{3+}, Cu^{2+}, and Yb^{3+} (41 %, 26 %, and 39 % for fructose; and 39 %, 30 %, and 30 % for xylulose + lyxose, respectively), which was expected due to the higher theoretical amount of Lewis acid sites added. On the other hand, the catalysts with Sc^{3+}, Fe^{3+}, and Sn^{4+} had practically the same distribution of products as their respective catalysts with 40 % exchanged Brønsted acid sites (FIGURES 4.1 and 4.2), indicating no effect from the additional Lewis acid sites. As the catalyst 100%-Fe(III)-Amb-45 still presented worse results than the Amb-45, we decided not to further study this cation for the M-Amb-45 catalysts. Interestingly, this cation in combination with Amb-15 presented very good results for HMF production (68 % HMF selectivity) [35], contrary to the results obtained herein. More studies and characterization must be done to investigate this.

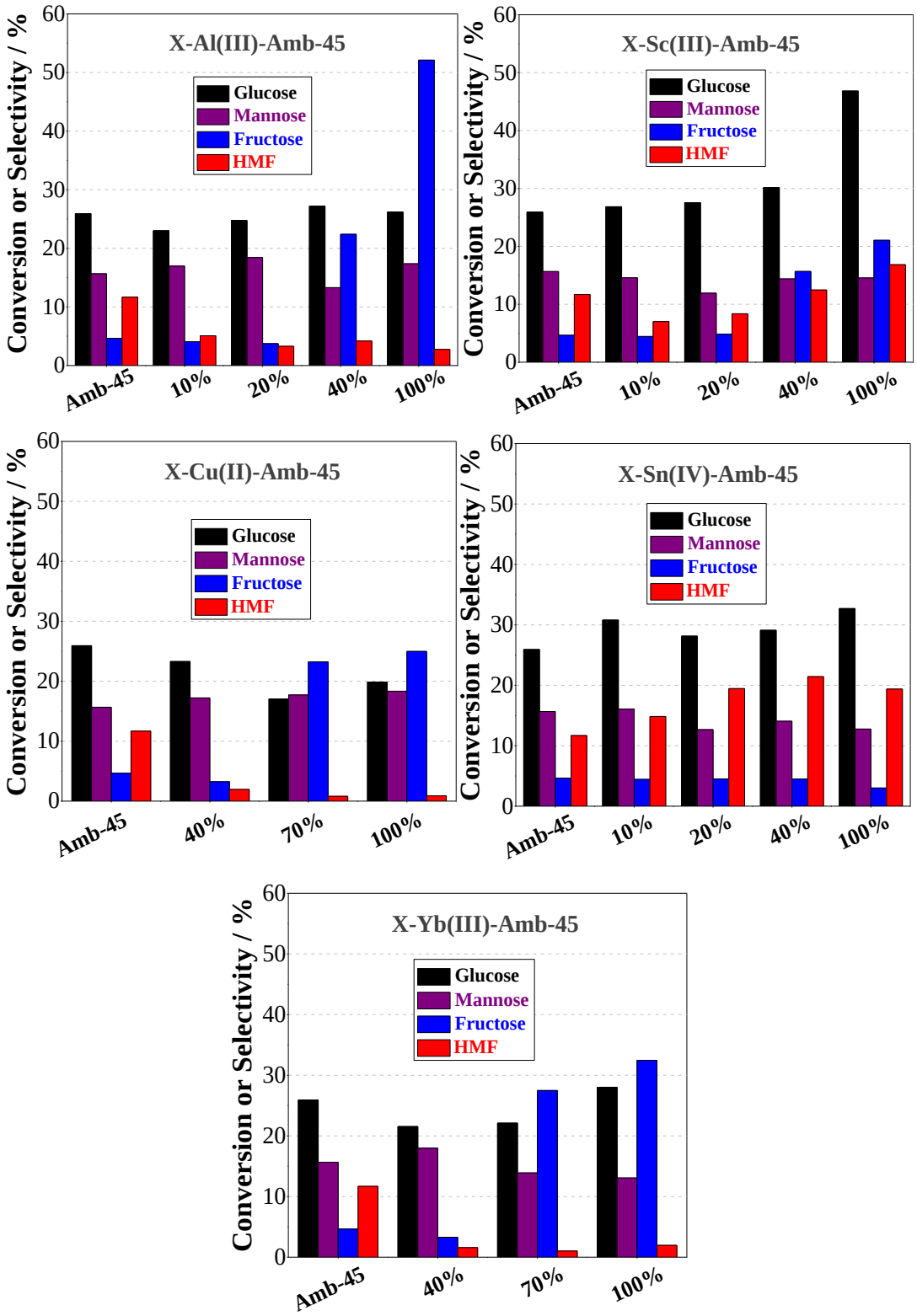

FIGURE 4.3 – Catalytic screening of the catalysts X-Al(III)-Amb-45, X-Sc(III)-Amb-45, X-Cu(II)-Amb-45, X-Sn(IV)-Amb-45, and X-Yb(III)-Amb-45 in the conversion of glucose into HMF, at 130 °C, in THF/H_2O = 4/1, 2 h of reaction, and 20 mg of catalyst (catalyst/substrate mass ratio = 0.50).

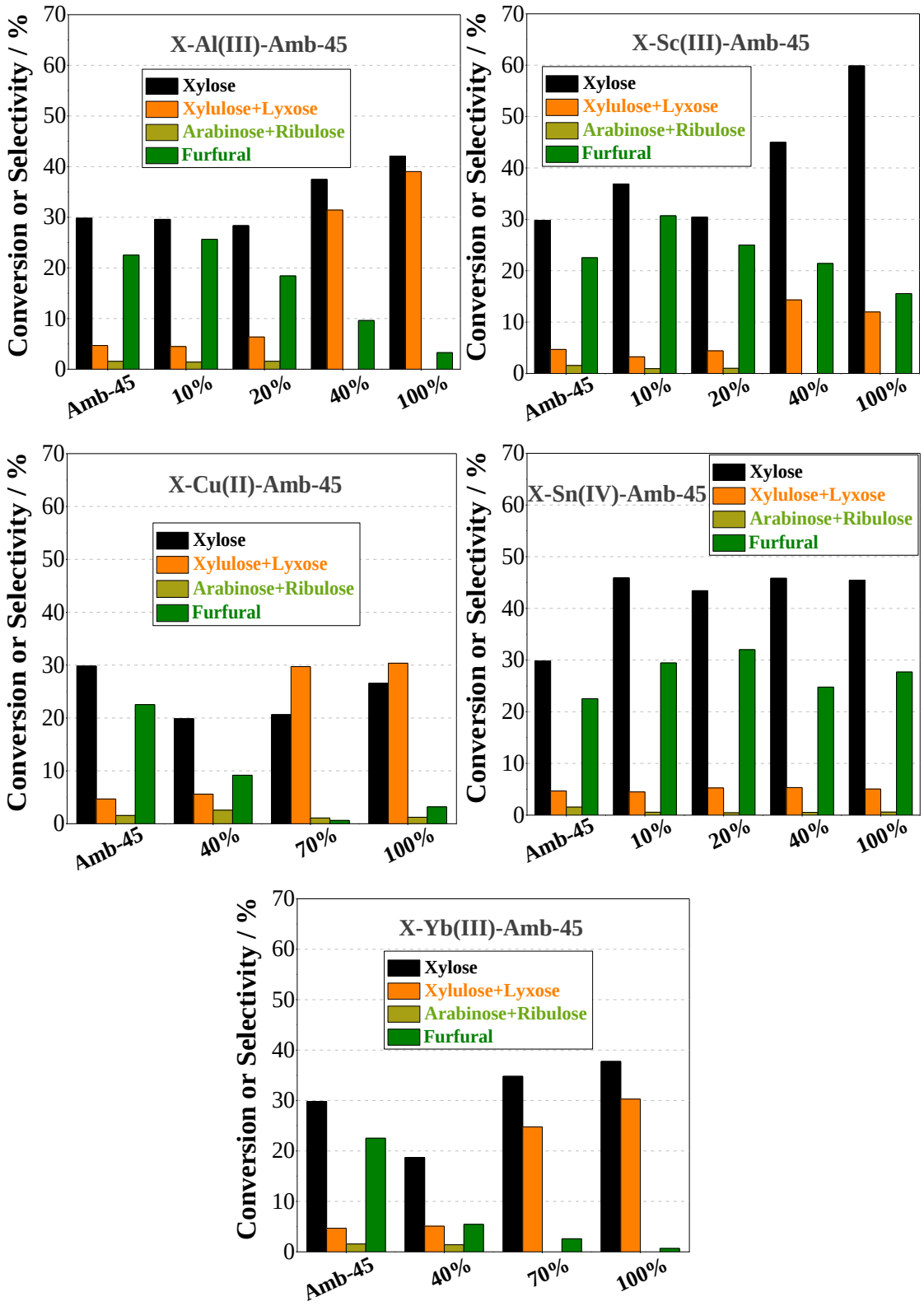

FIGURE 4.4 – Catalytic screening of the catalysts X-Al(III)-Amb-45, X-Sc(III)-Amb-45, X-Cu(II)-Amb-45, X-Sn(IV)-Amb-45, and X-Yb(III)-Amb-45 in the conversion of xylose into furfural, at 160 °C, in THF/H_2O = 4/1, 30 min of reaction, and 10 mg of catalyst (catalyst/substrate mass ratio = 0.25).

The *L/B* ratio can be tuned by adjusting the amount of metallic cation exchanged during the partial ion exchange process [35]. For this reason, we selected the most promising metallic cations from the previous screening (Al^{3+}, Sc^{3+}, Cu^{2+}, Sn^{4+}, and Yb^{3+}) and studied additional percentages of exchanged Brønsted acid sites in the M-Amb-45 catalysts (FIGURES 4.3 and 4.4). For the catalysts with Al^{3+}, Cu^{2+}, and Yb^{3+}, the higher the percentage, the lower the platform molecule selectivities and the higher the fructose and xylulose + lyxose selectivities. In short, these catalysts can be considered only isomerization catalysts. This result is intriguing because, even at low percentages, where the *L/B* ratio may be low due to the excess of Brønsted acid sites, the isomers formed are not dehydrated into platform molecules. A possible hypothesis is that these metallic cations provide strong Lewis acid sites, leading to a strong adsorption of the isomers produced at those sites, which prevents them from undergoing dehydration. Further characterization is necessary to assess the concentration and strength of the acid sites in these catalysts.

The materials with Sc^{3+}, in turn, presented higher conversions as the percentage increased, with an enhancement in the selectivities for fructose, xylulose + lyxose, and HMF; and a decrease in furfural selectivity. Even though these catalysts show activity for the isomers and platform molecules, they cannot be considered good because they are not selective for only one product. In any case, the best *L/B* ratio for HMF production was found with the catalyst 100%-Sc(III)-Amb-45 (16 % HMF selectivity at 46 % glucose conversion); whereas for furfural production, the catalyst 10%-Sc(III)-Amb-45 exhibited the best results (30 % furfural selectivity at 36 % xylose conversion).

Lastly, the materials with Sn^{4+} exhibited an enhancement in the monosaccharide conversion and platform molecule selectivities as the percentage increased up to 20 %; after that, the results reached a plateau (respectively 28 % and 43 % glucose and xylose conversions, and 19 % and 32 % HMF and furfural

selectivities), which may be explained by a possible saturation of the metallic cations added. As mentioned previously, this catalyst presents a *L/B* ratio for platform molecule production, and considering the earlier discussion on the strength of Lewis acid sites, it may have weaker Lewis acid sites compared to Al^{3+}, Cu^{2+}, and Yb^{3+} catalysts, which could result in less strong adsorption of the isomers produced at these sites, leaving them available for dehydration at the Brønsted acid sites. Recent studies with bifunctional tin carbon-based catalysts for these reactions have indeed shown that the most efficient catalysts for platform molecule production, in addition to having a good balance of Brønsted and Lewis acid sites, possess acidic sites with low and medium strength [163,164].

Notably, the effect of the *L/B* ratio on the conversion of monosaccharides into platform molecules is more pronounced for niobium phosphates (Chapter 1, FIGURE 2.7 and FIGURE 2.9) than for ion-exchanged bifunctional carbons. In the latter case, the strength of the Lewis acid sites likely plays a crucial role in these conversions, with stronger sites (Al^{3+}, Cu^{2+}, and Yb^{3+}) leading to isomers; intermediate strength sites (Sc^{3+}) leading to both isomers and platform molecules, and weaker sites (Sn^{4+}) leading to platform molecules. Additionally, another important factor to consider is that, during the partial ion exchange procedure, the sulfonic acid groups, responsible for monosaccharide dehydration, have their protons exchanged with metallic cations, reducing the number of active acid sites for dehydration and the ratio between stronger and weaker Brønsted acid sites (N_S/N_W), which, according to FIGURE 3.9, results in catalysts with low TON_{Furan}. The concentration and strength of both Brønsted and Lewis acid sites in the ion-exchanged bifunctional carbons must be characterized to identify the key parameter driving the conversion of monosaccharides into platform molecules in these catalysts.

For the kinetic studies, the bifunctional catalyst 20%-Sn(IV)-Amb-45 and the Lewis acid catalysts 100%-Al(III)-Amb-45, 100%-Cu(II)-Amb-45,

and 100%-Yb(III)-Amb-45 were selected.

4.3.2 - Kinetic studies

For the kinetic studies, the catalyst mass for the dehydration of glucose was increased from 20 mg to 150 mg to achieve faster reactions. In the dehydration of xylose, 10 mg of catalyst was sufficient to maintain fast reaction rates, so this amount was used for the kinetic studies. The kinetic studies of the Amb-45 and 20%-Sn(IV)-Amb-45 (FIGURES 4.5 and 4.6) generally show that, over the reaction time, the monosaccharide conversions increase and the isomer selectivities decrease. The mass balance also decreases over the time, due to the formation of humins [111], condensation reactions, degradation, and/or decomposition [33]. Regarding the platform molecules, the furfural selectivities also increase; however, the HMF selectivities increase up to 1 hour of reaction, reaching a plateau. The catalyst 20%-Sn(IV)-Amb-45, in comparison with the Amb-45, exhibited an increase in the monosaccharide conversions (approximately 5 %) and HMF selectivities (between 5 – 10 %), with a plateau of HMF selectivity between 40 – 45 %; nevertheless, the furfural selectivities remain the same in both cases (approximately 45 % at 60 min of reaction). We can conclude, therefore, that the bifunctional catalyst increased the reaction rate of both reactions and specifically enhanced HMF production, which is in agreement with the literature [33,34]. These results confirm the synergistic effect of Lewis and Brønsted acid sites of this catalyst in the direct production of platform molecules from glucose and xylose.

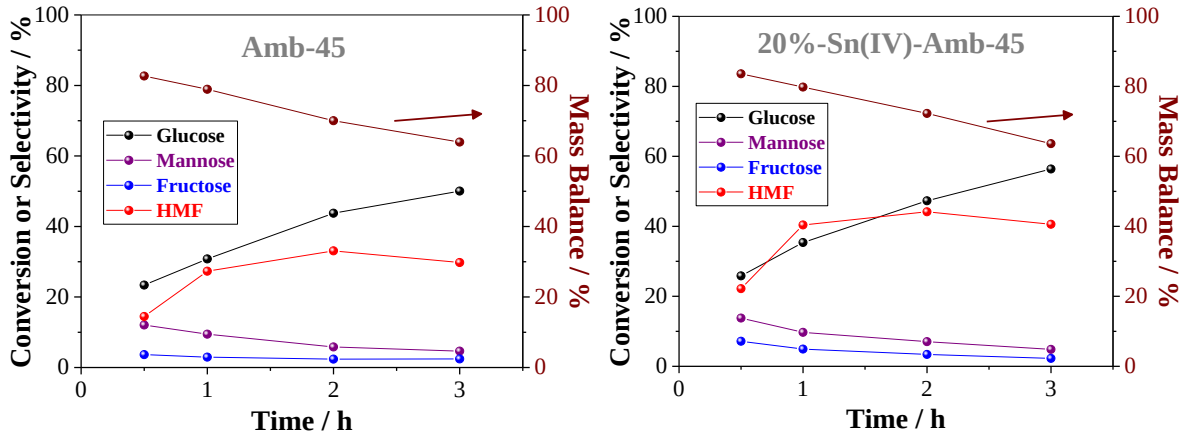

FIGURE 4.5 – Kinetic studies of the HMF promoters in the conversion of glucose into HMF, at 130 °C, in THF/H_2O = 4/1, and 150 mg of catalyst (catalyst/substrate mass ratio = 3.75).

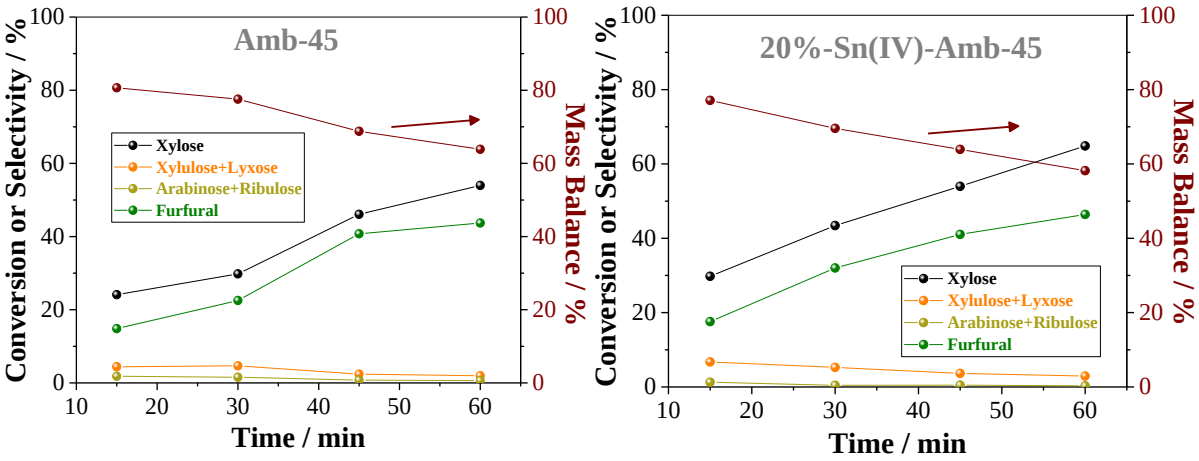

FIGURE 4.6 – Kinetic studies of the furfural promoters in the conversion of xylose into furfural, at 160 °C, in THF/H_2O = 4/1, and 10 mg of catalyst (catalyst/substrate mass ratio = 0.25).

Bifunctional tin carbon-based catalysts have been studied for the conversion of glucose and xylose to platform molecules in the literature. By incorporating SnO_x nanoparticles on sulfonated carbon microspheres, it was possible to achieve 90 % HMF selectivity at 92 % glucose conversion at 180 °C for 2 hours, and 85 % furfural selectivity at 95 % xylose conversion at 170 °C for 2 hours, using in both cases THF/H_2O biphasic solvent system with 1.5 mol/L NaCl [165]. In a similar solvent system, bifunctional tin-based silica-carbon catalysts achieved 83 % HMF selectivity at 95 % glucose conversion at 175 °C

for 2 hours [166], and bifunctional solid acid tin oxide/carbon catalysts achieved 91 % HMF selectivity at 92 % glucose conversion at 180 °C for 2 hours [164]. Lignin-derived carbon-supported tin oxides have shown HMF selectivity close to 86 % at 58 % glucose conversion, with a reaction temperature of 190 °C, reaction time of 3 hours, and a THF/H_2O volume ratio of 4:1 (biphasic system according to the authors) [163]. To the best of our knowledge, no studies using bifunctional tin carbon-based catalysts in a monophasic THF/H_2O system have been performed yet. In any case, further studies are necessary to optimize the reaction conditions and further improve platform molecule selectivities for the tin-exchanged bifunctional carbons prepared herein.

On the other hand, the kinetic curves of the isomerization catalysts (FIGURES 4.7 and 4.8) show high selectivities for fructose and xylulose + lyxose in conversions between 15 – 30 %, which decrease over the reaction time, along with the mass balance, while the monosaccharide conversions and platform molecule selectivities increase. The best isomerization catalysts were 100%-Al(III)-Amb-45 and 100%-Yb(III)-Amb-45. Although the former catalyst exhibited 5 % less glucose conversion than the latter over the reaction time (FIGURE 4.7), it was 5 – 10 % more selective for fructose, achieving an impressive fructose selectivity of 59 % at 30 min of reaction. For the xylose conversion (FIGURE 4.8), the former catalyst was more active (showing a difference of 5 – 10 % in xylose conversion) and more selective for xylulose + lyxose (showing a difference of 5 – 10 % in selectivity), achieving 42 % selectivity after 15 min of reaction. For this reason, the catalyst 100%-Al(III)-Amb-45 can be considered the best isomerization catalyst of this study.

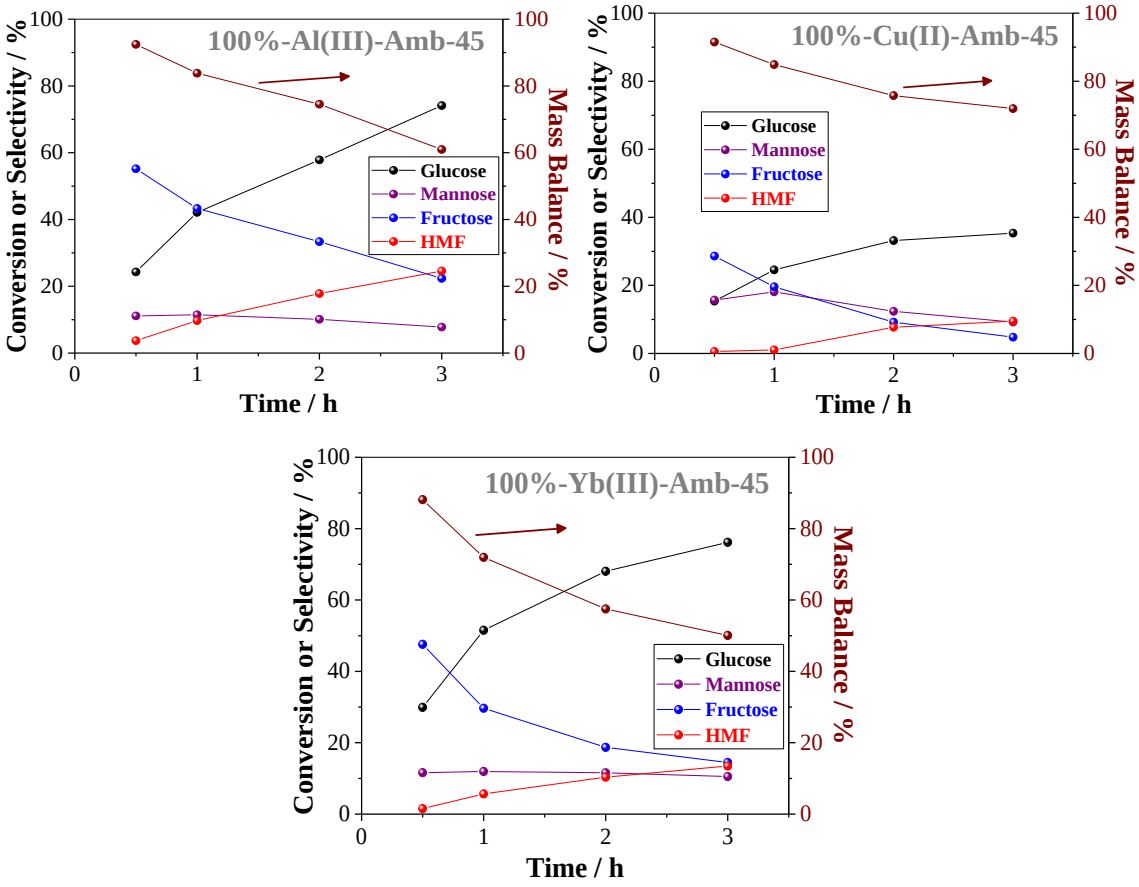

FIGURE 4.7 – Kinetic studies of the isomerization catalysts in the conversion of glucose into HMF, at 130 °C, in THF/H_2O = 4/1, and 150 mg of catalyst (catalyst/substrate mass ratio = 3.75).

There are many studies on glucose isomerization into fructose using aluminum carbon-based catalysts. Hydrochar microsphere-supported Al catalysts with a hierarchically porous structure showed 93 % fructose selectivity at 35 % glucose conversion in water at 160 °C for 20 minutes [167]. Biochar, graphitic oxide, and graphene oxide were used as carbon supports to synthesize Al-impregnated heterogeneous catalysts, achieving fructose selectivities of 51 %, 52 %, and 60 % at glucose conversions of 69 %, 66 %, and 49 %, respectively, in water at 140 °C [168]. Al-loaded functional lignin biopolymer produced 69 % fructose selectivity at 85 % glucose conversion in ethanol at 140 °C in a 30-minute reaction time [169]. An aluminum-hydrochar catalyst in an acetone/water reaction medium produced 93 % fructose selectivity at 43 % glucose conversion at 160 °C

for 20 minutes [170]. In a similar solvent system, another aluminum-hydrochar catalyst, prepared by impregnating aluminum on swollen cellulose-derived hydrochar, achieved 72 % fructose selectivity at 23 % glucose conversion at 160 °C for 10 minutes [171]. To the best of our knowledge, aluminum carbon-based catalysts have not yet been used for the isomerization of xylose to xylulose. In any case, further studies are necessary to optimize the reaction conditions and improve isomer selectivities for the aluminum-exchanged bifunctional carbons prepared herein.

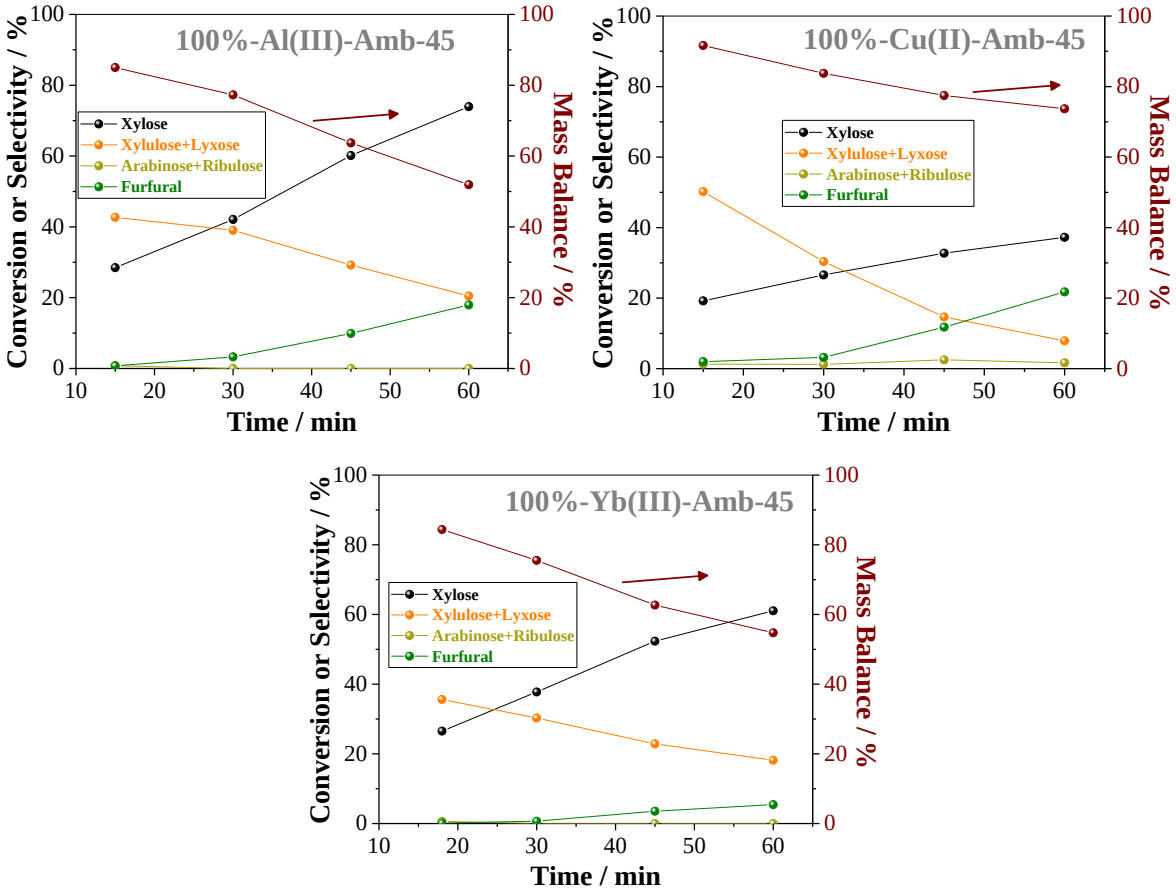

FIGURE 4.8 – Kinetic studies of the isomerization catalysts in the conversion of xylose into furfural, at 160 °C, in THF/H_2O = 4/1, and 10 mg of catalyst (catalyst/substrate mass ratio = 0.25).

Since 100%-Al(III)-Amb-45, 100%-Cu(II)-Amb-45, and 100%-Yb(III)-Amb-45 are primarily isomerization catalysts, we conducted a final test

combining these catalysts with an equal amount of pure Amb-45 to create a bifunctional environment for producing platform molecules. The results (FIGURE 4.9) indicated that the catalytic performance of the combination was practically the same as that of the Amb-45, suggesting that the Lewis acid catalysts were somehow inhibited, and only pure Amb-45 was active. An experimental observation during these experiments was that both catalysts in the solvent system used (THF/H_2O = 4/1) agglutinated into a ball-shaped material. In contrast, for the reactions with individual catalysts, the materials were well-dispersed in the solvent system. Considering this, the ball-shaped material may have consisted of a core of Lewis acid sites surrounded by a shell of Brønsted acid sites. Since the latter were the only sites in contact with the liquid reaction, they may have been the only ones active in the dehydration of monosaccharides. Characterizations need to be performed to confirm this hypothesis. In any case, more Brønsted acid catalysts must be combined and studied with these Lewis acid catalysts to promote the dehydration of the isomers into platform molecules.

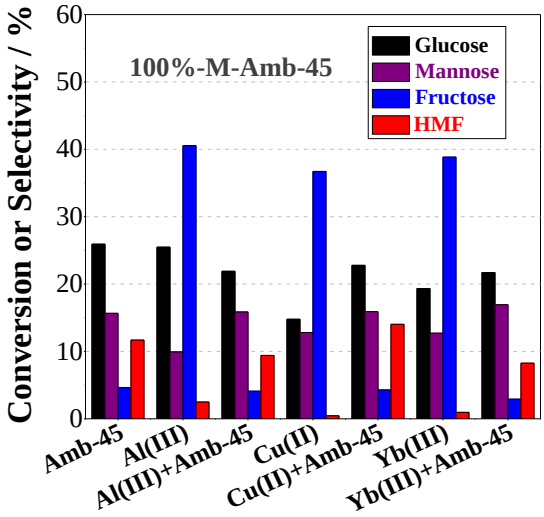

FIGURE 4.9 – Catalytic performance of the isomerization catalysts in combination with pure Amb-45 in the conversion of glucose into HMF, at 130 °C, in THF/H_2O = 4/1, and 2 h of reaction. For the reactions with single catalysts, a mass of 20 mg of catalyst were used (catalyst/substrate mass ratio = 0.50); for the reactions combining two catalysts, 20 mg of each were used (catalysts/substrate mass ratio = 1.00).

After this first study with the X-M-Amb-45 catalysts and the preliminary results with 40%-M-CMK-8-PSA, we can conclude that the best metallic cation to produce platform molecules is Sn^{4+}, and the best to produce isomers is Al^{3+}. In future studies, we will prepare new bifunctional carbons of CMK-8-PSA with Sn^{4+} and Al^{3+}. The same catalytic and kinetic studies carried out for X-M-Amb-45 will be performed for these new catalysts.

4.3.3 - Preliminary characterization

The main characterization of this chapter, the quantification of Lewis and Brønsted acid sites, has not been performed yet. So far, we have only performed Scanning Electron Microscopy with Energy Dispersive X-ray Spectroscopy (SEM-EDS) on some X-M-Amb-45 catalysts to estimate their chemical composition (TABLE 4.1). The basic chemical composition of Amb-45 is C, O, S, and Cl. After the partial ion exchange procedure, the respective metallic cations were detected, with concentrations ranging between 0.1 and 2.0 mmol g^{-1}. In the case of X-Sc(III)-Amb-45 catalysts, there is indeed an observed decrease in the Sc^{3+} concentration as the percentage of theoretical exchanged Brønsted acid sites decreases (1.4 to 1.0 mmol g^{-1} for 100% and 40%-Sc(III), respectively). On the other hand, the X-Sn(IV)-Amb-45 catalysts presented the same concentration of Sn^{4+} (0.1 mmol g^{-1}), explaining the similar catalytic results observed for both materials (FIGURES 4.3 and 4.4). In this case, 20 % of exchanged sites is likely the limit of exchange; further addition of Sn^{4+} does not exchange any more Brønsted acid sites.

Furthermore, it is possible to compare the *S/M* ratio of these materials (TABLE 4.1), since the partial ion exchange procedure considers the exchange of the sulfonic acid protons by metallic cations [35]. The catalyst with the lowest value is 100%-Cu(II)-Amb-45 (*S/M* = 1.9), which presents the metallic cation with the lowest valence. Indeed, the lower the metallic cation valence, the lower

its Lewis acidity and consequently the sulfonate groups bonded to it. The catalysts with trivalent cations (Al^{3+}, Sc^{3+} and Yb^{3+}) showed ratios between 2.1 and 2.8. Clearly, 40%-Sc(III)-Amb-45 exhibited a higher ratio than 100%-Sc(III)-Amb-45 (2.8 and 2.3, respectively), since the former has a lower Sc^{3+} concentration than the latter. On the other hand, the other 100%-M-Amb-45 trivalent catalysts presented a linear correlation between their *S/M* ratios and their ionic radius (FIGURE 4.10), showing that metallic cations with the same valence but larger ionic radius can bond with more sulfonate groups. The catalysts with Sn^{4+}, in turn, exhibited *S/M* ratios between 25.0 and 27.5. As this metallic cation is tetravalent, it was indeed expected to have *S/M* ratios higher than those of the trivalent catalysts; however, these results are very high. More characterizations need to be performed to understand them. Lastly, the real exchanged percentage of Brønsted acid sites was calculated (TABLE 4.1), showing that the partial ion exchange procedure does not occur equimolarly, but depends on the valence and the ionic radius of the metallic cation.

TABLE 4.1 – Chemical composition of some X-M-Amb-45 catalysts, by SEM-EDS.

Amb-45 Catalysts	**Chemical Composition (mmol g^{-1})**										
	C	**O**	**S**	**Cl**	**Al**	**Sc**	**Cu**	**Sn**	**Yb**	***S/M* Ratio**	**Real Exchanged Percentage[a] (%)**
Amb-45	44.6	10.2	3.3	5.5	-	-	-	-	-	-	-
100%-Al(III)	43.2	9.6	3.4	4.9	1.7	-	-	-	-	2.1	71.2
100%-Sc(III	38.3	11.6	3.2	5.3	-	1.4	-	-	-	2.3	59.6
40%-Sc(III)	43.3	10.5	3.0	4.8	-	1.0	-	-	-	2.8	45.1
100%-Cu(II)	33.2	10.5	3.7	5.6	-	-	1.9	-	-	1.9	81.5
100%-Sn(IV)	42.4	9.7	3.6	5.7	-	-	-	0.1	-	25.1	6.3
20%-Sn(IV)	44.5	9.1	3.5	5.5	-	-	-	0.1	-	27.4	5.5
100%-Yb(III)	31.8	8.8	3.1	5.3	-	-	-	-	1.1	2.8	47.7

[a] The Amb-45 concentration of stronger acid sites by potentiometric titration, which is 2.31 mmol g^{-1}, is considered 100 %.

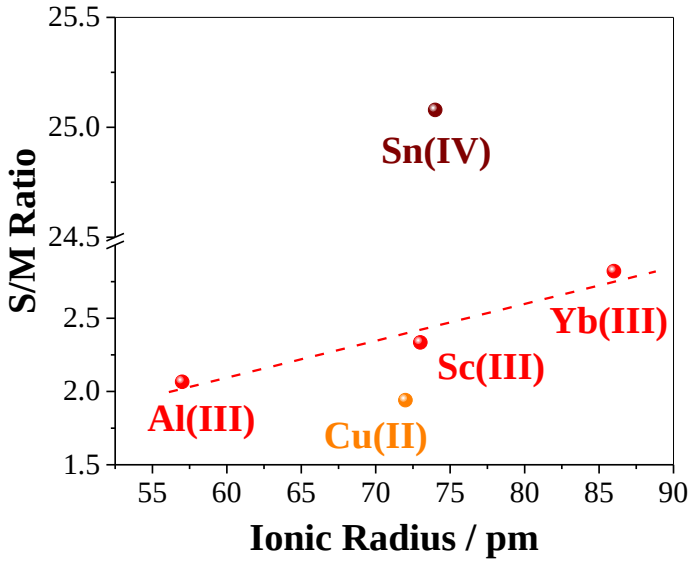

FIGURE 4.10 – Correlation between *S/M* ratio with the *M* ionic radius, for 100%-M-Amb-45 catalysts.

4.4 - Conclusions

In this chapter, we focused on performing the partial ion-exchange of two sulfonated carbons (hand-made CMK-8-PSA and commercial Amb-45) with metallic cations possessing good Lewis acidity for isomerization (Al^{3+}, Sc^{3+}, Fe^{3+}, Cu^{2+}, Sn^{4+}, Yb^{3+}) to produce ion-exchanged bifunctional carbons with different *L/B* ratios for dehydrating glucose and xylose into HMF and furfural, respectively. From the catalytic screening of the materials prepared herein, the strength of the Lewis acid sites likely plays a crucial role in the monosaccharide conversion, with stronger sites (Al^{3+}, Cu^{2+}, and Yb^{3+}) leading to isomers; intermediate strength sites (Sc^{3+}) leading to both isomers and platform molecules, and weaker sites (Sn^{4+}) leading to platform molecules.

The catalyst 20%-Sn(IV)-Amb-45 has the best *L/B* ratio for platform molecule production, exhibiting HMF selectivity of 41 % at 57 % glucose conversion after 3 h of reaction, and furfural selectivity of 47 % at 65 % xylose

conversion after 1 h of reaction. On the other hand, the catalysts 100%-Al(III)-Amb-45, 100%-Cu(II)-Amb-45, and 100%-Yb(III)-Amb-45 were promising for isomerization reactions, with 100%-Al(III)-Amb-45 presenting outstanding results: fructose selectivity of 59 % at 23 % glucose conversion after 30 min of reaction, and xylulose + lyxose selectivity of 42 % at 25 % xylose conversion after 15 min of reaction.

We also conducted a test combining these isomerization catalysts with an equal amount of pure Amb-45 to create a bifunctional environment for producing platform molecules; however, the Lewis acid catalysts were somehow inhibited, and only pure Amb-45 was active in the dehydration, producing HMF in low yields. More Brønsted acid catalysts must be combined and studied with this Lewis acid catalyst to promote the dehydration of the isomers into platform molecules.

The metallic cations were indeed detected by SEM-EDS, and their concentrations ranged from 0.1 to 2.0 mmol g^{-1}. The results also showed that lower valence metallic cations resulted in a lower bond with sulfonate groups (low *S/M* ratio), and as the metallic valence increases, the *S/M* ratio also increases, indicating more sulfonate group interaction. Moreover, with trivalent cations, a linear correlation between *S/M* ratio and ionic radius was found, suggesting that metallic cations with the same valence but larger ionic radius can bond with more sulfonate groups. The unexpectedly high *S/M* ratios for Sn^{4+} (between 25.0 and 27.5) suggest the need for further investigation.

In future studies, we will prepare new bifunctional carbons of CMK-8-PSA with Sn^{4+} and Al^{3+}. The same catalytic and kinetic studies carried out for X-M-Amb-45 will be performed for these new catalysts. More characterization regarding the concentration and strength of both Brønsted and Lewis acid sites must be done to identify the key parameter driving the conversion of monosaccharides into platform molecules in these catalysts.

4.5 - Acknowledgments

J.L.V thanks FAPESP for the PhD fellowship (2019/02132-8 and 2020/04109-0).

5 - THESIS CONCLUSIONS

Much more than just producing a highly efficient catalyst for the dehydration of monosaccharides into HMF and furfural, we have thoroughly investigated the catalyst composition and/or surface acidity of different mesoporous acidic catalysts, and their impacts on catalytic performance for the production of platform molecules.

In the first chapter, with niobium phosphates, it was demonstrated that altering synthesis parameters affects the *P/Nb* molar ratio, which in turn influences the Lewis/Brønsted acid site (*L/B*) ratio and overall catalytic activity. High *L/B* ratios correlate linearly with reaction rates for HMF and furfural production from glucose and xylose, respectively, indicating the importance of tuning the surface acidity balance.

Based on that, we tried to synthesize a controlled bifunctional carbon catalyst with the best *L/B* ratio for those reactions. First, we prepared sulfonated carbons with varying concentrations of stronger (sulfonic acid groups) and weaker acid sites (carboxylic acid, alcohol, phenol groups) for the dehydration of fructose and xylose into HMF and furfural, respectively. From this study, it was found that the ratio between stronger and weaker acid sites (N_S/N_W) crucially impacts catalytic performance, with optimal yields and turnover numbers achieved at N_S/N_W ratios of 2 – 4, suggesting a synergistic role of both types of acid sites in the catalytic mechanism.

Finally, we selected two sulfonated carbons and performed ion-exchange with various metallic cations to produce ion-exchanged bifunctional carbons with different *L/B* ratios. Even though no characterization regarding surface acidity has been performed yet, the strength of the Lewis acid sites likely plays a crucial role in the monosaccharide conversion, with stronger sites (Al^{3+}, Cu^{2+}, and Yb^{3+}) leading to isomers; intermediate strength sites (Sc^{3+}) leading to both isomers and platform molecules, and weaker sites (Sn^{4+}) leading to platform

molecules. The catalyst with 20 % of Brønsted acid sites exchanged with Sn^{4+} (20%-Sn(IV)-Amb-45) showed promising results for HMF and furfural production, achieving an HMF selectivity of 41 % at 57 % glucose conversion, and a furfural selectivity of 47 % at 65 % xylose conversion.

6 - REFERENCES

[1] F. Wang, J.D. Harindintwali, Z. Yuan, M. Wang, F. Wang, S. Li, Z. Yin, L. Huang, Y. Fu, L. Li, S.X. Chang, L. Zhang, J. Rinklebe, Z. Yuan, Q. Zhu, L. Xiang, D.C.W. Tsang, L. Xu, X. Jiang, J. Liu, N. Wei, M. Kästner, Y. Zou, Y.S. Ok, J. Shen, D. Peng, W. Zhang, D. Barceló, Y. Zhou, Z. Bai, B. Li, B. Zhang, K. Wei, H. Cao, Z. Tan, L. bin Zhao, X. He, J. Zheng, N. Bolan, X. Liu, C. Huang, S. Dietmann, M. Luo, N. Sun, J. Gong, Y. Gong, F. Brahushi, T. Zhang, C. Xiao, X. Li, W. Chen, N. Jiao, J. Lehmann, Y.G. Zhu, H. Jin, A. Schäffer, J.M. Tiedje, J.M. Chen, Technologies and perspectives for achieving carbon neutrality, Innovation. 2 (2021). https://doi.org/10.1016/j.xinn.2021.100180.

[2] M. Antar, D. Lyu, M. Nazari, A. Shah, X. Zhou, D.L. Smith, Biomass for a sustainable bioeconomy: An overview of world biomass production and utilization, Renew. Sustain. Energy Rev. 139 (2021) 110691. https://doi.org/10.1016/j.rser.2020.110691.

[3] L. Chen, G. Msigwa, M. Yang, A.I. Osman, S. Fawzy, D.W. Rooney, P.S. Yap, Strategies to achieve a carbon neutral society: a review, Environ. Chem. Lett. 20 (2022) 2277–2310. https://doi.org/10.1007/s10311-022-01435-8.

[4] J. Rogelj, D. Huppmann, V. Krey, K. Riahi, L. Clarke, M. Gidden, Z. Nicholls, M. Meinshausen, A new scenario logic for the Paris Agreement long-term temperature goal, Nature. 573 (2019) 357–363. https://doi.org/10.1038/s41586-019-1541-4.

[5] A. Anca-Couce, C. Hochenauer, R. Scharler, Bioenergy technologies, uses, market and future trends with Austria as a case study, Renew. Sustain. Energy Rev. 135 (2021) 110237. https://doi.org/10.1016/j.rser.2020.110237.

[6] L. Li, J. Lin, N. Wu, S. Xie, C. Meng, Y. Zheng, X. Wang, Y. Zhao, Review and outlook on the international renewable energy development, Energy Built Environ. 3 (2022) 139–157. https://doi.org/10.1016/j.enbenv.2020.12.002.

[7] K. Calvin, A. Cowie, G. Berndes, A. Arneth, F. Cherubini, J. Portugal-Pereira, G. Grassi, J. House, F.X. Johnson, A. Popp, M. Rounsevell, R. Slade, P. Smith, Bioenergy for climate change mitigation: Scale and sustainability, GCB Bioenergy. 13 (2021) 1346–1371. https://doi.org/10.1111/gcbb.12863.

[8] E. De Jong, A. Higson, P. Walsh, M. Wellisch, Bio-based Chemicals: Value added products from biorefineries, IEA Bioenergy, Task42 Biorefinery. (2012) 36. http://www.ieabioenergy.com/wp-content/uploads/2013/10/Task-42-Biobased-Chemicals-value-added-products-from-biorefineries.pdf.

[9] B. Annevelink, L.G. Chavez, R. Van Ree, I.V. Gursel, Global biorefinery status report 2022, 2022.

[10] J.J. Bozell, G.R. Petersen, Technology development for the production of biobased products from biorefinery carbohydrates - The US Department of Energy's "top 10" revisited, Green Chem. 12 (2010) 539–554. https://doi.org/10.1039/b922014c.

[11] IMARC Group, Furfural Market Report by Process (Quaker Batch Process, Chinese Batch Process, Rosenlew Continuous Process, and Others), Raw Material (Corn Cobs, Rice Husk, Sugarcane Bagasse, and Others), Application (Furfuryl Alcohol, Solvent, and Others), (2024) 1–10. https://www.imarcgroup.com/furfural-market.

[12] IMARC Group, 5-Hydroxymethylfurfural Market Report by Grade (Industrial Grade, Food Grade), End User (Flavor and Fragrance Industry, Pharmaceutical Industry, and Others), and Region 2023-2028, Mark. Res. Rep. (2023) 1–12. https://www.imarcgroup.com/5-hydroxymethylfurfural-market.

[13] Y.Y. Gorbanev, S.K. Klitgaard, J.M. Woodley, C.H. Christensen, A. Riisager, Gold-catalyzed aerobic oxidation of 5-hydroxymethylfurfural in water at ambient temperature, ChemSusChem. 2 (2009) 672–675. https://doi.org/10.1002/cssc.200900059.

[14] Y. Román-Leshkov, C.J. Barrett, Z.Y. Liu, J.A. Dumesic, Production of dimethylfuran for liquid fuels from biomass-derived carbohydrates, Nature. 447 (2007) 982–985. https://doi.org/10.1038/nature05923.
[15] J.M.R. Gallo, M.A. Trapp, The chemical conversion of biomass-derived saccharides: An overview, J. Braz. Chem. Soc. 28 (2017) 1586–1607. https://doi.org/10.21577/0103-5053.20170009.
[16] R. Alamillo, M. Tucker, M. Chia, Y. Pagán-Torres, J. Dumesic, The selective hydrogenation of biomass-derived 5-hydroxymethylfurfural using heterogeneous catalysts, Green Chem. 14 (2012) 1413–1419. https://doi.org/10.1039/c2gc35039d.
[17] M. Intelligence, Furfural Market Size & Share Analysis - Growth Trends & Forecasts (2024 - 2029), (2024) 1–9. https://www.mordorintelligence.com/industry-reports/furfural-market.
[18] S. Sitthisa, D.E. Resasco, Hydrodeoxygenation of furfural over supported metal catalysts: A comparative study of Cu, Pd and Ni, Catal. Letters. 141 (2011) 784–791. https://doi.org/10.1007/s10562-011-0581-7.
[19] N. Alonso-Fagúndez, I. Agirrezabal-Telleria, P.L. Arias, J.L.G. Fierro, R. Mariscal, M.L. Granados, Aqueous-phase catalytic oxidation of furfural with H<inf>2</inf>O<inf>2</inf>: High yield of maleic acid by using titanium silicalite-1, RSC Adv. 4 (2014) 54960–54972. https://doi.org/10.1039/c4ra11563e.
[20] D.A. Simonetti, J.A. Dumesic, Catalytic strategies for changing the energy content and achieving C-C coupling in biomass-derived oxygenated hydrocarbons, ChemSusChem. 1 (2008) 725–733. https://doi.org/10.1002/cssc.200800105.
[21] P. Verdeguer, N. Merat, L. Rigal, A. Gaset, Optimization of experimental conditions for the catalytic oxidation of furfural to furoic acid, J. Chem. Technol. & Biotechnol. 61 (1994) 97–102. https://doi.org/10.1002/jctb.280610203.
[22] S. Kang, J. Fu, G. Zhang, From lignocellulosic biomass to levulinic acid: A review on acid-catalyzed hydrolysis, Renew. Sustain. Energy Rev. 94 (2018) 340–362. https://doi.org/10.1016/j.rser.2018.06.016.
[23] R.S. Rinaldi Ferdi, R. Rinaldi, F. Schüth, R.S. Rinaldi Ferdi, Acid Hydrolysis of Cellulose as the Entry Point into Biorefinery Schemes, ChemSusChem. 2 (2009) 1096–1107. https://doi.org/10.1002/cssc.200900188.
[24] T. Istasse, A. Richel, Mechanistic aspects of saccharide dehydration to furan derivatives for reaction media design, RSC Adv. 10 (2020) 23720–23742. https://doi.org/10.1039/d0ra03892j.
[25] A. Ricci, B. Di Rienzo, F. Pepi, A. Troiani, S. Garzoli, P. Giacomello, Acid-catalysed glucose dehydration in the gas phase: a mass spectrometric approach, J. Mass Spectrom. 50 (2015) 228–234. https://doi.org/https://doi.org/10.1002/jms.3525.
[26] G. Yang, E.A. Pidko, E.J.M.M. Hensen, Mechanism of Bronsted acid-catalyzed conversion of carbohydrates, J. Catal. 295 (2012) 122–132. https://doi.org/10.1016/j.jcat.2012.08.002.
[27] D.W. Harris, M.S. Feather, Mechanism of the interconversion of D-glucose, D-mannose, and D-fructose in acid solution, J. Am. Chem. Soc. 97 (1975) 178–181. https://doi.org/10.1021/ja00834a031.
[28] S. Ramchander, M.S. Feather, An intramolecular C-2 → C-1 hydrogen transfer during the acid-catalyzed conversion of d-xylose to d-threo-pentulose (d-xylulose), Arch. Biochem. Biophys. 178 (1977) 576–580. https://doi.org/10.1016/0003-9861(77)90228-4.
[29] K.R. Enslow, A.T. Bell, The Role of Metal Halides in Enhancing the Dehydration of Xylose to Furfural, ChemCatChem. 7 (2015) 479–489. https://doi.org/https://doi.org/10.1002/cctc.201402842.

[30] B. Danon, G. Marcotullio, W. De Jong, Mechanistic and kinetic aspects of pentose dehydration towards furfural in aqueous media employing homogeneous catalysis, Green Chem. 16 (2014) 39–54. https://doi.org/10.1039/c3gc41351a.
[31] L. Hu, Z. Wu, Y. Jiang, X. Wang, A. He, J. Song, J. Xu, S. Zhou, Y. Zhao, J. Xu, Recent advances in catalytic and autocatalytic production of biomass-derived 5-hydroxymethylfurfural, Renew. Sustain. Energy Rev. 134 (2020) 110317. https://doi.org/10.1016/j.rser.2020.110317.
[32] T.M.C. Hoang, E.R.H. van Eck, W.P. Bula, J.G.E. Gardeniers, L. Lefferts, K. Seshan, Humin based by-products from biomass processing as a potential carbonaceous source for synthesis gas production, Green Chem. 17 (2015) 959–972. https://doi.org/10.1039/c4gc01324g.
[33] J.L. Vieira, M. Almeida-Trapp, A. Mithöfer, W. Plass, J.M.R. Gallo, Rationalizing the conversion of glucose and xylose catalyzed by a combination of Lewis and Brønsted acids, Catal. Today. 344 (2020) 92–101. https://doi.org/10.1016/j.cattod.2018.10.032.
[34] J.M.R. Gallo, D.M. Alonso, M.A. Mellmer, J.A. Dumesic, Production and upgrading of 5-hydroxymethylfurfural using heterogeneous catalysts and biomass-derived solvents, Green Chem. 15 (2013) 85–90. https://doi.org/10.1039/c2gc36536g.
[35] S. Xu, C. Yin, D. Pan, F. Hu, Y. Wu, Y. Miao, L. Gao, G. Xiao, Efficient conversion of glucose into 5-hydroxymethylfurfural using a bifunctional Fe 3+ modified Amberlyst-15 catalyst, Sustain. Energy Fuels. 3 (2019) 390–395. https://doi.org/10.1039/c8se00499d.
[36] J. Pimenta Lorenti, E. Scolari, N.M. Cabral, C. Bisio, J.M.R. Gallo, Isomerization and Epimerization of Glucose Catalyzed by Sn-Containing Mesoporous Silica, Ind. Eng. Chem. Res. 60 (2021) 12821–12833. https://doi.org/10.1021/acs.iecr.1c01781.
[37] J. Liu, B.B. Yang, X.Q. Wang, C.L. Liu, R.Z. Yang, W.S. Dong, Glucose conversion to methyl levulinate catalyzed by metal ion-exchanged montmorillonites, Appl. Clay Sci. 141 (2017) 118–124. https://doi.org/10.1016/j.clay.2017.02.017.
[38] S. Luo, L. Zhu, A. Talukdar, G. Zhang, X. Mi, J.P. Cheng, P.G. Wang, Recent advances in rare earth-metal triflate catalyzed organic synthesis in green media, Mini. Rev. Org. Chem. 2 (2005) 177–202. https://doi.org/10.2174/1570193053544472.
[39] I. Delidovich, R. Palkovits, Catalytic Isomerization of Biomass-Derived Aldoses: A Review, ChemSusChem. 9 (2016) 547–561. https://doi.org/10.1002/cssc.201501577.
[40] B. Girisuta, L.P.B.M. Janssen, H.J. Heeres, Green Chemicals: A Kinetic Study on the Conversion of Glucose to Levulinic Acid, Chem. Eng. Res. Des. 84 (2006) 339–349. https://doi.org/10.1205/cherd05038.
[41] J.M.R.. A. Gallo Ricardo; Dumesic, James A., Acid-functionalized mesoporous carbons for the continuous production of 5-hydroxymethylfurfural, J. Mol. Catal. A Chem. 422 (2016) 13–17. https://doi.org/10.1016/j.molcata.2016.01.005.
[42] E.I. Gürbüz, J.M.R. Gallo, D.M. Alonso, S.G. Wettstein, W.Y. Lim, J.A. Dumesic, Conversion of hemicellulose into furfural using solid acid catalysts in γ-valerolactone, Angew. Chemie - Int. Ed. 52 (2013) 1270–1274. https://doi.org/10.1002/anie.201207334.
[43] V. Choudhary, S. Caratzoulas, D.G. Vlachos, Insights into the isomerization of xylose to xylulose and lyxose by a Lewis acid catalyst, Carbohydr. Res. 368 (2013) 89–95. https://doi.org/10.1016/j.carres.2012.12.019.
[44] B. Li, S. Varanasi, P. Relue, High yield aldose–ketose transformation for isolation and facile conversion of biomass sugar to furan, Green Chem. 15 (2013) 2149–2157. https://doi.org/10.1039/c3gc40795k.
[45] V. Choudhary, S.I. Sandler, D.G. Vlachos, Conversion of Xylose to Furfural Using Lewis and Brønsted Acid Catalysts in Aqueous Media, ACS Catal. 2 (2012) 2022–2028. https://doi.org/10.1021/cs300265d.

[46] R. Schlögl, Heterogeneous catalysis, Angew. Chemie - Int. Ed. 54 (2015) 3465–3520. https://doi.org/10.1002/anie.201410738.
[47] L.A. Petrov, Y. Alhamed, A. Al-Zahrani, M. Daous, Role of chemical kinetics in the heterogeneous catalysis studies, Cuihua Xuebao/Chinese J. Catal. 32 (2011) 1085–1112. https://doi.org/10.1016/S1872-2067(10)60225-2.
[48] W. Wei, S. Wu, Experimental and kinetic study of glucose conversion to levulinic acid in aqueous medium over Cr/HZSM-5 catalyst, Fuel. 225 (2018) 311–321. https://doi.org/10.1016/j.fuel.2018.03.120.
[49] T. Dallas Swift, H. Nguyen, A. Anderko, V. Nikolakis, D.G. Vlachos, Tandem Lewis/Brønsted homogeneous acid catalysis: conversion of glucose to 5-hydoxymethylfurfural in an aqueous chromium(<scp>iii</scp>) chloride and hydrochloric acid solution, Green Chem. 17 (2015) 4725–4735. https://doi.org/10.1039/C5GC01257K.
[50] H. Nguyen, V. Nikolakis, D.G. Vlachos, Mechanistic Insights into Lewis Acid Metal Salt-Catalyzed Glucose Chemistry in Aqueous Solution, ACS Catal. 6 (2016) 1497–1504. https://doi.org/10.1021/acscatal.5b02698.
[51] K. Lamminpää, J. Ahola, J. Tanskanen, Kinetics of xylose dehydration into furfural in formic acid, Ind. Eng. Chem. Res. 51 (2012) 6297–6303. https://doi.org/10.1021/ie2018367.
[52] B.F.M. Kuster, H.M.G. Temmink, The influence of pH and weak-acid anions on the dehydration of d-fructose, Carbohydr. Res. 54 (1977) 185–191. https://doi.org/10.1016/s0008-6215(00)84808-9.
[53] I.K.M. Yu, D.C.W. Tsang, Conversion of biomass to hydroxymethylfurfural: A review of catalytic systems and underlying mechanisms, Bioresour. Technol. 238 (2017) 716–732. https://doi.org/https://doi.org/10.1016/j.biortech.2017.04.026.
[54] J.A. Dumesic, J.M.R. Gallo, D. Alonso, Method to convert monosaccharides to 5-(hydroxymethyl) furfural (hmf) using biomass-derived solvents, 2014. http://www.google.com/patents/US20140107355.
[55] M.A. Mellmer, C. Sener, J.M.R. Gallo, J.S. Luterbacher, D.M. Alonso, J.A. Dumesic, Solvent effects in acid-catalyzed biomass conversion reactions, Angew. Chemie - Int. Ed. 53 (2014) 11872–11875. https://doi.org/10.1002/anie.201408359.
[56] A.H. Motagamwala, K. Huang, C.T. Maravelias, J.A. Dumesic, Solvent system for effective near-term production of hydroxymethylfurfural (HMF) with potential for long-term process improvement, Energy Environ. Sci. 12 (2019) 2212–2222. https://doi.org/10.1039/c9ee00447e.
[57] Y. Román-Leshkov, J.N. Chheda, J.A. Dumesic, Phase Modifiers Promote Efficient Production of Hydroxymethylfurfural from Fructose, Science. 312 (2006) 1933–1937. https://doi.org/10.1126/science.1126337.
[58] Y. Zhu, W. Li, Y. Lu, T. Zhang, H. Jameel, H. Chang, L. Ma, Production of furfural from xylose and corn stover catalyzed by a novel porous carbon solid acid in γ-valerolactone, RSC Adv. 7 (2017) 29916–29924. https://doi.org/10.1039/c7ra03995f.
[59] T. Dallas Swift, H. Nguyen, A. Anderko, V. Nikolakis, D.G. Vlachos, Tandem Lewis/Brønsted homogeneous acid catalysis: conversion of glucose to 5-hydoxymethylfurfural in an aqueous chromium(iii) chloride and hydrochloric acid solution, Green Chem. 17 (2015) 4725–4735. https://doi.org/10.1039/c5gc01257k.
[60] R. Zhang, X. Lu, Y. Liu, X. Wang, S. Zhang, Kinetic Study of Dilute Nitric acid Treatment of Corn Stover at Relatively High Temperature, Chem. Eng. Technol. 34 (2011) 409–414. https://doi.org/10.1002/ceat.201000258.
[61] J.L. Vieira, G. Paul, G.D. Iga, N.M. Cabral, J.M.C. Bueno, C. Bisio, J.M.R. Gallo, Niobium phosphates as bifunctional catalysts for the conversion of biomass-derived monosaccharides, Appl. Catal. A Gen. 617 (2021) 118099-NA.

https://doi.org/10.1016/j.apcata.2021.118099.
[62] J.L. Vieira, E.A. Santos, C. Ribeiro, J.M.R. Gallo, The Impact of the Ratio Between Stronger and Weaker Acid Sites on the Production of 5-Hydroxymethylfurfural and Furfural from Monosaccharides, ChemCatChem. 202301666 (2024) 1–11. https://doi.org/10.1002/cctc.202301666.
[63] M.S. Masnadi, H. El-Houjeiri, D. Schunack, Y. Li, J. Englander, A. Badahdah, J.-C. Monfort, J. Anderson, T. Wallington, J. Bergerson, D. Gordon, J. Koomey, S. Przesmitzki, I. Azevedo, X. Bi, J. Duffy, G. Heath, G. Keoleian, C. McGlade, A. Brandt, Global carbon intensity of crude oil production, Science (80-.). 361 (2018) 851–853. https://doi.org/10.1126/science.aar6859.
[64] E4tech, Re-Cord, Wur, From the Sugar Platform to biofuels and biochemicals, Final Rep. Eur. Comm. Dir. Energy. (2015) 183. https://ec.europa.eu/energy/sites/ener/files/documents/EC Sugar Platform final report.pdf.
[65] J.J. Bozell, G.R. Petersen, Technology development for the production of biobased products from biorefinery carbohydrates — The US Department of Energy's "top 10" revisited, Green Chem. 12 (2010) 539–55. https://doi.org/10.1039/b922014c.
[66] G. Gibson, The Synthesis and Evolution of a Supermodel, Science (80-.). 307 (2005) 1890–1891. https://doi.org/10.1126/science.1109835.
[67] E. Nikolla, Y. Román-Leshkov, M. Moliner, M.E.E. Davis, "One-pot" synthesis of 5-(hydroxymethyl)furfural from carbohydrates using tin-beta zeolite, Acs Catal. 1 (2011) 408–410. https://doi.org/10.1021/cs2000544.
[68] M. Moliner, Y. Roman-Leshkov, M.E. Davis, Tin-containing zeolites are highly active catalysts for the isomerization of glucose in water, Proc. Natl. Acad. Sci. 107 (2010) 6164–6168. https://doi.org/10.1073/pnas.1002358107.
[69] Y.J. Pagan-Torres, T.F. Wang, J.M.R. Gallo, B.H. Shanks, J.A. Dumesic, Production of 5-Hydroxymethylfurfural from Glucose Using a Combination of Lewis and Bronsted Acid Catalysts in Water in a Biphasic Reactor with an Alkylphenol Solvent, Acs Catal. 2 (2012) 930–934. https://doi.org/Doi 10.1021/Cs300192z.
[70] J.M.R. Gallo, D.M. Alonso, M.A. Mellmer, J.H. Yeap, H.C. Wong, J.A. Dumesic, Production of furfural from lignocellulosic biomass using beta zeolite and biomass-derived solvent, Top. Catal. 56 (2013) 1775–1781. https://doi.org/10.1007/s11244-013-0113-3.
[71] I. Agirrezabal-Telleria, C. García-Sancho, P. Maireles-Torres, P.L. Arias, Dehydration of xylose to furfural using a Lewis or Brönsted acid catalyst and N2 stripping, Cuihua Xuebao/Chinese J. Catal. 34 (2013) 1402–1406. https://doi.org/10.1016/s1872-2067(12)60599-3.
[72] J.P. Lorenti, E. Scolari, E.M. Albuquerque, M.A. Fraga, J.M.R. Gallo, Tailoring Sn-SBA-15 properties for catalytic isomerization of glucose, Appl. Catal. A Gen. 581 (2019) 37–42. https://doi.org/https://doi.org/10.1016/j.apcata.2019.05.009.
[73] V. Choudhary, A.B. Pinar, S.I. Sandler, D.G. Vlachos, R.F. Lobo, Xylose isomerization to xylulose and its dehydration to furfural in aqueous media, Acs Catal. 1 (2011) 1724–1728. https://doi.org/10.1021/cs200461t.
[74] K. Nakajima, Y. Baba, R. Noma, M. Kitano, J. N. Kondo, S. Hayashi, M. Hara, J.N. Kondo, S. Hayashi, M. Hara, Nb2O5·nH2O as a Heterogeneous Catalyst with Water-Tolerant Lewis Acid Sites, J. Am. Chem. Soc. 133 (2011) 4224–4227. https://doi.org/10.1021/ja110482r.
[75] N. V. Gromov, O.P. Taran, V.S. Semeykina, I.G. Danilova, A. V. Pestunov, E. V. Parkhomchuk, V.N. Parmon, Solid Acidic NbOx/ZrO2 Catalysts for Transformation of Cellulose to Glucose and 5-Hydroxymethylfurfural in Pure Hot Water, Catal. Letters. 147 (2017) 1485–1495. https://doi.org/10.1007/s10562-017-2056-y.

[76] M.N. Catrinck, E.S. Ribeiro, R.S. Monteiro, R.M. Ribas, M.H.P.P. Barbosa, R.F. Teófilo, Direct conversion of glucose to 5-hydroxymethylfurfural using a mixture of niobic acid and niobium phosphate as a solid acid catalyst, Fuel. 210 (2017) 67–74. https://doi.org/10.1016/j.fuel.2017.08.035.
[77] C. Fang, W. Wu, H. Li, T. Yang, W. Zhao, Z. Wang, S. Yang, Production of bio-based furfural from xylose over a recyclable niobium phosphate (NbOPO3) catalyst, Energy Sources, Part A Recover. Util. Environ. Eff. 39 (2017) 2072–2077. https://doi.org/10.1080/15567036.2017.1402103.
[78] X. Li, K. Peng, X. Liu, Q. Xia, Y. Wang, Comprehensive Understanding of the Role of Brønsted and Lewis Acid Sites in Glucose Conversion into 5-Hydromethylfurfural, ChemCatChem. 9 (2017) 2739–2746. https://doi.org/10.1002/cctc.201601203.
[79] N.K. Gupta, A. Fukuoka, K. Nakajima, Amorphous Nb2O5 as a Selective and Reusable Catalyst for Furfural Production from Xylose in Biphasic Water and Toluene, Acs Catal. 7 (2017) 2430–2436. https://doi.org/10.1021/acscatal.6b03682.
[80] A. Aronne, M. Di Serio, R. Vitiello, N.J. Clayden, L. Minieri, C. Imparato, A. Piccolo, P. Pernice, P. Carniti, A. Gervasini, An Environmentally Friendly Nb-P-Si Solid Catalyst for Acid-Demanding Reactions, J. Phys. Chem. C. 121 (2017) 17378–17389. https://doi.org/10.1021/acs.jpcc.7b05886.
[81] B. Guo, L. Ye, G. Tang, L. Zhang, B. Yue, S.C.E. Tsang, H. He, Effect of Brønsted/Lewis Acid Ratio on Conversion of Sugars to 5-Hydroxymethylfurfural over Mesoporous Nb and Nb-W Oxides, Chinese J. Chem. 35 (2017) 1529–1539. https://doi.org/10.1002/cjoc.201700084.
[82] N.T. do Prado, T.E. Souza, A.R.T. Machado, P.P. Souza, R.S. Monteiro, L.C.A. Oliveira, Enhanced catalytic activity for fructose conversion on nanostructured niobium oxide after hydrothermal treatment: Effect of morphology and porous structure, J. Mol. Catal. A Chem. 422 (2016) 23–34. https://doi.org/https://doi.org/10.1016/j.molcata.2016.01.021.
[83] H.T. Kreissl, K. Nakagawa, Y.K. Peng, Y. Koito, J. Zheng, S.C.E. Tsang, Niobium oxides: Correlation of acidity with structure and catalytic performance in sucrose conversion to 5-hydroxymethylfurfural, J. Catal. 338 (2016) 329–339. https://doi.org/10.1016/j.jcat.2016.03.007.
[84] P. Carniti, A. Gervasini, F. Bossola, V. Dal Santo, Cooperative action of Brønsted and Lewis acid sites of niobium phosphate catalysts for cellobiose conversion in water, Appl. Catal. B Environ. 193 (2016) 93–102. https://doi.org/10.1016/j.apcatb.2016.04.012.
[85] H.G. Bernal, A.M.R. Galletti, G. Garbarino, G. Busca, E. Finocchio, NbP catalyst for furfural production: FT IR studies of surface properties, Appl. Catal. A Gen. 502 (2015) 388–398. https://doi.org/10.1016/j.apcata.2015.06.031.
[86] R.S. de Carvalho, F. de A. Rodrigues, R.S. Monteiro, W.L. da Silva Faria, Optimization of Furfural Synthesis from Xylose Using Niobic Acid and Niobium Phosphate as Catalysts, Waste and Biomass Valorization. 10 (2019) 2673–2680. https://doi.org/10.1007/s12649-018-0272-3.
[87] V.. V. Ordomsky, V.L. Sushkevich, J.C. Schouten, J. Van Der Schaaf, T.A. Nijhuis, Glucose dehydration to 5-hydroxymethylfurfural over phosphate catalysts, J. Catal. 300 (2013) 37–46. https://doi.org/10.1016/j.jcat.2012.12.028.
[88] Y. Zhang, J. Wang, X. Li, X. Liu, Y. Xia, B. Hu, G. Lu, Y. Wang, Direct conversion of biomass-derived carbohydrates to 5-hydroxymethylfurural over water-tolerant niobium-based catalysts, Fuel. 139 (2015) 301–307. https://doi.org/10.1016/j.fuel.2014.08.047.
[89] B. Pholjaroen, N. Li, Z. Wang, A. Wang, T. Zhang, Dehydration of xylose to furfural over niobium phosphate catalyst in biphasic solvent system, J. Energy Chem. 22 (2013) 826–832. https://doi.org/10.1016/S2095-4956(14)60260-6.

[90] N.K. Mal, M. Fujiwara, Synthesis of hexagonal and cubic super-microporous niobium phosphates with anion exchange capacity and catalytic properties, Chem. Commun. 2 (2002) 2702–2703. https://doi.org/10.1039/b207976c.
[91] N.K. Mal, A. Bhaumik, M. Fujiwara, M. Matsukata, Novel organic–inorganic hybrid and organic-free mesoporous niobium oxophosphate synthesized in the presence of an anionic surfactant, Microporous Mesoporous Mater. 93 (2006) 40–45. https://doi.org/https://doi.org/10.1016/j.micromeso.2006.02.001.
[92] N.K. Mal, A. Bhaumik, P. Kumar, M. Fujiwara, Microporous niobium phosphates and catalytic properties prepared by a supramolecular templating mechanism, Chem. Commun. (2003) 872–873. https://doi.org/10.1039/B300323J.
[93] D. Massiot, F. Fayon, M. Capron, I. King, S. Le Calvé, B. Alonso, J.-O. Durand, B. Bujoli, Z. Gan, G. Hoatson, Modelling one- and two-dimensional solid-state NMR spectra, Magn. Reson. Chem. 40 (2002) 70–76. https://doi.org/https://doi.org/10.1002/mrc.984.
[94] C.A. Emeis, Determination of Integrated Molar Extinction Coefficients for Infrared Absorption Bands of Pyridine Adsorbed on Solid Acid Catalysts, J. Catal. 141 (1993) 347–354. https://doi.org/https://doi.org/10.1006/jcat.1993.1145.
[95] A. Taouli, W. Reschetilowski, Comparative study of MCM-41 acidity by using the integrated molar extinction coefficients for infrared absorption bands of adsorbed ammonia, Stud. Surf. Sci. Catal. 142 B (2002) 1315–1322. https://www.scopus.com/inward/record.uri?eid=2-s2.0-0036937668&partnerID=40&md5=17b09261af1a3d7521625bd82ae6665a.
[96] Q. Sun, A. Auroux, J. Shen, Surface acidity of niobium phosphate and steam reforming of dimethoxymethane over CuZnO/Al2O3–NbP complex catalysts, J. Catal. 244 (2006) 1–9. https://doi.org/https://doi.org/10.1016/j.jcat.2006.07.027.
[97] V.L. Sushkevich, V. V. Ordomsky, I.I. Ivanova, Synthesis of isoprene from formaldehyde and isobutene over phosphate catalysts, Appl. Catal. A Gen. 441–442 (2012) 21–29. https://doi.org/https://doi.org/10.1016/j.apcata.2012.06.034.
[98] Y. Zhang, J. Wang, J. Ren, X. Liu, X. Li, Y. Xia, G. Lu, Y. Wang, Mesoporous niobium phosphate: An excellent solid acid for the dehydration of fructose to 5-hydroxymethylfurfural in water, Catal. Sci. Technol. 2 (2012) 2485–2491. https://doi.org/10.1039/c2cy20204b.
[99] A. Sarkar, P. Pramanik, Synthesis of mesoporous niobium oxophosphate using niobium tartrate precursor by soft templating method, Microporous Mesoporous Mater. 117 (2009) 580–585. https://doi.org/https://doi.org/10.1016/j.micromeso.2008.08.001.
[100] G. Paul, C. Bisio, I. Braschi, M. Cossi, G. Gatti, E. Gianotti, L. Marchese, Combined solid-state NMR, FT-IR and computational studies on layered and porous materials, Chem. Soc. Rev. 47 (2018) 5684–5739. https://doi.org/10.1039/c7cs00358g.
[101] J.P. Lourenço, M.F. Ribeiro, F.R. Ribeiro, J. Rocha, Z. Gabelica, Solid-state NMR and powder XRD studies of the structure of SAPO-40 upon hydration–dehydration cycles, J. Chem. Soc., Faraday Trans. 91 (1995) 2213–2215. https://doi.org/10.1039/FT9959102213.
[102] Y. Watanabe, A. Koiwai, H. Takeuchi, S.A. Hyodo, S. Noda, Multinuclear NMR studies on the thermal stability of SAPO-34, J. Catal. 143 (1993) 430–436. https://doi.org/10.1006/jcat.1993.1287.
[103] J.M.R. Gallo, C. Bisio, G. Gatti, L. Marchese, H.O. Pastore, Physicochemical characterization and surface acid properties of mesoporous [Al]-SBA-15 obtained by direct synthesis, Langmuir. 26 (2010) 5791–5800. https://doi.org/10.1021/la903661q.
[104] A. Ramírez, B.L. Lopez, L. Sierra, Study of the acidic sites and their modifications in mesoporous silica synthesized in acidic medium under quiescent conditions, J. Phys. Chem. B. 107 (2003) 9275–9280. https://doi.org/10.1021/jp0351472.

[105] B. Chakraborty, B. Viswanathan, Surface acidity of MCM-41 by in situ IR studies of pyridine adsorption, Catal. Today. 49 (1999) 253–260. https://doi.org/10.1016/s0920-5861(98)00431-3.
[106] T. Barzetti, E. Selli, D. Moscotti, L. Forni, Pyridine and ammonia as probes for FTIR analysis of solid acid catalysts, J. Chem. Soc. Trans. 92 (1996) 1401–1407. https://doi.org/10.1039/ft9969201401.
[107] Q. Sun, Y. Fu, H. Yang, A. Auroux, J. Shen, Dehydration of methanol to dimethyl ether over Nb2O5 and NbOPO4 catalysts: Microcalorimetric and FT-IR studies, J. Mol. Catal. A Chem. 275 (2007) 183–193. https://doi.org/https://doi.org/10.1016/j.molcata.2007.06.008.
[108] A. Travert, A. Vimont, J.C. Lavalley, V. Montouillout, M. Rodríguez Delgado, J.J. Cuart Pascual, C. Otero Areán, Evidence for discrepancy between the surface lewis acid site strength and infrared spectra of adsorbed molecules: The case of boria-silica, J. Phys. Chem. B. 108 (2004) 16499–16507. https://doi.org/10.1021/jp0479365.
[109] S. Impellizzeri, S. Simoncelli, C. Fasciani, M.L. Marin, G.L. Hallett-Tapley, G.K. Hodgson, J.C. Scaiano, Mechanistic insights into the Nb2O5 and niobium phosphate catalyzed in situ condensation of a fluorescent halochromic assembly, Catal. Sci. Technol. 5 (2015) 169–175. https://doi.org/10.1039/c4cy00703d.
[110] M.A. Mellmer, C. Sanpitakseree, B. Demir, P. Bai, K. Ma, M. Neurock, J.A. Dumesic, Solvent-enabled control of reactivity for liquid-phase reactions of biomass-derived compounds, Nat. Catal. 1 (2018) 199–207. https://doi.org/10.1038/s41929-018-0027-3.
[111] Z. Xu, Y. Yang, P. Yan, Z. Xia, X. Liu, Z.C. Zhang, Mechanistic understanding of humin formation in the conversion of glucose and fructose to 5-hydroxymethylfurfural in [BMIM]Cl ionic liquid †, (2020). https://doi.org/10.1039/d0ra05641c.
[112] K.I. Hadjiivanov, G.N. Vayssilov, Characterization of oxide surfaces and zeolites by carbon monoxide as an IR probe molecule, in: B.C. Gates, H. Knozinger (Eds.), Adv. Catal. Vol 47, Elsevier Academic Press Inc, San Diego, USA, 2002: pp. 307–511. https://doi.org/10.1016/S0360-0564(02)47008-3.
[113] R. Rinaldi, F. Schüth, Design of solid catalysts for the conversion of biomass, Energy Environ. Sci. 2 (2009) 610–626. https://doi.org/10.1039/b902668a.
[114] H.P. Xiong Hien N.; Datye, Abhaya K., Hydrothermally stable heterogeneous catalysts for conversion of biorenewables, Green Chem. 16 (2014) 4627–4643. https://doi.org/10.1039/c4gc01152j.
[115] H. Xiong, T.J. Schwartz, N.I. Andersen, J.A. Dumesic, A.K. Datye, Graphitic-Carbon Layers on Oxides: Toward Stable Heterogeneous Catalysts for Biomass Conversion Reactions, Angew. Chem. Int. Ed. Engl. 54 (2015) 7939–7943. https://doi.org/10.1002/anie.201502206.
[116] R.M. Ravenelle, F. Schübler, A. Damico, N. Danilina, J.A. Van Bokhoven, J.A. Lercher, C.W. Jones, C. Sievers, Stability of zeolites in hot liquid water, J. Phys. Chem. C. 114 (2010) 19582–19595. https://doi.org/10.1021/jp104639e.
[117] V. V. Ordomsky, J. van der Schaaf, J.C. Schouten, T.A. Nijhuis, Fructose Dehydration to 5-Hydroxymethylfurfural over Solid Acid Catalysts in a Biphasic System, ChemSusChem. 5 (2012) 1812–1819. https://doi.org/10.1002/cssc.201200072.
[118] D.M. Alonso, J.M.R. Gallo, M.A. Mellmer, S.G. Wettstein, J.A. Dumesic, Direct conversion of cellulose to levulinic acid and gamma-valerolactone using solid acid catalysts, Catal. Sci. Technol. 3 (2013) 927–931. https://doi.org/10.1039/c2cy20689g.
[119] R. Otomo, T. Yokoi, J.N. Kondo, T. Tatsumi, Dealuminated Beta zeolite as effective bifunctional catalyst for direct transformation of glucose to 5-hydroxymethylfurfural, Appl. Catal. A Gen. 470 (2014) 318–326. https://doi.org/10.1016/j.apcata.2013.11.012.
[120] R. Li, Q. Lin, J. Ren, X. Yang, Y. Wang, L. Kong, Dealuminated Hβ zeolite for

selective conversion of fructose to furfural and formic acid, Green Energy Environ. 9 (2024) 311–320. https://doi.org/10.1016/j.gee.2022.06.003.
[121] J.S. Kruger, V. Nikolakis, D.G. Vlachos, Aqueous-phase fructose dehydration using Brønsted acid zeolites: Catalytic activity of dissolved aluminosilicate species, Appl. Catal. A Gen. 469 (2014) 116–123. https://doi.org/10.1016/j.apcata.2013.09.030.
[122] A.J. Crisci, M.H. Tucker, J.A. Dumesic, S.L. Scott, Bifunctional solid catalysts for the selective conversion of fructose to 5-hydroxymethylfurfural, Top. Catal. 53 (2010) 1185–1192. https://doi.org/10.1007/s11244-010-9560-2.
[123] A.J. Crisci, M.H. Tucker, M.-Y. Lee, S.G. Jang, J.A. Dumesic, S.L. Scott, Acid-Functionalized SBA-15-Type Silica Catalysts for Carbohydrate Dehydration, ACS Catal. 1 (2011) 719–728. https://doi.org/10.1021/cs2001237.
[124] M.H. Tucker, A.J. Crisci, B.N. Wigington, N. Phadke, R. Alamillo, J. Zhang, S.L. Scott, J.A. Dumesic, Acid-Functionalized SBA-15-Type Periodic Mesoporous Organosilicas and Their Use in the Continuous Production of 5-Hydroxymethylfurfural, ACS Catal. 2 (2012) 1865–1876. https://doi.org/10.1021/cs300303v.
[125] N.W. Dulie, B. Woldeyes, H.D. Demsash, Synthesis of lignin-carbohydrate complex-based catalyst from Eragrostis tef straw and its catalytic performance in xylose dehydration to furfural, Int. J. Biol. Macromol. 171 (2021) 10–16. https://doi.org/10.1016/j.ijbiomac.2020.12.213.
[126] W. Li, T. Zhang, G. Pei, Catalytic conversion of corn stover into furfural over carbon-based solid acids, BioResources. 13 (2018) 1425–1440. https://doi.org/10.15376/biores.13.1.1425-1440.
[127] R. Liu, J. Chen, X. Huang, L. Chen, L. Ma, X. Li, Conversion of fructose into 5-hydroxymethylfurfural and alkyl levulinates catalyzed by sulfonic acid-functionalized carbon materials, Green Chem. 15 (2013) 2895–2903. https://doi.org/10.1039/c3gc41139g.
[128] L. Xing, R. Liu, F. Jing, M. Xu, J. He, Loading behavior of p-toluenesulfonic acid in biochar and its application to prepare 5-hydroxymethylfurfural, BioResources. 17 (2022) 2705–2726. https://doi.org/10.15376/biores.17.2.2705-2726.
[129] R.P. Rocha, M.F.R. Pereira, J.L. Figueiredo, Characterisation of the surface chemistry of carbon materials by temperature-programmed desorption: An assessment, Catal. Today. 418 (2023) 114136. https://doi.org/10.1016/j.cattod.2023.114136.
[130] R.S. Nunes, G.M. Reis, L.M. Vieira, D. Mandelli, W.A. Carvalho, Ultra-Fast Selective Fructose Dehydration Promoted by a Kraft Lignin Sulfonated Carbon Under Microwave Heating, Catal. Letters. 151 (2021) 398–408. https://doi.org/10.1007/s10562-020-03305-w.
[131] H. Tang, N. Li, G. Li, W. Wang, A. Wang, Y. Cong, Dehydration of Carbohydrates to 5-Hydroxymethylfurfural over Lignosulfonate-Based Acidic Resin, ACS Sustain. Chem. Eng. 6 (2018) 5645–5652. https://doi.org/10.1021/acssuschemeng.8b00757.
[132] K. Li, J. Chen, Y. Yan, Y. Min, H. Li, F. Xi, J. Liu, P. Chen, Quasi-homogeneous carbocatalysis for one-pot selective conversion of carbohydrates to 5-hydroxymethylfurfural using sulfonated graphene quantum dots, Carbon N. Y. 136 (2018) 224–233. https://doi.org/10.1016/j.carbon.2018.04.087.
[133] W. Wang, X. Cao, H. Guo, X. Yang, N. Guo, Y. Ma, Carbon-based solid acid derived from lignin and polyvinyl chloride for conversion of xylose and crop wastes to furfural, Mol. Catal. 524 (2022) 112329. https://doi.org/10.1016/j.mcat.2022.112329.
[134] G. Chen, Q. Sun, J. Xu, L. Zheng, J. Rong, B. Zong, Sulfonic Derivatives as Recyclable Acid Catalysts in the Dehydration of Fructose to 5-Hydroxymethylfurfural in Biphasic Solvent Systems., ACS Omega. 6 (2021) 6798–6809. https://doi.org/10.1021/acsomega.0c05857.

[135] H. Tang, N. Li, F. Chen, G. Li, A. Wang, Y. Cong, X. Wang, T. Zhang, Highly efficient synthesis of 5-hydroxymethylfurfural with carbohydrates over renewable cyclopentanone-based acidic resin, Green Chem. 19 (2017) 1855–1860. https://doi.org/10.1039/c7gc00673j.
[136] X. Yu, Y. Chu, L. Zhang, H. Shi, M. Xie, L. Peng, X. Guo, W. Li, N. Xue, W. Ding, Adjacent acid sites cooperatively catalyze fructose to 5-hydroxymethylfurfural in a new, facile pathway, J. Energy Chem. 47 (2020) 112–117. https://doi.org/10.1016/j.jechem.2019.11.020.
[137] R. Zhong, B.F. Sels, Sulfonated mesoporous carbon and silica-carbon nanocomposites for biomass conversion, Appl. Catal. B Environ. 236 (2018) 518–545. https://doi.org/10.1016/j.apcatb.2018.05.012.
[138] H.L. Peng, J.B. Zhang, J.Y. Zhang, F.Y. Zhong, P.K. Wu, K. Huang, J.P. Fan, F. Liu, Chitosan-derived mesoporous carbon with ultrahigh pore volume for amine impregnation and highly efficient CO2 capture, Chem. Eng. J. 359 (2019) 1159–1165. https://doi.org/10.1016/j.cej.2018.11.064.
[139] D. Zhao, Q. Huo, J. Feng, B.F. Chmelka, G.D. Stucky, Nonionic Triblock and Star Diblock Copolymer and Oligomeric Surfactant Syntheses of Highly Ordered, Hydrothermally Stable, Mesoporous Silica Structures, J. Am. Chem. Soc. 120 (1998) 6024–6036. https://doi.org/10.1021/ja974025i.
[140] S. Jun, J. Sang Hoon, R. Ryoo, M. Kruk, M. Jaroniec, Z. Liu, T. Ohsuna, O. Terasaki, Synthesis of new, nanoporous carbon with hexagonally ordered mesostructure [5], J. Am. Chem. Soc. 122 (2000) 10712–10713. https://doi.org/10.1021/ja002261e.
[141] S. Jun, R. Ryoo, Aluminum Impregnation into Mesoporous Silica Molecular Sieves for Catalytic Application to Friedel–Crafts Alkylation, J. Catal. 195 (2000) 237–243. https://doi.org/https://doi.org/10.1006/jcat.2000.2999.
[142] S. Che, K. Lund, T. Tatsumi, S. Iijima, S.H. Joo, R. Ryoo, O. Terasaki, Direct observation of 3D mesoporous structure by scanning electron microscopy (SEM): SBA-15 silica and CMK-5 carbon, Angew. Chemie - Int. Ed. 42 (2003) 2182–2185. https://doi.org/10.1002/anie.200250726.
[143] F. Kleitz, S.H. Choi, R. Ryoo, Cubic Ia3d large mesoporous silica: Synthesis and replication to platinum nanowires, carbon nanorods and carbon nanotubes, Chem. Commun. 9 (2003) 2136–2137. https://doi.org/10.1039/b306504a.
[144] P. Valle-Vigón, M. Sevilla, A.B. Fuertes, Functionalization of mesostructured silica-carbon composites, Mater. Chem. Phys. 139 (2013) 281–289. https://doi.org/10.1016/j.matchemphys.2013.01.036.
[145] A. Takagaki, M. Toda, M. Okamura, J.N. Kondo, S. Hayashi, K. Domen, M. Hara, Esterification of higher fatty acids by a novel strong solid acid, Catal. Today. 116 (2006) 157–161. https://doi.org/https://doi.org/10.1016/j.cattod.2006.01.037.
[146] X. Wang, R. Liu, M.M. Waje, Z. Chen, Y. Yan, K.N. Bozhilov, P. Feng, Sulfonated ordered mesoporous carbon as a stable and highly active protonic acid catalyst, Chem. Mater. 19 (2007) 2395–2397. https://doi.org/10.1021/cm070278r.
[147] P. Alexandridis, U. Olsson, B. Lindman, A Record Nine Different Phases (Four Cubic, Two Hexagonal, and One Lamellar Lyotropic Liquid Crystalline and Two Micellar Solutions) in a Ternary Isothermal System of an Amphiphilic Block Copolymer and Selective Solvents (Water and Oil), Langmuir. 14 (1998) 2627–2638. https://doi.org/10.1021/la971117c.
[148] R. Zhong, B.F. Sels, Sulfonated mesoporous carbon and silica-carbon nanocomposites for biomass conversion, Appl. Catal. B Environ. 236 (2018) 518–545. https://doi.org/10.1016/j.apcatb.2018.05.012.

[149] B. Freitas, W.G. Nunes, D.M. Soares, F.C. Rufino, C.M. Moreira, L.M. Da Silva, H. Zanin, Robust, flexible, freestanding and high surface area activated carbon and multi-walled carbon nanotubes composite material with outstanding electrode properties for aqueous-based supercapacitors, Mater. Adv. 2 (2021) 4264–4276. https://doi.org/10.1039/d0ma00783h.
[150] M.A. Pimenta, G. Dresselhaus, M.S. Dresselhaus, L.G. Cançado, A. Jorio, R. Saito, Studying disorder in graphite-based systems by Raman spectroscopy, Phys. Chem. Chem. Phys. 9 (2007) 1276–1291. https://doi.org/10.1039/b613962k.
[151] P. Lazar, R. Mach, M. Otyepka, Spectroscopic Fingerprints of Graphitic, Pyrrolic, Pyridinic, and Chemisorbed Nitrogen in N-Doped Graphene, J. Phys. Chem. C. 123 (2019) 10695–10702. https://doi.org/10.1021/acs.jpcc.9b02163.
[152] P. Valle-Vigón, M. Sevilla, A.B. Fuertes, Sulfonated mesoporous silica-carbon composites and their use as solid acid catalysts, Appl. Surf. Sci. 261 (2012) 574–583. https://doi.org/10.1016/j.apsusc.2012.08.059.
[153] L. Peng, A. Philippaerts, X. Ke, J. Van Noyen, F. De Clippel, G. Van Tendeloo, P.A. Jacobs, B.F. Sels, Preparation of sulfonated ordered mesoporous carbon and its use for the esterification of fatty acids, Catal. Today. 150 (2010) 140–146. https://doi.org/10.1016/j.cattod.2009.07.066.
[154] L. Geng, G. Yu, Y. Wang, Y. Zhu, Ph-SO3H-modified mesoporous carbon as an efficient catalyst for the esterification of oleic acid, Appl. Catal. A Gen. 427–428 (2012) 137–144. https://doi.org/10.1016/j.apcata.2012.03.044.
[155] B. Chang, J. Fu, Y. Tian, X. Dong, Multifunctionalized ordered mesoporous carbon as an efficient and stable solid acid catalyst for biodiesel preparation, J. Phys. Chem. C. 117 (2013) 6252–6258. https://doi.org/10.1021/jp312820g.
[156] L. Geng, Y. Wang, G. Yu, Y. Zhu, Efficient carbon-based solid acid catalysts for the esterification of oleic acid, Catal. Commun. 13 (2011) 26–30. https://doi.org/10.1016/j.catcom.2011.06.014.
[157] D. Song, S. An, B. Lu, Y. Guo, J. Leng, Arylsulfonic acid functionalized hollow mesoporous carbon spheres for efficient conversion of levulinic acid or furfuryl alcohol to ethyl levulinate, Appl. Catal. B Environ. 179 (2015) 445–457. https://doi.org/10.1016/j.apcatb.2015.05.047.
[158] P.F. Siril, N.R. Shiju, D.R. Brown, K. Wilson, Optimising catalytic properties of supported sulfonic acid catalysts, Appl. Catal. A Gen. 364 (2009) 95–100. https://doi.org/10.1016/j.apcata.2009.05.032.
[159] L. Xing, R. Liu, F. Jing, M. Xu, J. He, Efficient Preparation of C6 Carbohydrate into 5-Hydroxymethylfurfural with a Combination of Monoclinic FePO4 and Carbon-Based Solid Acid Catalyst Prepared from Papermaking Sludge, ChemistrySelect. 7 (2022) NA-NA. https://doi.org/10.1002/slct.202200008.
[160] Z. Zhang, D.W. Flaherty, Modified potentiometric titration method to distinguish and quantify oxygenated functional groups on carbon materials by pKa and chemical reactivity, Carbon N. Y. 166 (2020) 436–445. https://doi.org/10.1016/j.carbon.2020.05.040.
[161] P.H. Finger, T.A. Osmari, M.S. Costa, J.M.C. Bueno, J.M.R. Gallo, The role of the interface between Cu and metal oxides in the ethanol dehydrogenation, Appl. Catal. A Gen. 589 (2020) 117236-NA. https://doi.org/10.1016/j.apcata.2019.117236.
[162] A. Takagaki, M. Ohara, S. Nishimura, K. Ebitani, One-pot formation of furfural from xylose via isomerization and successive dehydration reactions over heterogeneous acid and base catalysts, Chem. Lett. 39 (2010) 838–840. https://doi.org/10.1246/cl.2010.838.
[163] S. Yan, L. Gan, K. Wang, K. Sun, Cost-effective bifunctional lignin-derived carbon supported tin oxide with efficient production of 5-hydroxymethylfurfural from glucose, Chinese J. Chem. Eng. 74 (2024) 154–164. https://doi.org/10.1016/j.cjche.2024.07.002.

[164] K. Wang, A. Rezayan, L. Si, Y. Zhang, R. Nie, T. Lu, J. Wang, C. Xu, Highly Efficient 5-Hydroxymethylfurfural Production from Glucose over Bifunctional SnOx/C catalyst, ACS Sustain. Chem. Eng. 9 (2021) 11351–11360. https://doi.org/10.1021/acssuschemeng.1c02870.
[165] Y. Zhong, Y. Liu, S. Wang, S. Hou, Y. Fan, Incorporation of tin oxide nanoparticles on sulfonated carbon microspheres as a bifunctional catalyst for efficient conversion of biomass-derived monosaccharides to 5-Hydroxymethylfurfural and furfural, Ind. Crops Prod. 208 (2024) 117913. https://doi.org/10.1016/j.indcrop.2023.117913.
[166] A. Rezayan, K. Wang, R. Nie, T. Lu, J. Wang, Y. Zhang, C. Charles Xu, Synthesis of bifunctional tin-based silica–carbon catalysts, Sn/KIT-1/C, with tunable acid sites for the catalytic transformation of glucose into 5-hydroxymethylfurfural, Chem. Eng. J. 429 (2022) 132261. https://doi.org/10.1016/j.cej.2021.132261.
[167] S. Zhang, K. Sheng, Y. Liang, J. Liu, S. E, X. Zhang, Green synthesis of aluminum-hydrochar for the selective isomerization of glucose to fructose, Sci. Total Environ. 727 (2020) 138743. https://doi.org/10.1016/j.scitotenv.2020.138743.
[168] X. Xiong, I.K.M. Yu, D.C.W. Tsang, L. Chen, Z. Su, C. Hu, G. Luo, S. Zhang, Y.S. Ok, J.H. Clark, Study of glucose isomerisation to fructose over three heterogeneous carbon-based aluminium-impregnated catalysts, J. Clean. Prod. 268 (2020) 122378. https://doi.org/10.1016/j.jclepro.2020.122378.
[169] J. Shan, H. Guo, J. Zhou, F. Shen, M. Qiu, J. Yang, R.L. Smith, X. Qi, Efficient isomerization of glucose to fructose over Al-loaded functional lignin biopolymer, Appl. Catal. B Environ. 353 (2024) 124095. https://doi.org/10.1016/j.apcatb.2024.124095.
[170] J. Liu, M. Yang, C. Gong, S. Zhang, K. Sheng, X. Zhang, Insights into the glucose isomerization mechanism of Al-hydrochar catalyst probed by Al-oxide species transformation, J. Environ. Chem. Eng. 9 (2021) 106721. https://doi.org/10.1016/j.jece.2021.106721.
[171] J. Liu, X. Zhang, L. Yang, U.A. Danhassan, S. Zhang, M. Yang, K. Sheng, X. Zhang, Glucose isomerization catalyzed by swollen cellulose derived aluminum-hydrochar, Sci. Total Environ. 777 (2021) 146037. https://doi.org/10.1016/j.scitotenv.2021.146037.
[172] V. Likodimos, T.A. Steriotis, S.K. Papageorgiou, G.E. Romanos, R.R.N. Marques, R.P. Rocha, J.L. Faria, M.F.R. Pereira, J.L. Figueiredo, A.M.T. Silva, P. Falaras, Controlled surface functionalization of multiwall carbon nanotubes by HNO3 hydrothermal oxidation, Carbon N. Y. 69 (2014) 311–326. https://doi.org/10.1016/j.carbon.2013.12.030.
[173] R. Xing, Y. Liu, Y. Wang, L. Chen, H. Wu, Y. Jiang, M. He, P. Wu, Active solid acid catalysts prepared by sulfonation of carbonization-controlled mesoporous carbon materials, Microporous Mesoporous Mater. 105 (2007) 41–48. https://doi.org/10.1016/j.micromeso.2007.06.043.
[174] M. Protić, A. Miltojević, B. Zoraja, M. Raos, I. Krstić, Application of thermogravimetry for determination of carbon content in biomass ash as an indicator of the efficiency of the combustion process, Teh. Vjesn. 28 (2021) 1762–1768. https://doi.org/10.17559/TV-20200508110940.

7 - ANNEX

7.1 - Chapter 1

7.1.1 - Synthesis of the Catalyst

7.1.1.1 - Synthesis of NbP-1

The NbP-1 was prepared by the addition of 50.0 mL of deionized water in 2.73 g of $NbCl_5$ under stirring, then 2.30 g of H_3PO_4 (85 % in water) and an additional 50 mL of water deionized were added. The mixture was stirred for 30 min, followed by adjusting the pH to 2.60 with NH_4OH (27 % in water). Then, the mixture was stirred for 5 min and the precipitate was separated by filtration. The solid was washed with 1.5 L of deionized water and transferred (still wet with the residual water of the filtration process) to a 50 mL Beaker containing a solution of 2.90 g of hexadecylamine in 20.0 mL of deionized water. The dispersion was stirred for 30 min, the pH adjusted to a value between 3.90 and 4.00 with concentrated H_3PO_4, and the solution stirred for another 30 min. The mixture was transferred to an autoclave and aged for 48 h at 65 °C. Finally, the white solid was filtered out and washed with 2.0 L of deionized water, dried overnight at room temperature, and calcined under air for 6 h at 550 °C (1 °C min^{-1}).

7.1.1.2 - Synthesis of NbP-2

The NbP-2 was prepared by the addition of 50.0 mL of deionized water in 2.73 g of $NbCl_5$ under stirring, then 2.30 g of H_3PO_4 (85 % in water) and an additional 50 mL of water deionized were added. The mixture was stirred for 30 min, followed by adjusting the pH to 2.60 with NH_4OH (27 % in water). Then, the mixture was stirred for 5 min and the precipitate was separated by filtration. The solid was washed with 1.5 L of deionized water and transferred (still wet with the residual water of the filtration process) to a 50 mL Beaker containing a solution of 3,90 g of sodium dodecyl sulfate (SDS) in 20.0 mL of deionized water.

The dispersion was stirred for 30 min, the pH adjusted to a value between 3.90 and 4.00 with concentrated NH_4OH, and the solution stirred for another 30 min. The mixture was transferred to an autoclave and aged for 48 h at 65 °C. Finally, the white solid was filtered out, washed with 2.0 L of deionized water, and dried overnight at room temperature. For the organic agent extraction method, it underwent a Soxhlet extraction process with a 0.10 mol L^{-1} HCl ethanolic solution for 22 h at 110 °C, followed by calcination under air for 6 h at 550 °C (1 °C min^{-1}).

7.1.1.3 - Synthesis of NbP-3

The NbP-3 was prepared by the addition of 50.0 mL of deionized water in 2.73 g of $NbCl_5$ under stirring, then 2.30 g of H_3PO_4 (85 % in water) and an additional 50 mL of water deionized were added. The mixture was stirred for 30 min, followed by adjusting the pH to 2.60 with NH_4OH (27 % in water). Then, the mixture was stirred for 5 min and the precipitate was separated by filtration. The solid was washed with 1.5 L of deionized water and transferred (still wet with the residual water of the filtration process) to a 50 mL Beaker containing a solution of 1.45 g of hexadecylamine in 10.0 mL of deionized water. The dispersion was stirred for 30 min, the pH adjusted to a value between 3.90 and 4.00 with concentrated H_3PO_4, and the solution stirred for another 30 min. The mixture was transferred to an autoclave and aged for 48 h at 90 °C. Finally, the white solid was filtered out and washed with 2.0 L of deionized water, dried overnight at room temperature, and calcined under air for 6 h at 550 °C (1 °C min^{-1}).

7.1.1.4 - Synthesis of NbP-4

The NbP-4 was prepared by the addition of 50.0 mL of deionized water in 2.73 g of $NbCl_5$ under stirring, then 2.30 g of H_3PO_4 (85 % in water) and

an additional 50.0 mL of water deionized were added. The mixture was stirred for 30 min, followed by adjusting the pH to 2.60 with NH_4OH (27 % in water). Then, the mixture was stirred for 5 min and the precipitate was separated by filtration. The solid was washed with 1.5 L of deionized water and transferred (still wet with the residual water of the filtration process) to a 50 mL Beaker containing a solution of 1.45 g of hexadecylamine in 10.0 mL of deionized water. The dispersion was stirred for 30 min, the pH adjusted to a value between 3.90 and 4.00 with concentrated H_3PO_4, and the solution stirred for another 30 min. The mixture was transferred to an autoclave and aged for 48 h at 65 °C. Finally, the white solid was filtered out and washed with 2.0 L of deionized water, dried overnight at room temperature, and calcined under air for 6 h at 450 °C (1 °C min^{-1}).

7.1.1.5 - Synthesis of NbP-5

The NbP-5 was prepared by the addition of 50.0 mL of deionized water in 2.73 g of $NbCl_5$ under stirring, then 2.30 g of H_3PO_4 (85 % in water) and an additional 50.0 mL of water deionized were added. The mixture was stirred for 30 min, followed by adjusting the pH to 2.60 with NH_4OH (27 % in water). Then, the mixture was stirred for 5 min and the precipitate was separated by filtration. The solid was washed with 1.5 L of deionized water and transferred (still wet with the residual water of the filtration process) to a 50 mL Beaker containing a solution of 1.45 g of hexadecylamine in 10.0 mL of deionized water. The dispersion was stirred for 30 min, the pH adjusted to a value between 3.90 and 4.00 with concentrated H_3PO_4, and the solution stirred for another 30 min. The mixture was transferred to an autoclave and aged for 48 h at 65 °C. Finally, the white solid was filtered out and washed with 2.0 L of deionized water, dried overnight at room temperature, and calcined under air for 6 h at 550 °C (1 °C min^{-1}).

7.1.1.6 - Synthesis of NbP-6

The NbP-6 was prepared by the addition of 50.0 mL of deionized water in 2.73 g of $NbCl_5$ under stirring, then 2.30 g of H_3PO_4 (85 % in water) and an additional 50.0 mL of water deionized were added. The mixture was stirred for 30 min, followed by adjusting the pH to 2.60 with NH_4OH (27 % in water). Then, the mixture was stirred for 5 min and the precipitate was separated by filtration. The solid was washed with 1.5 L of deionized water and transferred (still wet with the residual water of the filtration process) to a 50 mL Beaker containing a solution of 1.45 g of hexadecylamine in 10.0 mL of deionized water. The dispersion was stirred for 30 min, the pH adjusted to a value between 3.90 and 4.00 with concentrated H_3PO_4, and the solution stirred for another 30 min. The mixture was transferred to an autoclave and aged for 48 h at 65 °C. Finally, the white solid was filtered out, washed with 2.0 L of deionized water, and dried overnight at room temperature. For the organic agent extraction method, it underwent a Soxhlet extraction process with a 0.10 mol L^{-1} HCl ethanolic solution for 22 h at 110 °C, followed by calcination under air for 6 h at 550 °C (1 °C min^{-1}).

7.1.1.7 - Synthesis of NbP-7

The NbP-7 was prepared by the addition of 100.0 mL of deionized water in 2.73 g of $NbCl_5$ under stirring and 2.30 g of H_3PO_4 (85 % in water). The mixture was stirred for 30 min, followed by adjusting the pH to 2.60 with NH_4OH (27 % in water). Then, the mixture was stirred for 5 min and the precipitate was separated by filtration. The solid was washed with 1.5 L of deionized water and transferred (still wet with the residual water of the filtration process) to a 50 mL Beaker containing a solution of 2.90 g of hexadecylamine in 20.0 mL of deionized water. The dispersion was stirred for 30 min, the pH adjusted to a value between 3.90 and 4.00 with concentrated H_3PO_4, and the solution stirred for another 30

min. The mixture was transferred to an autoclave and aged for 48 h at 65 °C. Finally, the white solid was filtered out, washed with 2.0 L of deionized water, and dried overnight at room temperature. For the organic agent extraction method, it underwent a Soxhlet extraction process with a 0.10 mol L^{-1} HCl ethanolic solution for 22 h at 110 °C, followed by calcination under air for 6 h at 550 °C (1 °C min^{-1}).

7.1.1.8 - Synthesis of NbP-8

The NbP-3 was prepared by the addition of 50.0 mL of deionized water in 2.73 g of $NbCl_5$ under stirring, then 2.30 g of H_3PO_4 (85 % in water) and an additional 50.0 mL of water deionized were added. The mixture was stirred for 30 min, followed by adjusting the pH to 2.60 with NH_4OH (27 % in water). Then, the mixture was stirred for 5 min and the precipitate was separated by filtration. The solid was washed with 1.5 L of deionized water and transferred (still wet with the residual water of the filtration process) to a 50 mL Beaker containing a solution of 1.45 g of hexadecylamine in 10.0 mL of deionized water. The dispersion was stirred for 30 min, the pH adjusted to a value between 3.90 and 4.00 with concentrated H_3PO_4, and the solution stirred for another 30 min. The mixture was transferred to an autoclave and aged for 48 h at 90 °C. Finally, the white solid was filtered out, washed with 2.0 L of deionized water, and dried overnight at room temperature. For the organic agent extraction method, it underwent a Soxhlet extraction process with a 0.10 mol L^{-1} HCl ethanolic solution for 22 h at 110 °C, followed by calcination under air for 6 h at 550 °C (1 °C min^{-1}).

7.1.1.9 - Synthesis of Nb_2O_5P

The phosphated niobium oxide was prepared by the addition of 200 mL of water in 5.0 g of niobium pentachloride and stirred vigorously for 10 min.

The pH was adjusted to 2.0 with concentrated ammonium hydroxide and the mixture stirred for 3 h. The solid was separated by centrifugation, washed thoroughly with water, and dried overnight. For phosphonation, 1.5 g of Nb_2O_5 prepared was dispersed in 30 mL of 1.0 mol L^{-1} of H_3PO_4 (85 % in water) and stirred for 48 h at room temperature. The solid was separated by centrifugation, washed thoroughly with water, and dried overnight.

7.1.2 - Rationalization of the synthesis methods

NbP-4, a sample prepared using hexadecylamine (HDA) as the surfactant, aged at 65 °C, and calcined at 400 °C displayed a *P/Nb* molar ratio of 0.64 (TABLE 2.2). Since the sample was brownish due to incomplete combustion of the organic surfactant, the calcination temperature was increased to 550 °C, leading to NbP-5, which presented a higher *P/Nb* molar ratio (0.76). A similar *P/Nb* ratio was obtained by extracting HDA Soxhlet before calcination at 500 °C (NbP-6). Therefore, higher temperatures of calcination promote a better reaction between NbO_x species and phosphate.

Since there is a clear effect of the temperature for an efficient introduction of phosphates in the final material, NbP-3 and NbP-8 were prepared similarly to NbP-5 and NbP-6 respectively, however, the aging temperature was performed at 90 °C (instead of 65 °C). In both cases, the *P/Nb* increased reaching nearly the values expected for a stoichiometric niobium oxyphosphate [$NbO(PO_4)$], as shown in TABLE 2.2.

Hence, from this set of synthesis, it was possible to conclude that increasing both temperatures of aging and calcination improves the introduction of phosphates in the final material, although, the increase in the aging temperate was more effective.

NbP-1 was prepared similarly to NbP-5 but increasing by two-fold the loading of HDA and water, which led to an increase in the *P/Nb* molar,

indicating that higher surfactant concentration might facilitate the nucleation of the phosphate species. NbP-7 synthesis differed from NbP-1 by the addition of twice more water for the niobium chloride hydrolysis. Surprisingly, this sample reached the highest *P/Nb* molar ratio (1.03), although its yield was very low.

To test a different surfactant, NbP-2 was prepared like NbP-1 but replacing HDA with sodium dodecyl sulfate (SDS). The material was the one with the lowest *P/Nb* ratio among the prepared herein. HDA is a neutral surfactant, but in reaction conditions, it protonates (HDA-H^+), while SDS is an anionic surfactant. Since phosphates are also negatively charged, it is possible that when the materials are nucleated by HDA-H^+, phosphate groups are attracted, while particles nucleated with SDS are less effective in attracting phosphate species. NbP-2 presented *P/Nb* ratio similar to the commercial catalyst NbP-C.

7.1.3 - Supplementary graphics

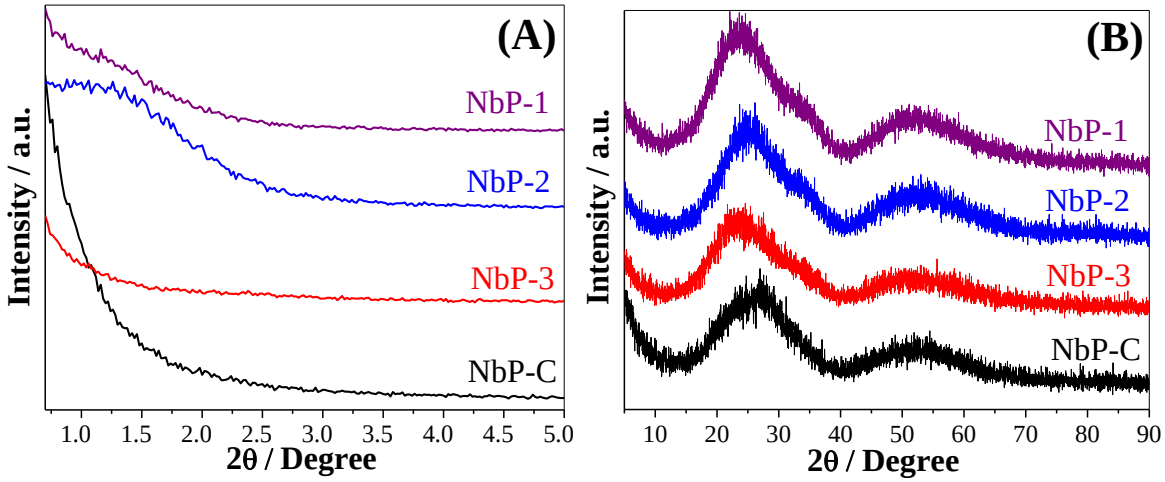

FIGURE A1.1 – Diffractograms of the samples at low (A) and high (B) angles.

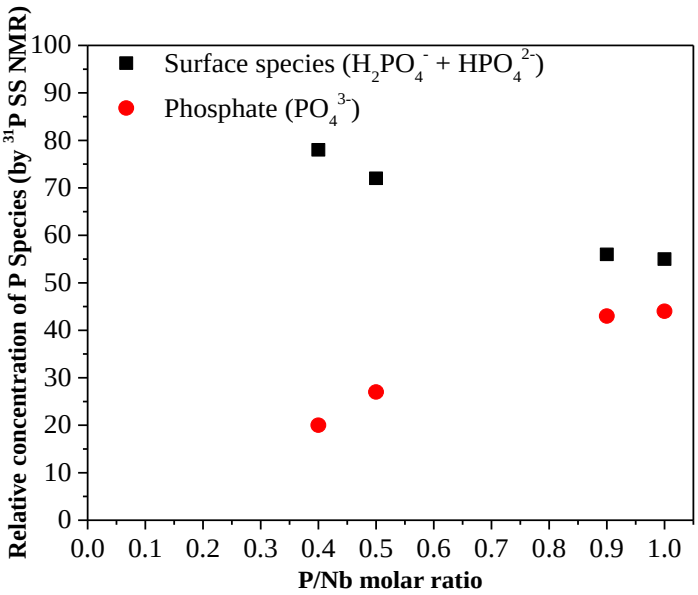

FIGURE A1.2 – Correlation between the relative concentration of surface and bulk P species found by ^{31}P SS NMR and the *P/Nb* molar ratio obtained by XRF.

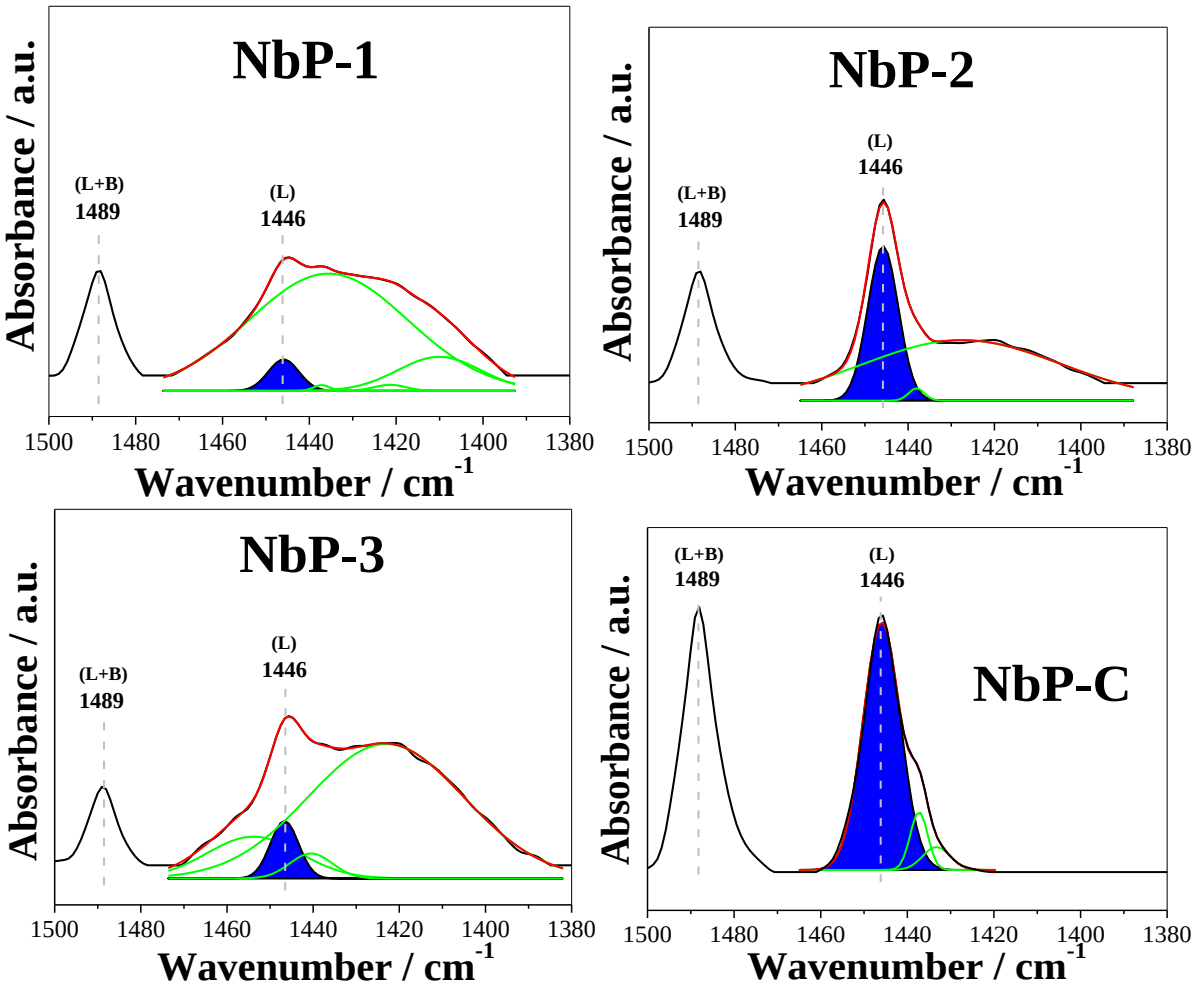

FIGURE A1.3 – Deconvoluted Lewis band at 1446 cm^{-1} after pyridine desorption at 100 °C.

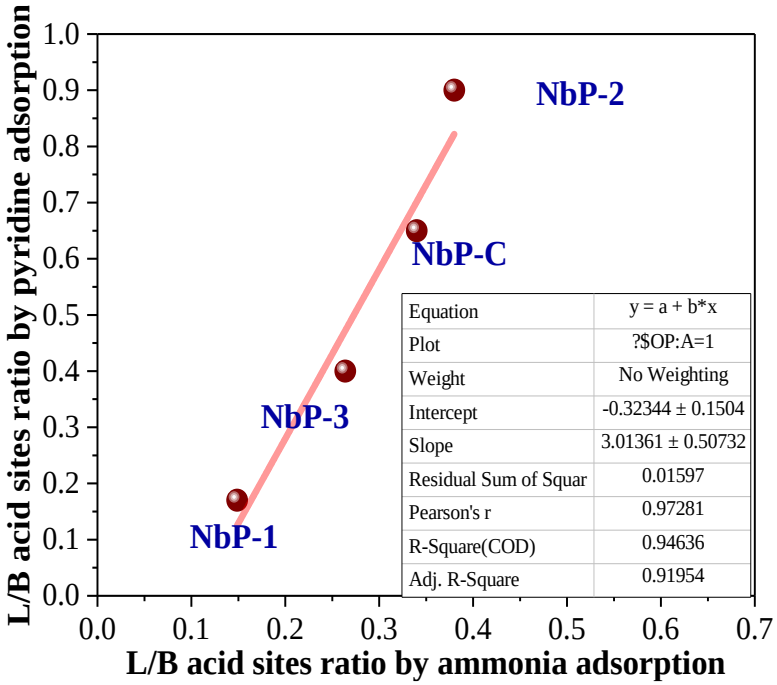

FIGURE A1.4 – Correlation between Brønsted/Lewis ratio obtained by pyridine and ammonia adsorption.

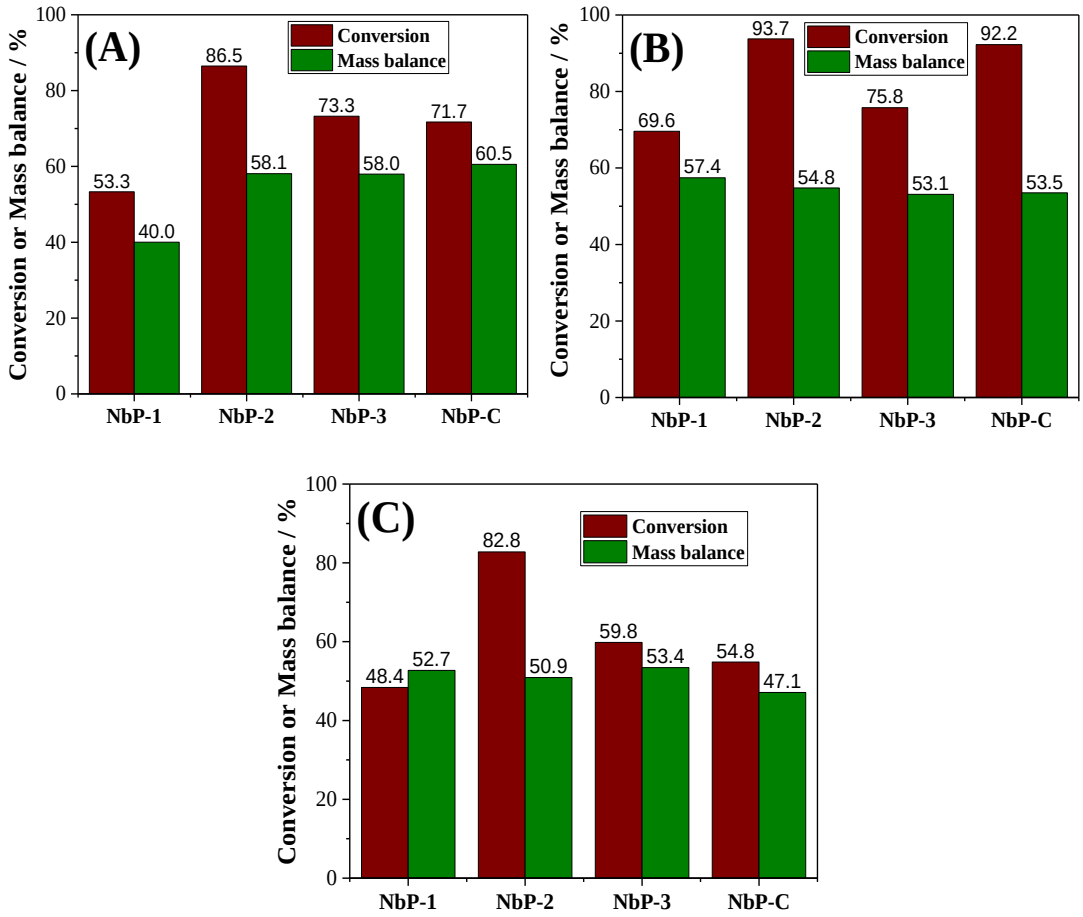

FIGURE A1.5 – Mass balance at the highest conversion obtained for (A) glucose in THF/H_2O, (B) xylose in THF/H_2O, and (C) xylose in pure water for the NbPs.

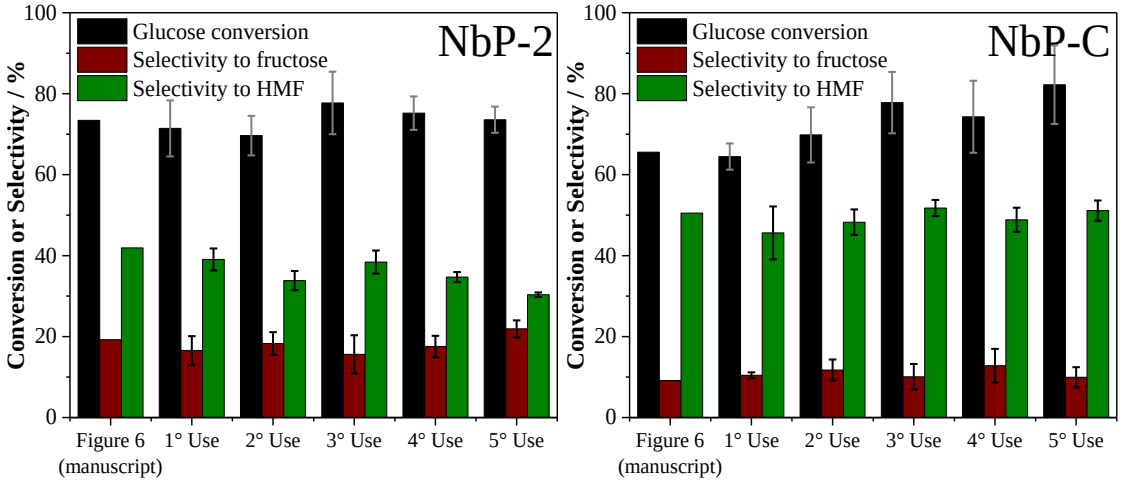

FIGURE A1.6 – Reuse of NbP-2 and NbP-C for the conversion of glucose in THF/H_2O = 4/1.

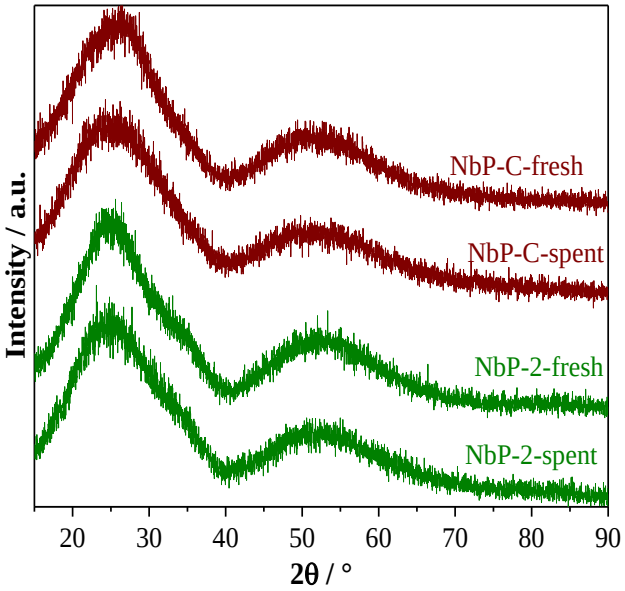

FIGURE A1.7 – XRD pattern of NbP-2 and NbP-C before (fresh) and after (spent) their use for the conversion of glucose.

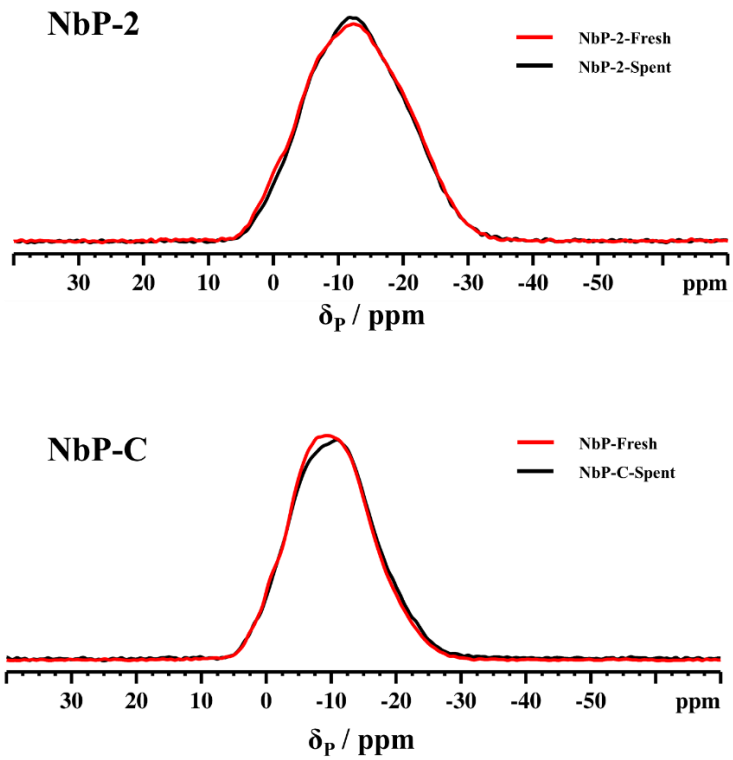

FIGURE A1.8 – ^{31}P NMR spectra for fresh and spent NbP-2 and NbP-C.

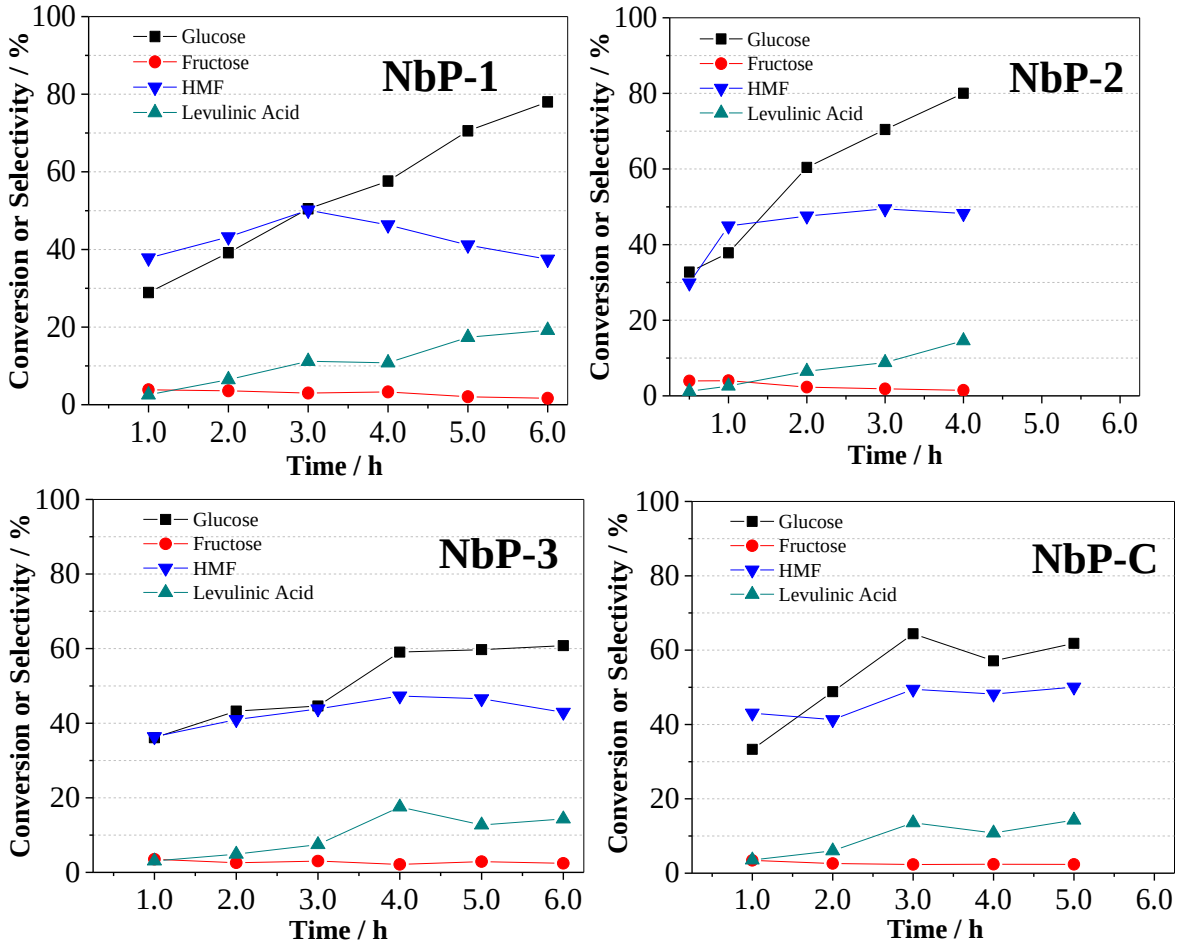

FIGURE A1.9 – Conversion of glucose catalyzed by the combination of 0.040 g of NbPs (catalyst/substrate mass ratio = 1.00) and HCl (0.18 mol L^{-1}) as a function of reaction time at 130 °C using THF/H_2O = 4/1 as solvent system.

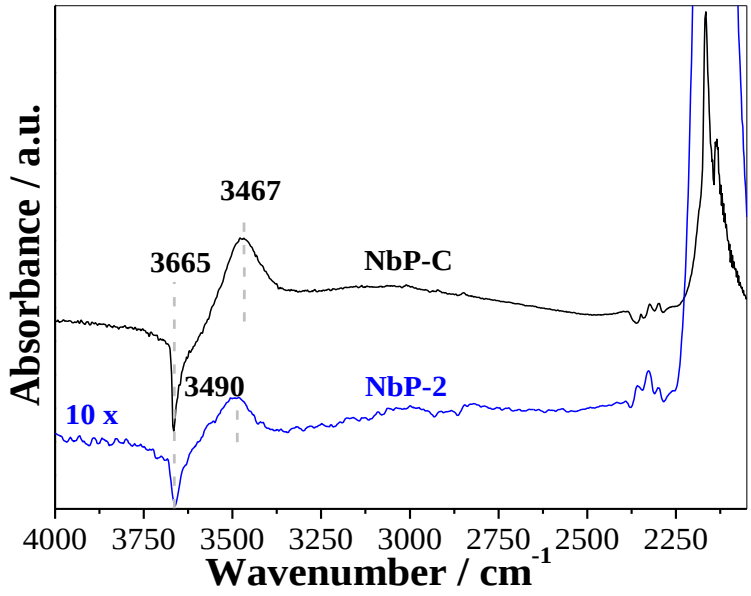

FIGURE A1.10 – Subtracted Infrared spectra of the catalysts at 50 mbar of CO.

7.2 - Chapter 2

7.2.1 - Supplementary graphics and tables

7.2.1.1 - Characterizations

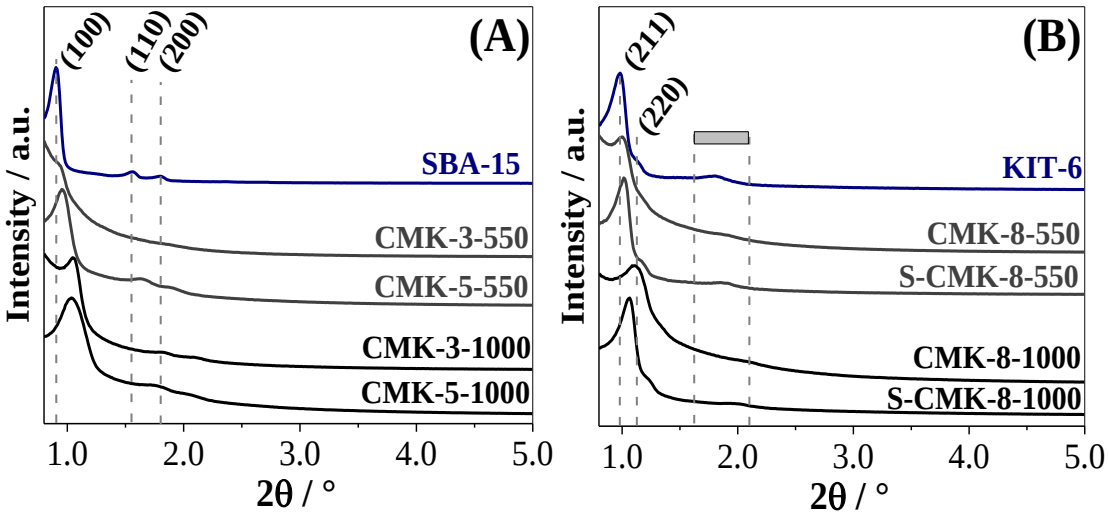

FIGURE A2.1 – XRD diffractograms of the templated carbons derived from the silica SBA-15 (A) and KIT-6 (B).

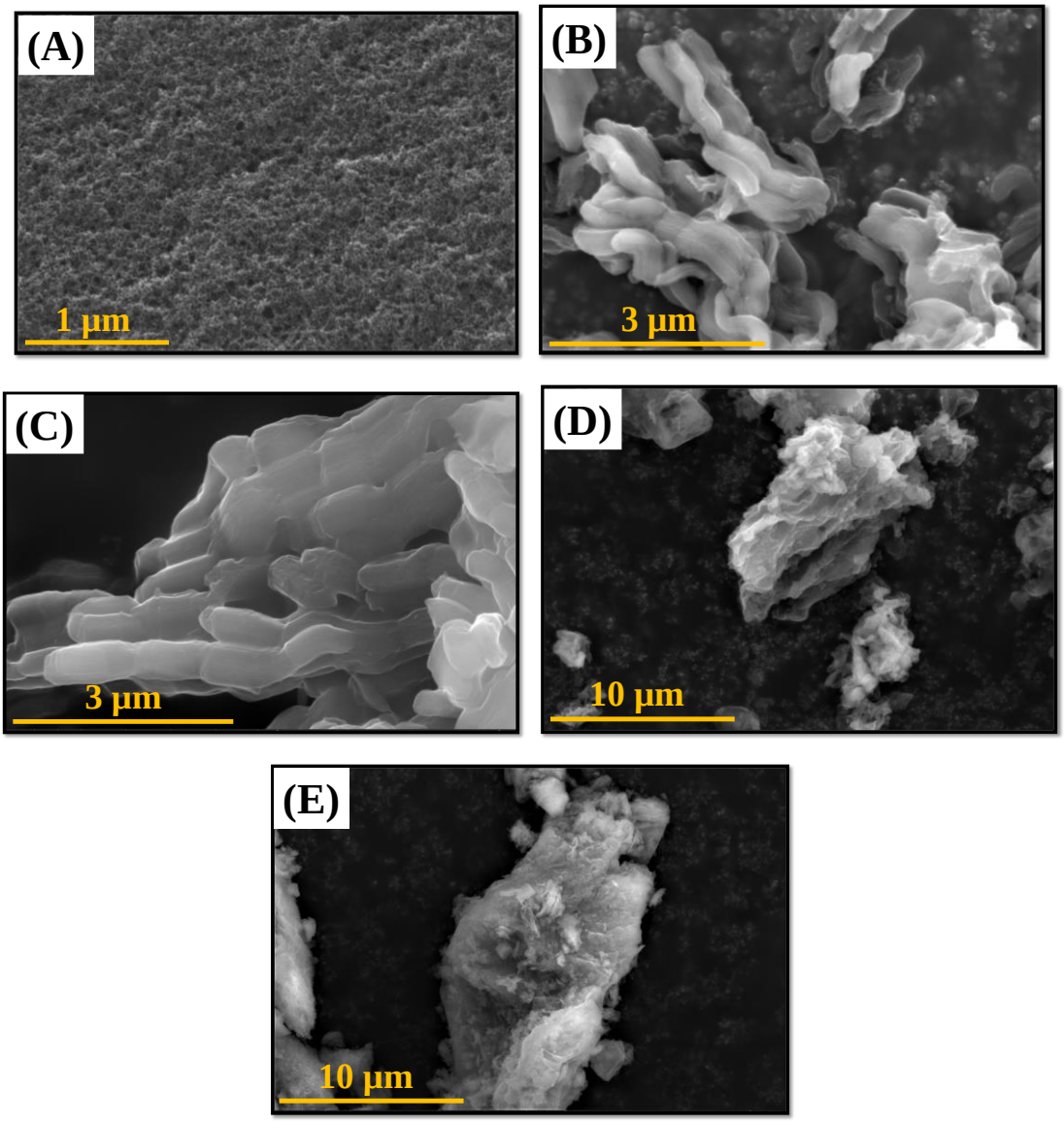

FIGURE A2.2 – SEM micrographs of the templated carbons C-Chi-550 (A), CMK-3-550 (B), CMK-5-550 (C), CMK-8-550 (D) and S-CMK-8-550 (E).

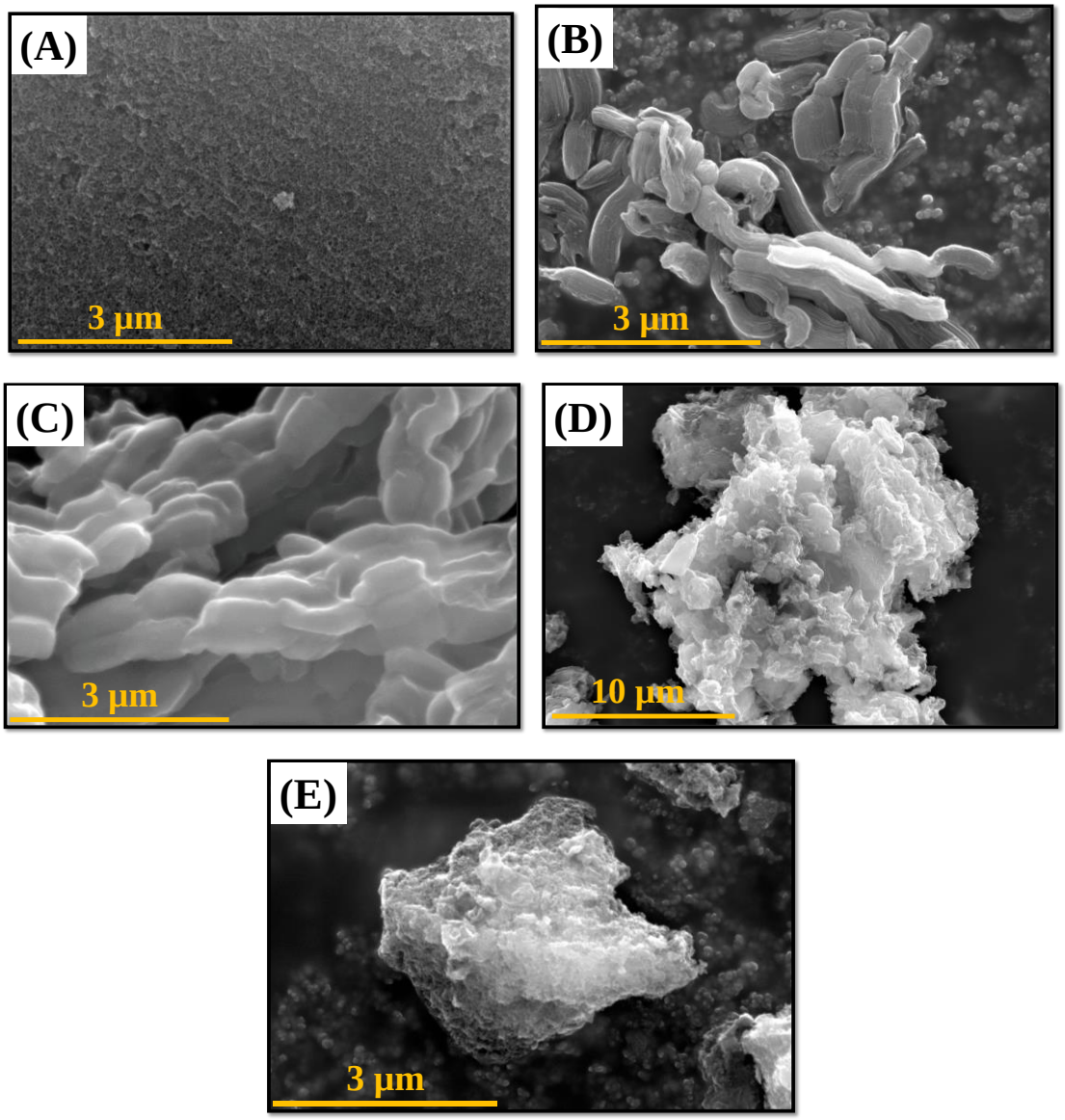

FIGURE A2.3 – SEM micrographs of the templated carbons C-Chi-1000 (A), CMK-3-1000 (B), CMK-5-1000 (C), CMK-8-1000 (D) and S-CMK-8-1000 (E).

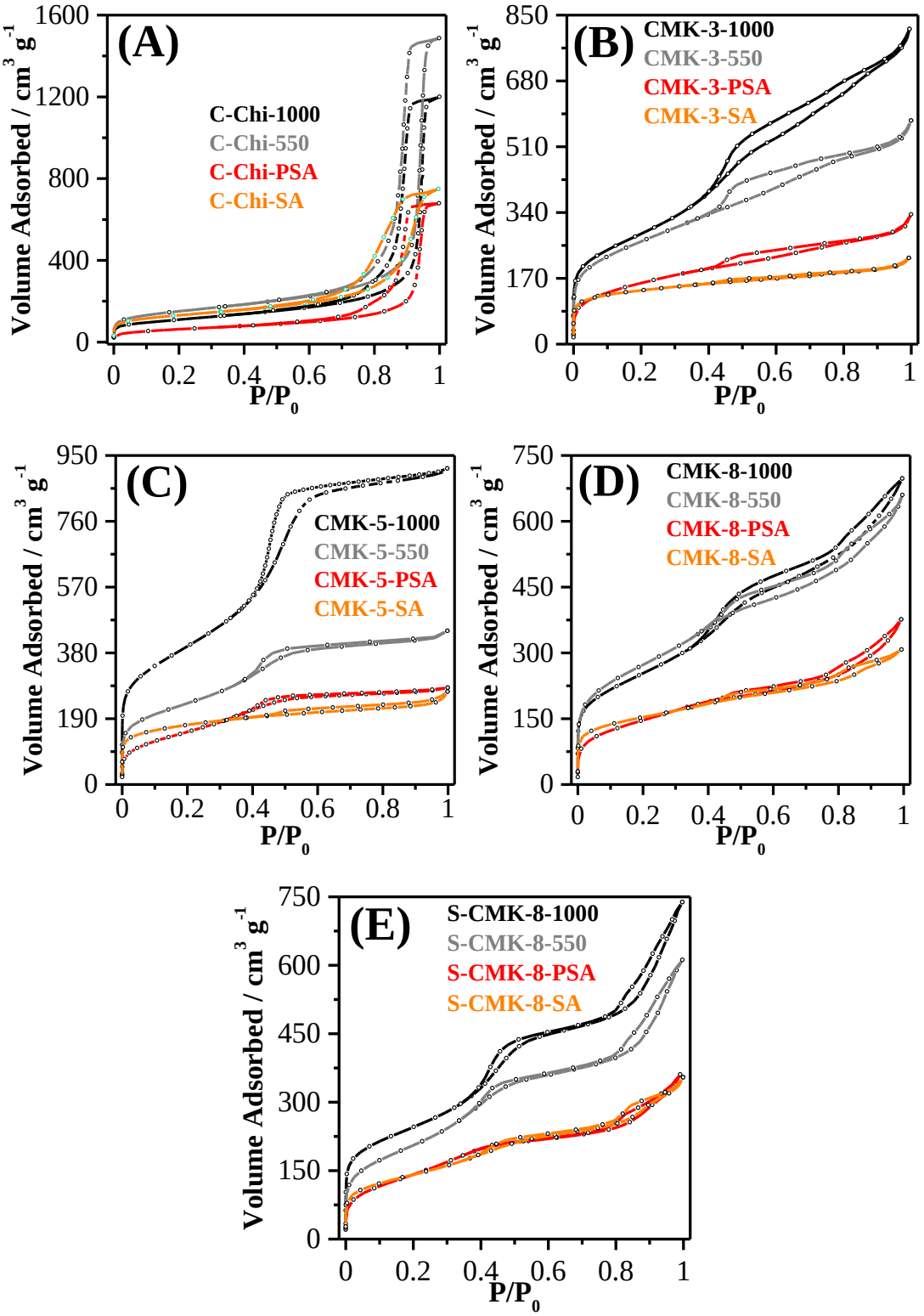

FIGURE A2.4 – Nitrogen physisorption isotherms of the templated carbons and sulfonated carbons of the groups C-Chi (A), CMK-3 (B), CMK-5 (C), CMK-8 (D), and S-CMK-8 (E).

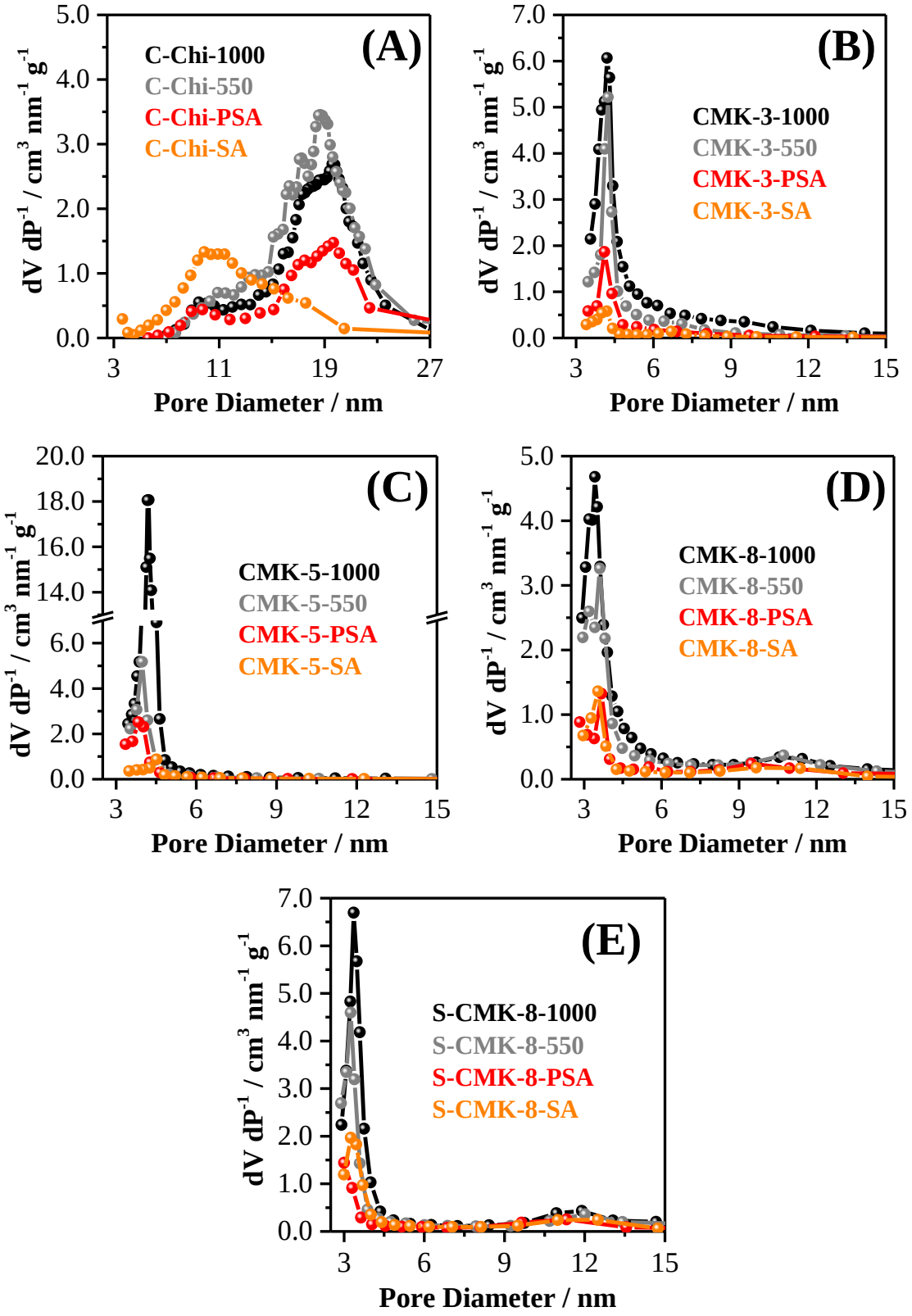

FIGURE A2.5 – Pore size distribution of the templated carbons and sulfonated carbons of the groups C-Chi (A), CMK-3 (B), CMK-5 (C), CMK-8 (D), and S-CMK-8 (E).

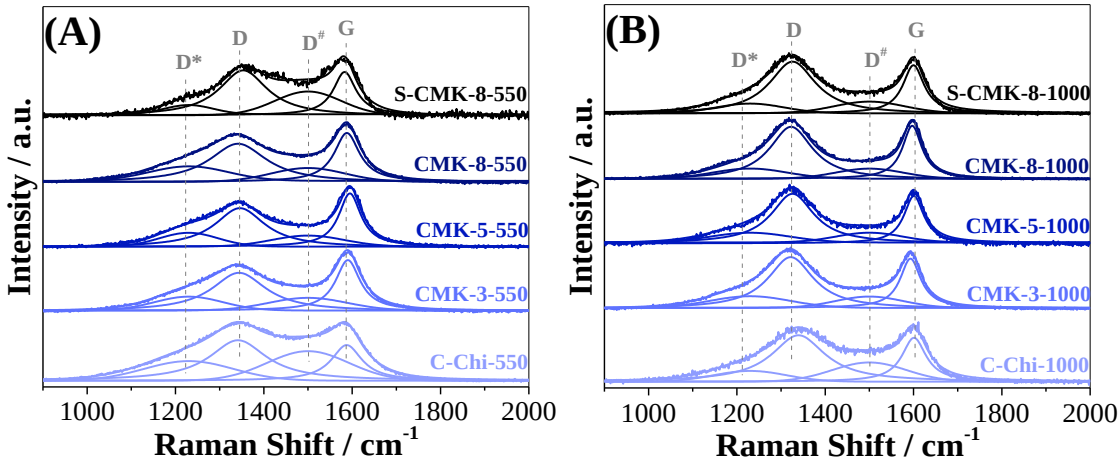

FIGURE A2.6 – Raman deconvoluted spectra of the templated carbons pyrolyzed at 550 °C (A) and 1000 °C (B).

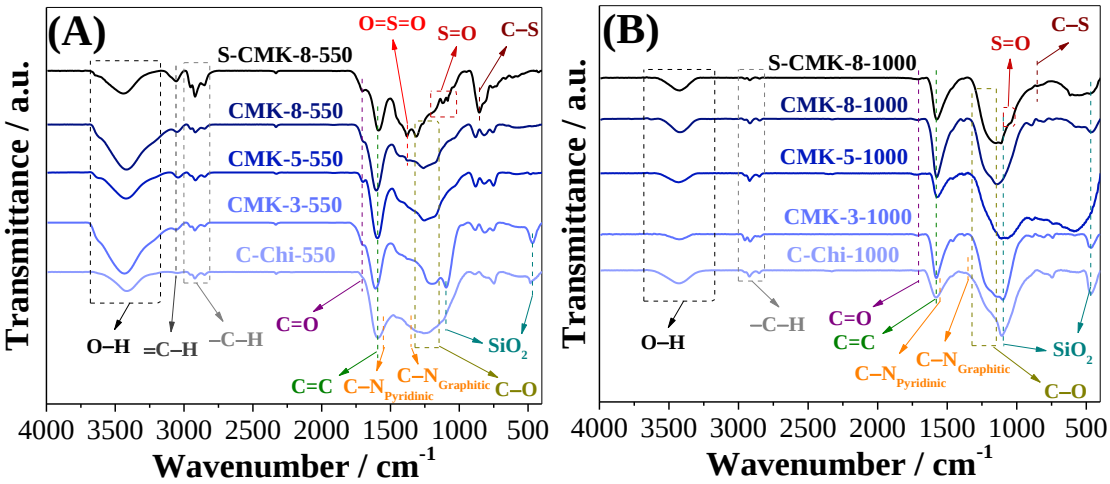

FIGURE A2.7 – FTIR spectra of the templated carbons pyrolyzed at 550 °C (A) and 1000 °C (B).

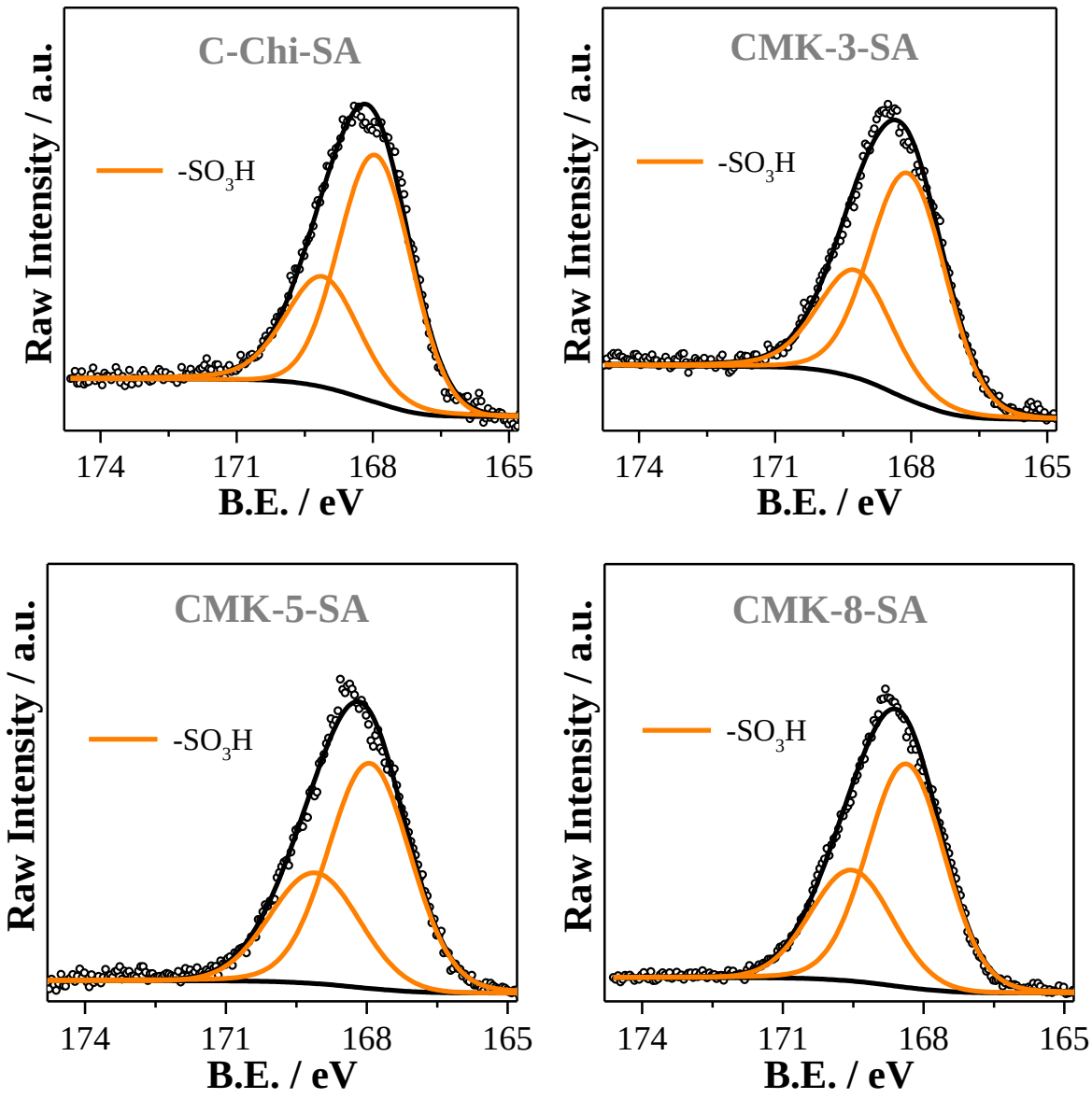

FIGURE A2.8 – High-resolution XPS spectra of *S 2*p with new deconvolutions for the sulfonated carbons functionalized with SA species.

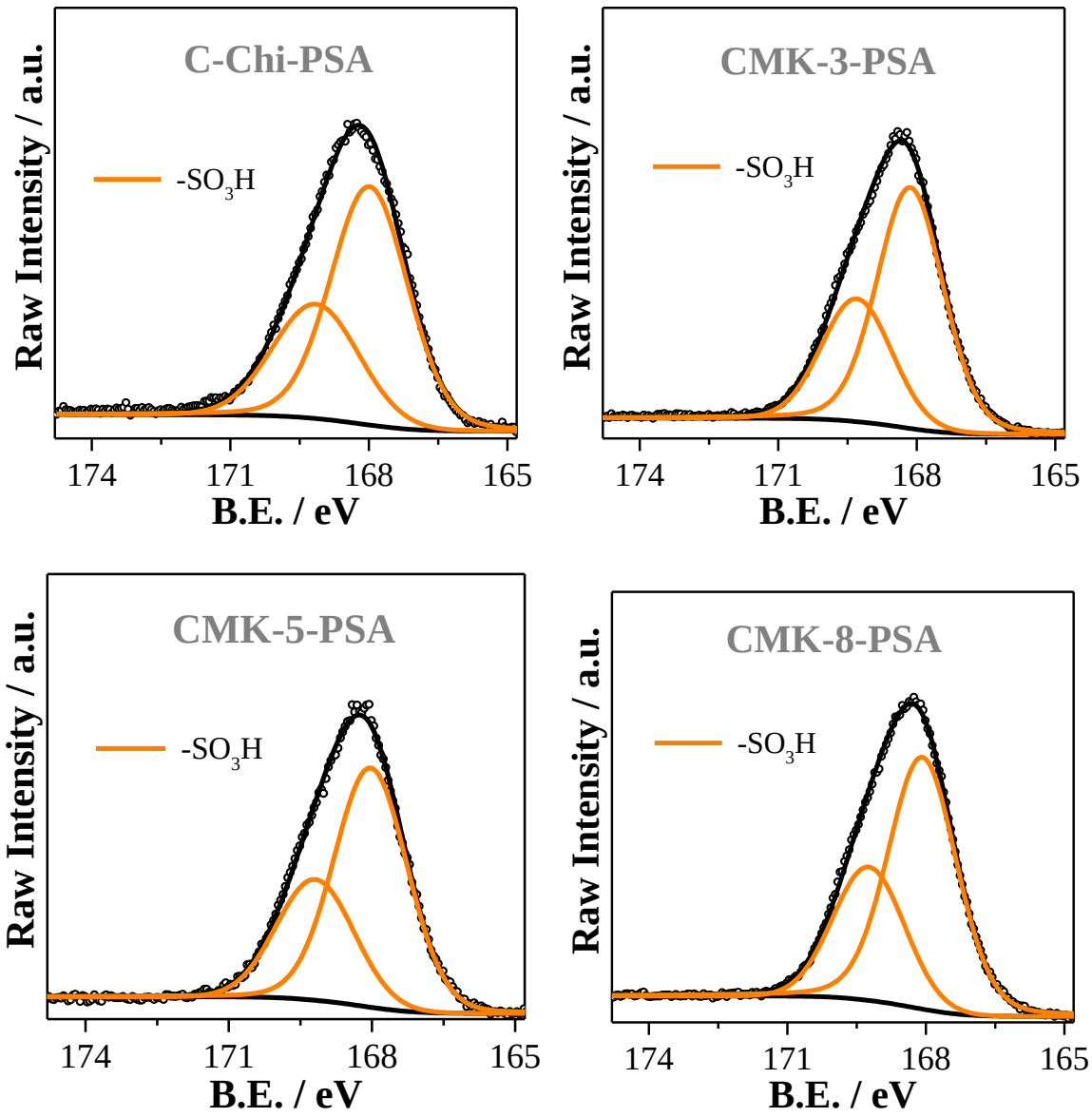

FIGURE A2.9 – High-resolution XPS spectra of *S 2*p with new deconvolutions for the sulfonated carbons functionalized with PSA species.

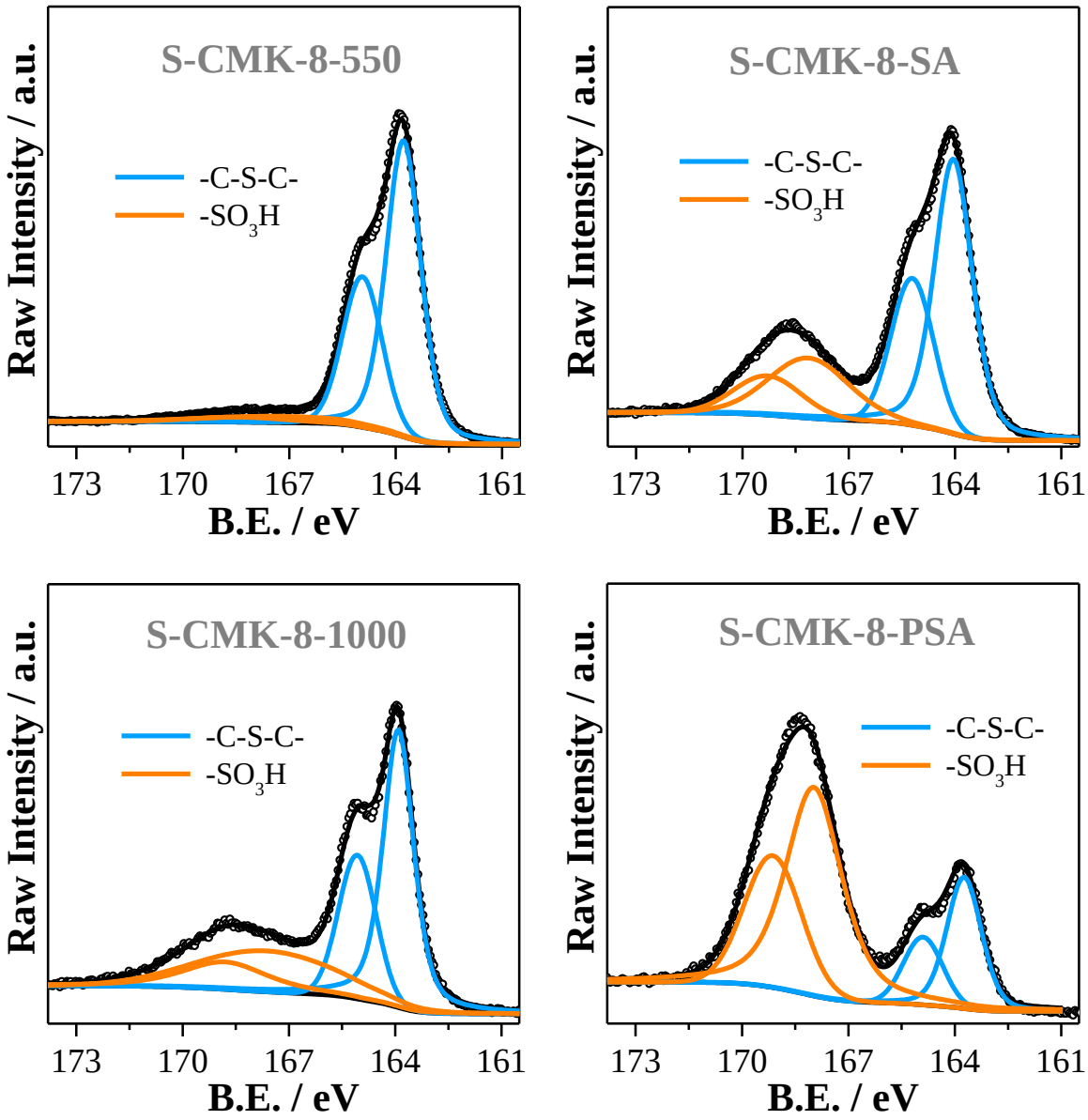

FIGURE A2.10 – High-resolution XPS spectra of *S 2*p with new deconvolutions for the templated carbons and sulfonated carbons of the group S-CMK-8.

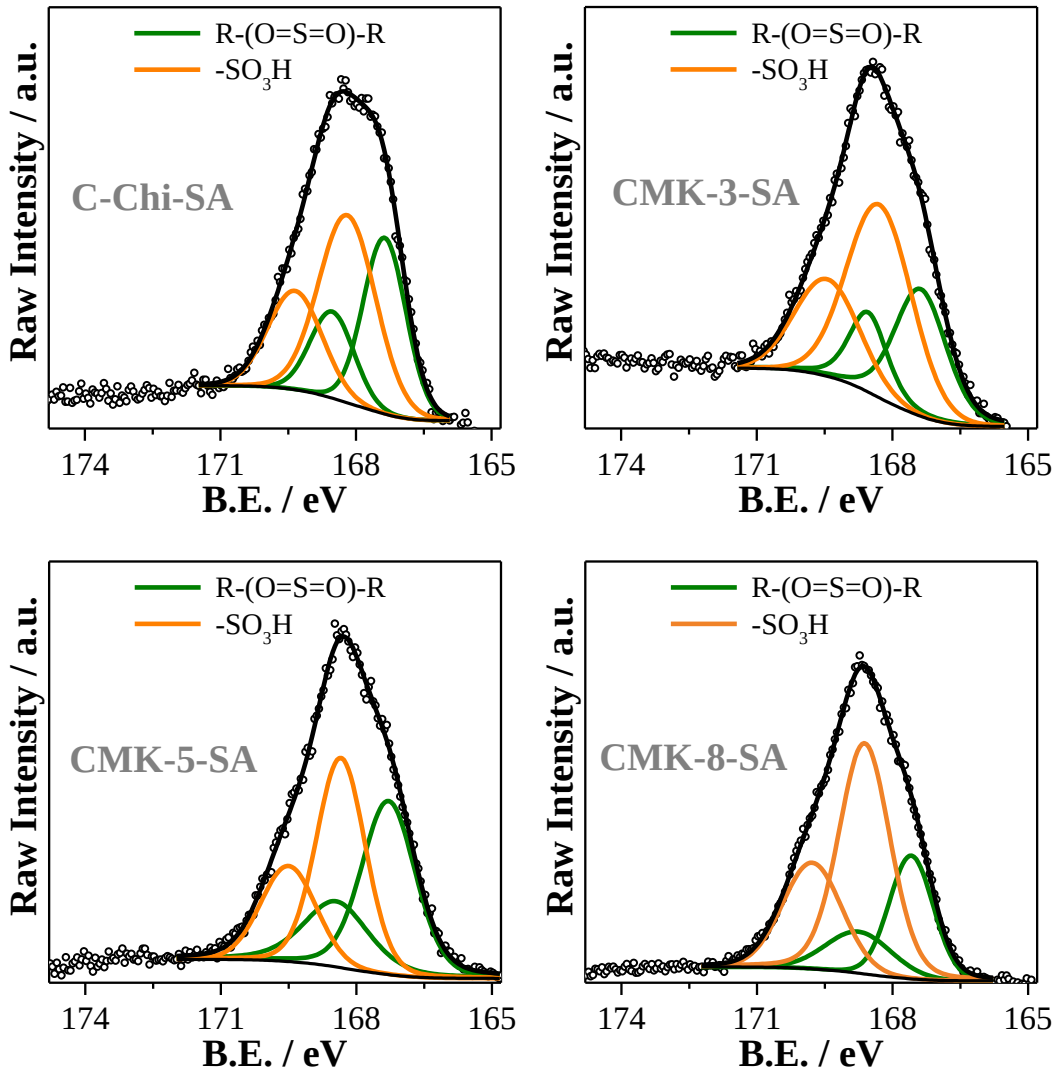

FIGURE A2.11 – High-resolution XPS spectra of *S 2*p for the sulfonated carbons functionalized with SA species.

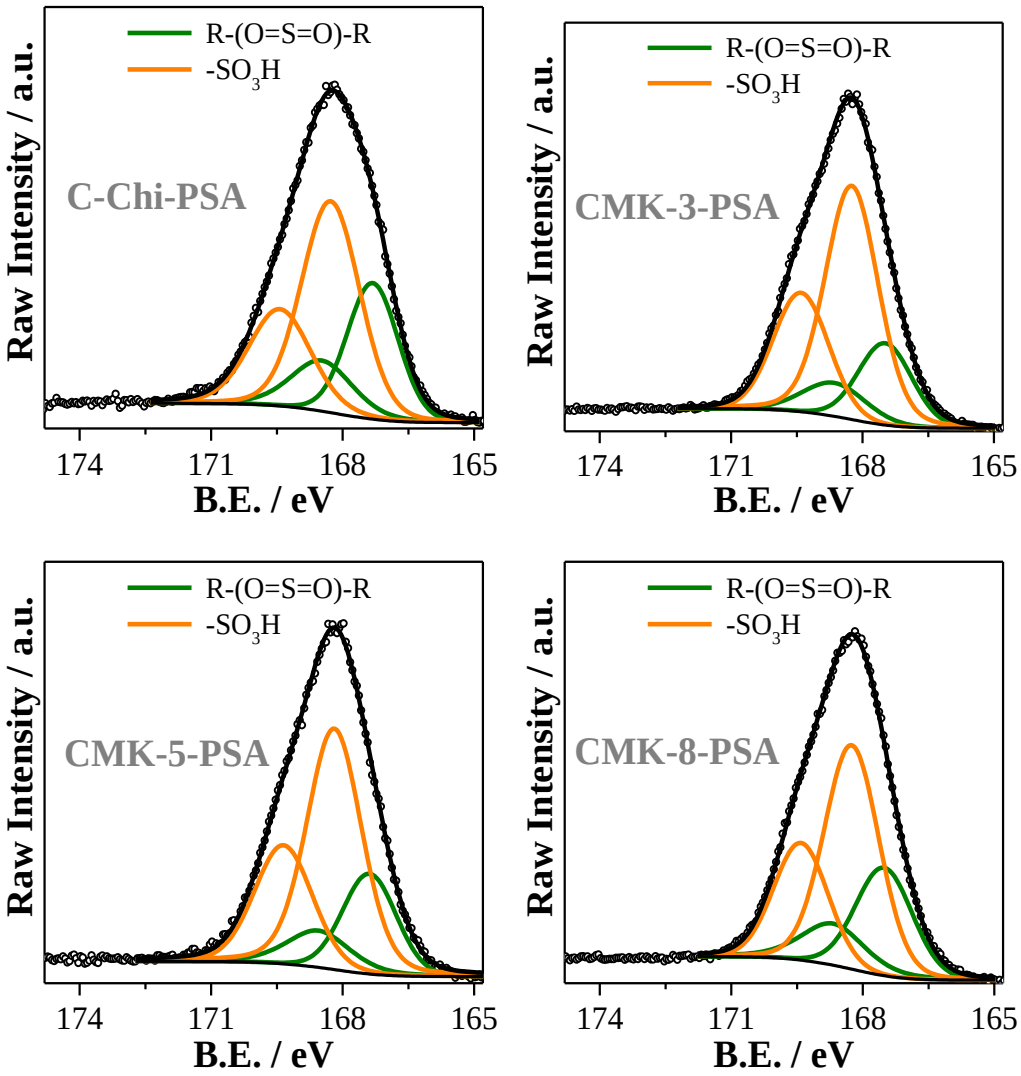

FIGURE A2.12 – High-resolution XPS spectra of *S 2*p for the sulfonated carbons functionalized with PSA species.

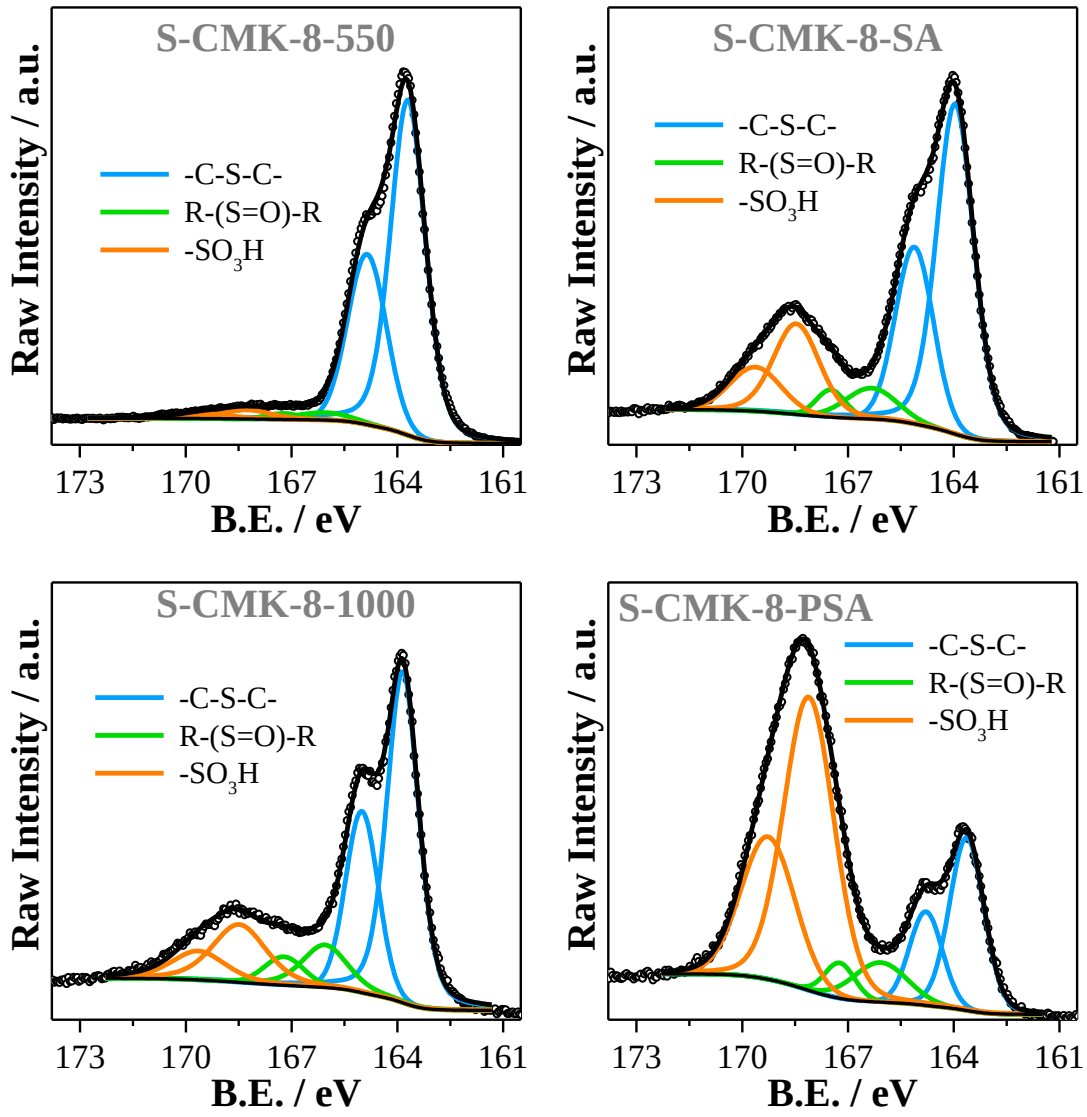

FIGURE A2.13 – High-resolution XPS spectra of *S 2*p for the templated carbons and sulfonated carbons of the group S-CMK-8.

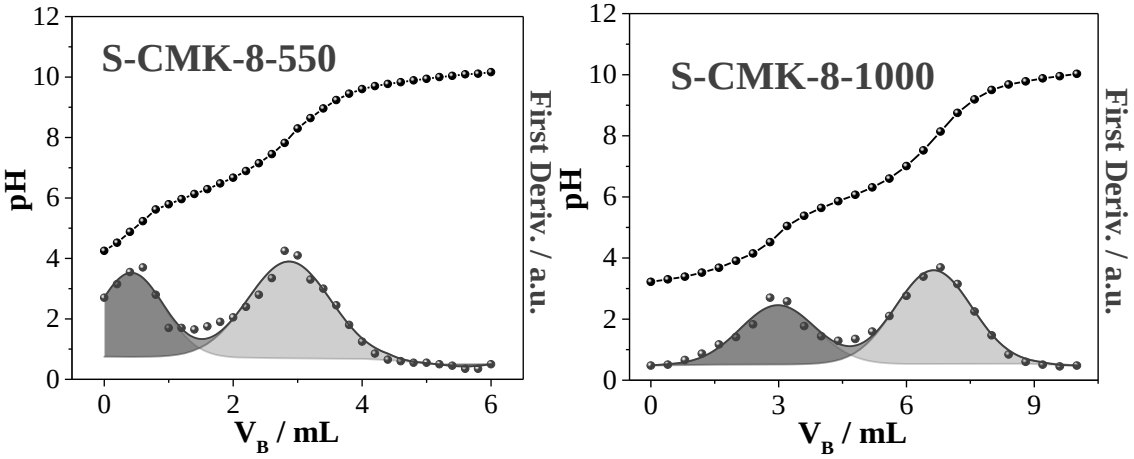

FIGURE A2.14 – Potentiometric titration and first derivative curves for the acidic templated carbons.

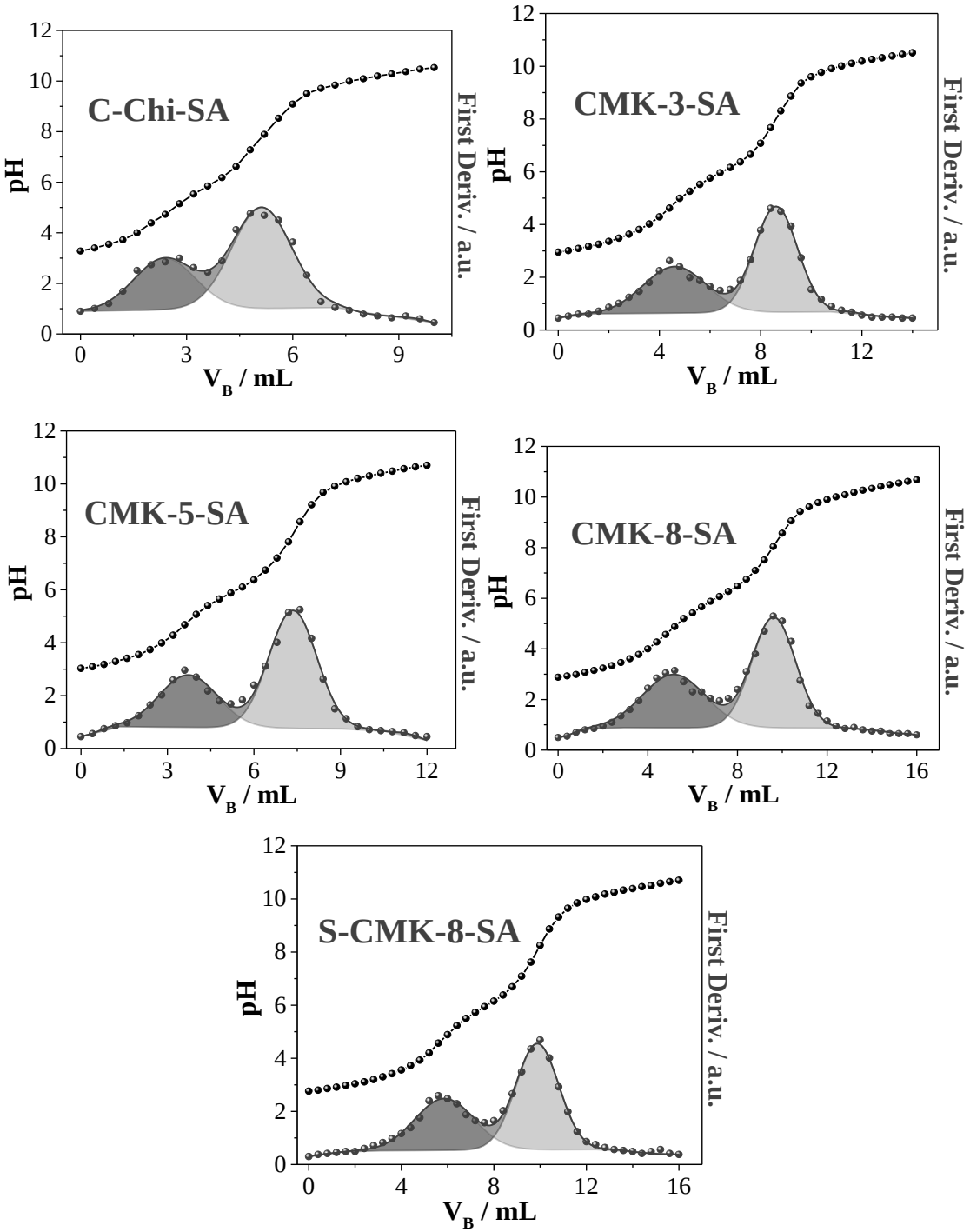

FIGURE A2.15 – Potentiometric titration and first derivative curves for the sulfonated carbons functionalized with SA species.

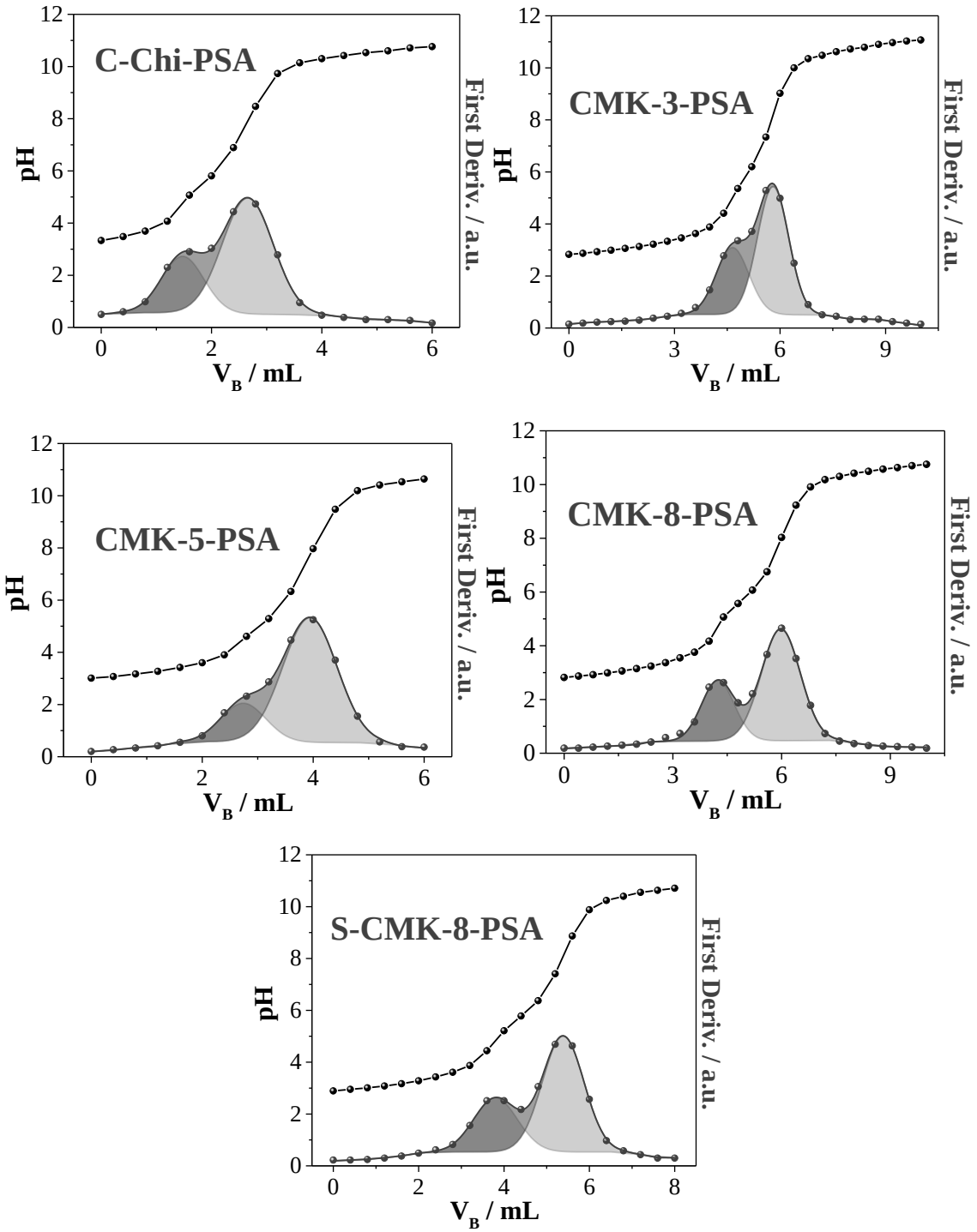

FIGURE A2.16 – Potentiometric titration and first derivative curves for the sulfonated carbons functionalized with PSA species.

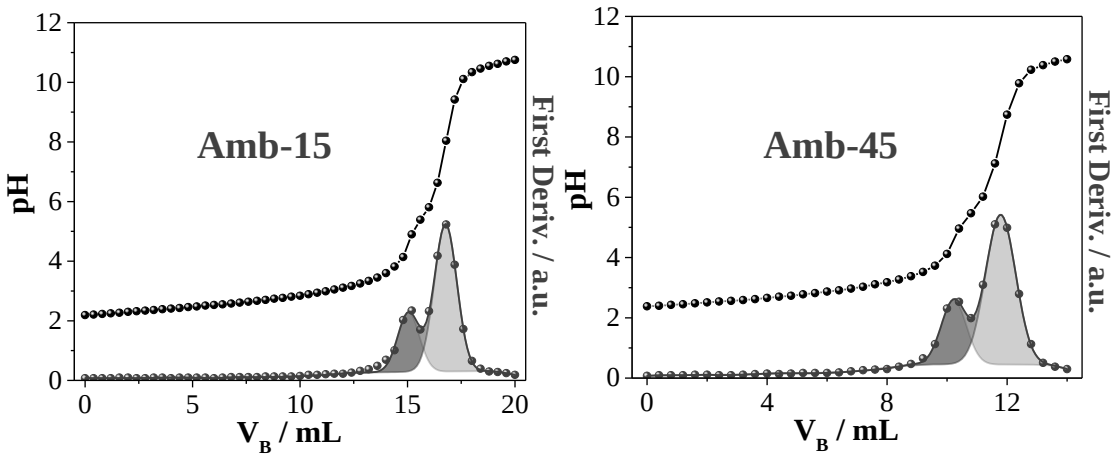

FIGURE A2.17 – Potentiometric titration and first derivative curves for the commercial Amberlysts.

TABLE A2.1 – Concentration of acid sites normalized by the surface area of the catalysts.

Catalysts	**Normalized concentration of acid sites (μmol m^{-2})**		
	Total	***Stronger***	***Weaker***
C-Chi-SA	2.50	1.16	1.34
C-Chi-PSA	2.68	1.49	1.19
CMK-3-SA	3.81	2.04	1.77
CMK-3-PSA	2.35	1.85	0.50
CMK-5-SA	2.64	1.34	1.30
CMK-5-PSA	1.60	1.11	0.49
CMK-8-SA	3.98	2.14	1.85
CMK-8-PSA	2.57	1.82	0.74
S-CMK-8-SA[a]	4.45	2.64	1.81
S-CMK-8-PSA[a]	2.36	1.67	0.70

[a] It was determined by ignoring the Poly-Th contribution.

TABLE A2.2 – Chemical composition determined by a combination of CHN analysis, potentiometric titration, and XPS spectra for *S 2*p and TGA in an oxidant environment.

Catalysts	Chemical composition (%)					
	C	H	N	S[a]	Si[b]	O[c]
C-Chi-550	69.44	1.74	9.44	-	1.82	17.57
C-Chi-SA	56.11	2.23	8.19	2.99	1.82	28.67
C-Chi-1000	41.27	0.08	2.15	-	5.90	50.61
C-Chi-PSA	38.37	0.77	1.87	1.68	5.90	51.41
CMK-3-550	62.26	2.28	-	-	4.38	31.09
CMK-3-SA	48.88	2.43	-	5.20	4.38	39.12
CMK-3-1000	83.35	0.46	-	-	3.02	13.17
CMK-3-PSA	55.47	3.25	-	4.53	3.02	33.73
CMK-5-550	80.82	3.48	-	-	0.66	15.05
CMK-5-SA	57.31	3.32	-	5.21	0.66	33.50
CMK-5-1000	86.59	0.35	-	-	0.64	12.43
CMK-5-PSA	57.21	2.56	-	2.73	0.64	36.86
CMK-8-550	77.34	2.05	-	-	0.72	19.89
CMK-8-SA	53.03	2.84	-	5.39	0.72	38.02
CMK-8-1000	81.64	1.10	-	-	1.12	16.15
CMK-8-PSA	55.71	3.18	-	4.63	1.12	35.37
S-CMK-8-550	71.62	0.96	-	1.67	0.12	25.63
S-CMK-8-SA	43.52	2.46	-	18.51	0.12	35.40
S-CMK-8-1000	76.53	0.72	-	2.15	3.99	16.62
S-CMK-8-PSA	55.37	2.77	-	4.28	3.99	33.60

[a] It was estimated from XPS spectra for *S 2*p and potentiometric titration.

[b] It was obtained from TGA analysis in an oxidant environment.

[c] It was calculated from the equation: $O = 100 - (C + H + N + S + Si)$

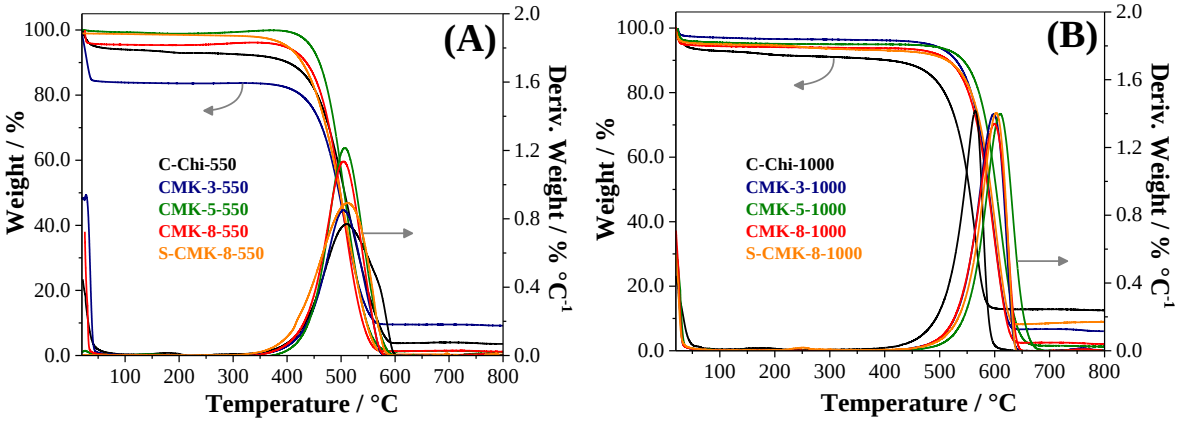

FIGURE A2.18 – Thermograms of the templated carbons pyrolyzed at 550 °C (A) and 1000 °C (B).

The stage of mass loss between 400 °C – 600 °C for the carbons pyrolyzed at 550 °C (FIGURE A2.18A) and between 450 °C – 700 °C for the carbons pyrolyzed at 1000 °C (FIGURE A2.18B), is due to the combustion of their carbon matrices [172]. The CMK carbons pyrolyzed at 1000 °C exhibit a maximum combustion temperature (represented by the maximum derivative weight) approximately 100 °C higher than those pyrolyzed at 550 °C; and C-Chi-1000 only 50 °C higher than C-Chi-550. These results firstly indicate that the carbons treated at higher pyrolysis temperature present more stable carbon matrices, due to their higher aromatization and lower susceptibility to oxidation [173]. Secondly, CMK carbons pyrolyzed at 1000 °C have a more stable carbon matrix than C-Chi-1000.

After the carbon matrix combustion, the remaining material can be assigned to the silica template [174]. The remaining silicon obtained for the templated carbons is less than 6 wt. % (TABLE A2.2).

7.2.1.2 - Catalytic studies

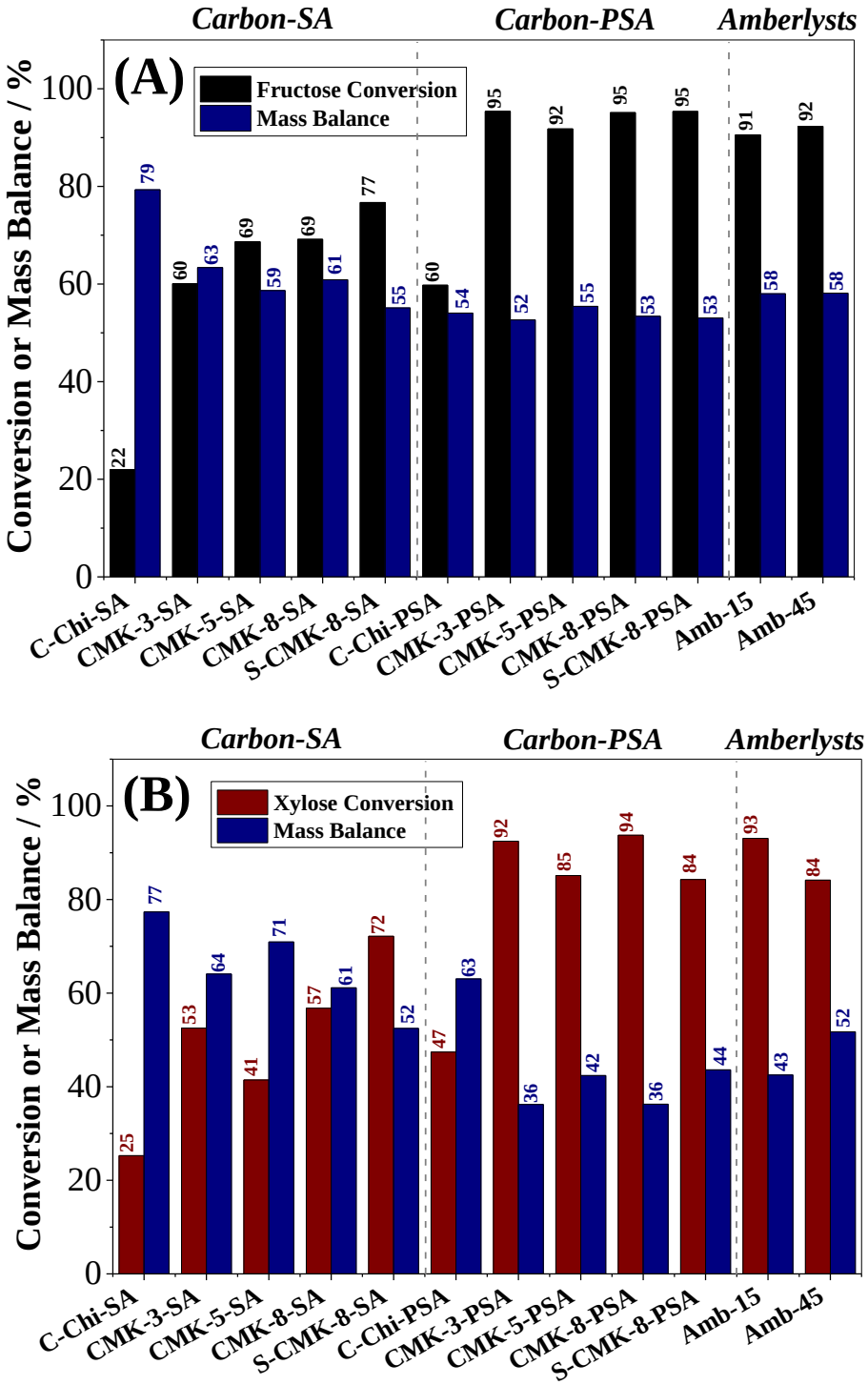

FIGURE A2.19 – Mass balance in the conversion of fructose into HMF (A) and xylose into furfural (B) for the sulfonated carbons and Amberlysts.

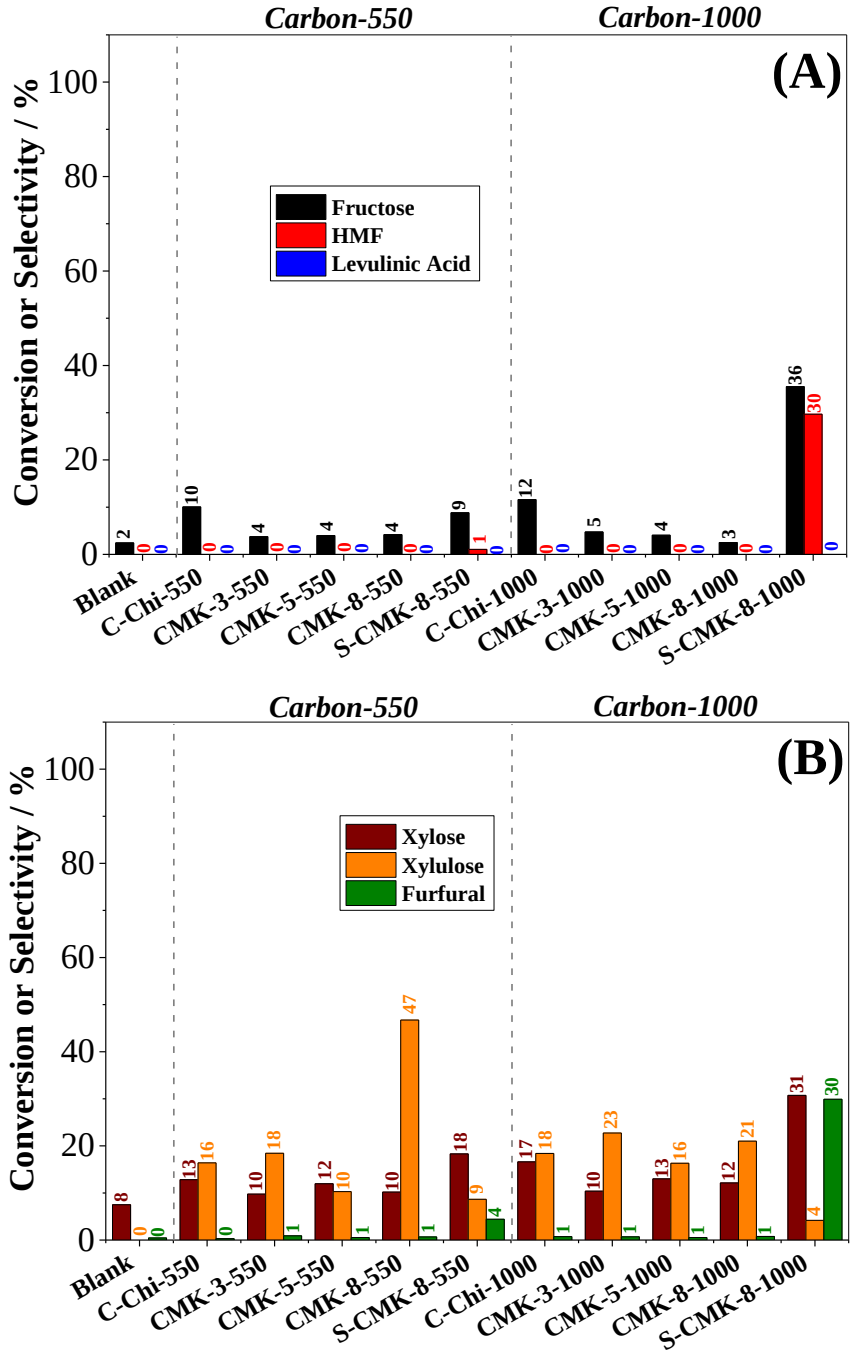

FIGURE A2.20 – Catalytic screening of the templated carbons for the conversion of fructose into HMF (A) and xylose into furfural (B) at 130 °C and 160 °C, respectively, in THF/H_2O = 4/1, 1 h of reaction and 50 mg of the carbon (catalyst/substrate mass ratio = 1.25).

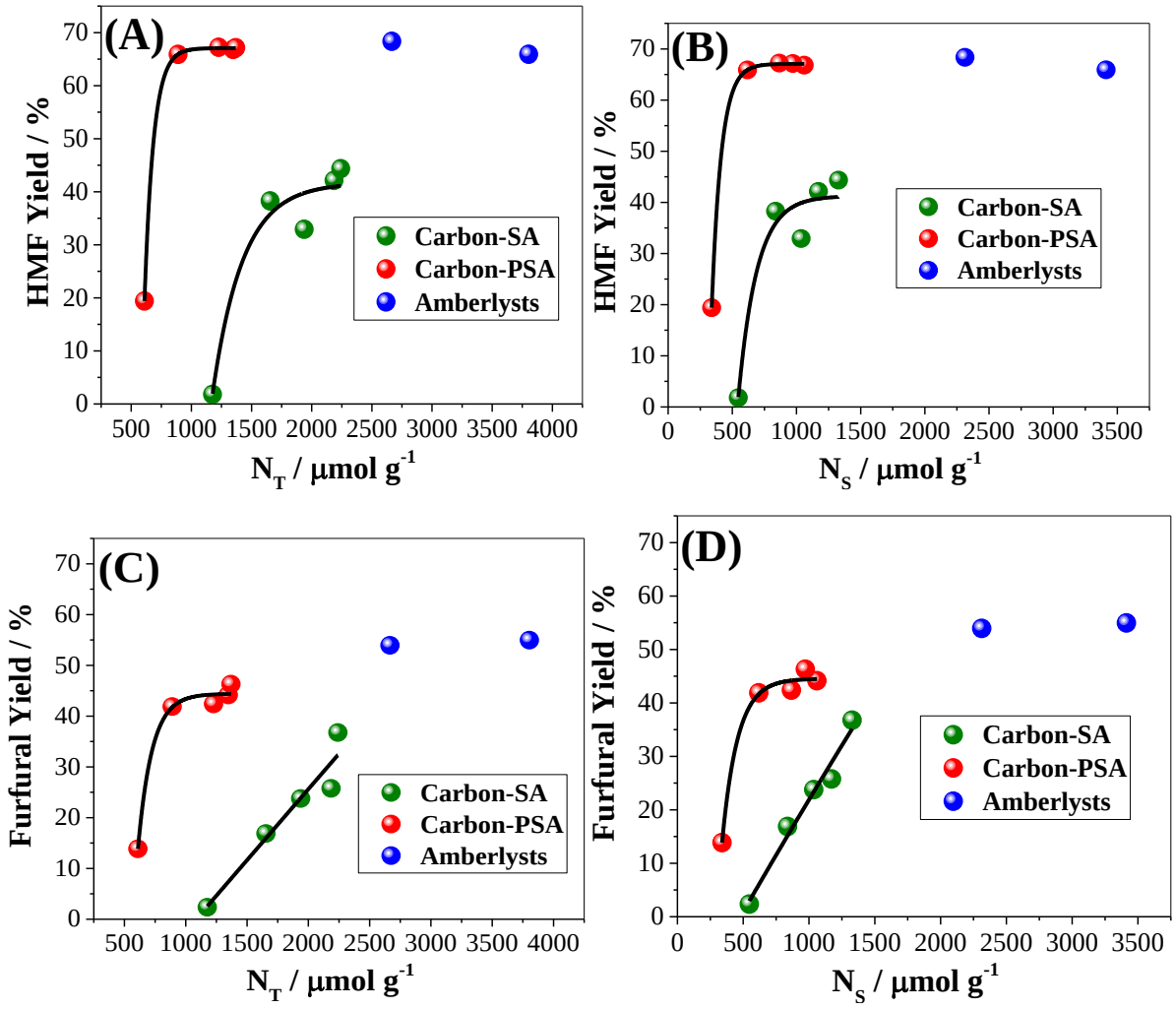

FIGURE A2.21 – Correlation of the concentration of total (A-C) and stronger (B-D) acid sites with the yield of HMF (A-B) and furfural (C-D) of the sulfonated carbons and Amberlysts.